# Examination of Structural Brain Changes and Cognitive Function in HIV using Advanced MRI Processing Techniques

Ryan Sanford
Department of Biomedical Engineering
McGill University, Montreal, Canada

December 2018

A thesis submitted to McGill University in partial fulfillment of the requirements for the degree of Doctor of Philosophy in Biomedical Engineering

## Abstract

The introduction of combination anti-retroviral therapy (cART) has dramatically improved the outlook for people living with HIV by reducing HIV-related morbidity and increasing life expectancy. Despite this, the rates of HIV-associated neurocognitive disorders (HAND) remain frequent. Such cognitive impairments remain clinically relevant as they can negatively impact performance in every day activities and reduce overall quality of life. The reasons for the persistence of HAND, despite cART, remains elusive with several proposed mechanisms including: irrecoverable brain injury that occurred prior to cART initiation; progressive brain injury caused by an active, destructive process in the brain; the presence of a comorbid condition causing additional neurological insults; and cerebral small vessel disease, a common cause of vascular cognitive impairment. The aim of this dissertation was to take advantage of advanced magnetic resonance imaging (MRI) processing tools and neuropsychological assessment to provide a clearer understanding into the neuropathogenesis of HIV and elucidate the causes of HAND in the cART era.

This is a manuscript-based dissertation composed of four separate papers. The first paper describes a cross-sectional study that reported brain volume reductions and poorer cognitive function in a group of HIV+ participants compared to demographically similar controls. We concluded that despite the majority of HIV+ participants being on cART with good viral control, regionally specific brain volume reductions and cognitive difficulties remained prevalent. However, given the cross-sectional nature of the study, we could not elucidate the extent to which these observations reflect changes before cART or ongoing brain injury, despite cART. This led to the second paper, where we sought to determine whether treated HIV+ individuals with undetectable viral loads experienced progressive brain atrophy and cognitive decline over a two-year period compared to demographically similar controls. Similar to the first study, we observed that the HIV+ group had smaller brain volumes and poorer cognitive function compared to the controls at all visits. However, the changes in brain volumes and cognitive function over time were similar between the groups. These results argue against an active, destructive process as the cause of the brain injury and, instead, supports the hypothesis that brain and cognitive changes occurring prior to cART initiation may be responsible for the cognitive impairment commonly found in people living with HIV. However, this hypothesis could not be verified as all the HIV+ participants included in the first two studies had chronic HIV infection (>1 year after exposure). This led to the

third study, which was a longitudinal study that aimed to map the natural course of structural brain changes occurring in early infection, prior to cART initiation, and the impact cART has on these changes. We observed that longer duration of untreated infection was correlated with greater brain atrophy and cortical thinning, while initiating treatment halted these changes. These findings verified the hypothesis that brain changes occur early in HIV infection before cART initiation and worsen with the absence of treatment. The final study investigated the synergistic effects between cerebral small vessel disease and HIV on the brain and cognition in people living with HIV. We observed that HIV+ participants did not have more severe cerebral small vessel disease compared to controls. However, worse cerebral small vessel disease was associated with reduced brain volumes and poorer cognitive function in all participants, regardless of HIV serostatus. These results suggested that HAND in the cART era may be a mix of injury caused by the virus before treatment initiation and subsequent cerebral small vessel disease.

Taken together, the results presented in this dissertation provide a unique narrative regarding the development of HAND in the cART era. The findings argue that the development of early neurobiological changes result in downstream cognitive deficits while subsequent cerebral small vessel disease may independently contribute to brain changes leading to additional cognitive problems. The combination of these independent processes most likely has a cumulative detrimental effect on brain structure and cognitive function resulting in the mild cognitive impairment that seem to be common in older people with long-standing, well-controlled HIV infection. These results emphasize the importance of starting cART early, adhering to cART, maintaining good viral control and optimizing vascular health to improve brain health and protect against decline.

## Résumé

L'introduction de la trithérapie antirétrovirale pour le VIH a profondément amélioré les perspectives des patients infectés par ce virus, en réduisant les comorbidités et en majorant l'espérance de vie. Malgré cela, la prévalence des troubles neurocognitifs liés au VIH reste élevée. Le déficit qui en résulte est significatif en termes de handicap, impactant les activités quotidiennes et la qualité de vie. Il est aujourd'hui difficile d'expliquer pourquoi de tels troubles persistent malgré la diffusion de la trithérapie. Les mécanismes proposés sont la survenue de lésions cérébrales avant traitement, un processus lésionnel chronique, ou bien les conséquences des comorbidités, telles qu'une atteinte vasculaire cérébrale. Le but de cette thèse était, à l'aide de techniques de traitement d'images novatrices appliquées à l'imagerie par résonnance magnétique (IRM) et d'évaluations neuropsychologiques exhaustives, d'apporter un éclairage nouveau sur la neuropathogénie du VIH et de comprendre la cause des troubles cognitifs liés à l'infection par ce virus.

Cette thèse se présente sous la forme d'un manuscrit de quatre papiers. La première étude s'agissait d'une étude transversale ayant mis en évidence des réductions du volume cérébral et une diminution des performances cognitives dans un groupe de patients VIH+ traités en comparaison avec un groupe contrôle aux mêmes caractéristiques démographiques. Nous en avions conclu que, malgré traitement efficace et bon contrôle virologique chez la majorité des patients VIH+, des réductions régionales spécifiques du volume cérébral et les troubles cognitifs étaient tout de même constatés. Toutefois, étant donné la nature transversale de l'étude, nous n'avions pas pu déterminer si ces changements survenaient avant traitement ou par une atteinte lésionnelle cérébrale progressive malgré le traitement. Dans la deuxième étude, nous avions pour objectif de comprendre si les patients VIH+ traités, avec charge virale indétectable, subissaient une atrophie cérébrale et un déclin cognitif progressifs sur une période de deux ans. De même que la première étude, nous avons observé que les patients VIH+ avaient un plus petit volume cérébral et de moins bonnes performances cognitives que les sujets du groupe contrôle. Cependant, les modifications de volume cérébral et des performances cognitives en fonction du temps étaient similaires entre les groupes. Ces résultats sont donc en défaveur d'un processus lésionnel chronique comme cause des lésions cérébrales, et plaident au contraire pour l'hypothèse selon laquelle des modifications cérébrales et cognitives survenant avant la mise en place de la trithérapie antirétrovirale seraient responsables du handicap cognitif constaté chez les personnes infectées par le VIH. Toutefois,

cette hypothèse n'avait pu être vérifiée, car tous les patients VIH+ inclus dans les première deux études étaient infectés par le VIH depuis plusieurs années et étaient déjà sous traitement efficace. Cela nous avait donc conduit à réaliser l'étude, qui était une étude longitudinale ayant pour but de suivre l'évolution des modifications cérébrales survenant au début de l'infection, avant l'initiation du traitement, et l'impact de la trithérapie antirétrovirale sur ces modifications. Nous avons pu observer qu'une plus longue période sans traitement était corrélée avec une atrophie cérébrale et corticale plus sévères, tandis que l'initiation du traitement stoppait ces changements. Ces résultats confirment l'hypothèse selon laquelle des modifications cérébrales surviennent tôt dans l'infection par le VIH, avant la mise en place du traitement. L'étude finale nous avions ici voulu étudier l'impact clinique de la maladie des petits vaisseaux cérébraux chez les personnes vivant avec le VIH. Nous avons constaté que les sujets VIH+ n'avaient pas une maladie des petits vaisseaux cérébraux plus sévère que les sujets contrôles. Toutefois, une maladie des petits vaisseaux cérébraux sévère impactait négativement le volume cérébral et les fonctions cognitives. Ces résultats suggèrent que les troubles neurocognitifs observés chez les patients infectés par le VIH pourraient en partie dépendre des effets de la maladie des petits vaisseaux cérébraux, en plus des dommages causés par le virus avant initiation du traitement.

En conclusion, les résultats rapportés dans cette thèse fournissent un récit unique en ce qui concerne le développement de troubles cognitifs liés au VIH à l'ère de la trithérapie antirétrovirale. Les résultats soutiennent que le développement de changements neurobiologiques précoces entraîne des déficits cognitifs en aval, alors que la maladie cérébrale des petits vaisseaux cérébraux qui en découle peut contribuer de manière indépendante à des modifications du cerveau conduisant à des problèmes cognitifs supplémentaires. La combinaison de ces processus indépendants a probablement un effet néfaste cumulatif sur la structure cérébrale et la fonction cognitive, ce qui entraîne une légère déficience cognitive qui semble être fréquente chez les personnes âgées atteintes d'une infection à VIH de longue date et bien contrôlée. Ces résultats mettent en lumière l'importance d'une bonne adhésion thérapeutique, du contrôle de la charge virale du contrôle des facteurs de risque cardiovasculaire pour prévenir l'aggravation des lésions cérébrales et le déclin cognitif.

## Acknowledgements

The completion of this dissertation could not be possible without the guidance, insight and encouragement from several wise people. First and foremost, I would like to thank my supervisor Dr. Louis Collins for his mentorship and outstanding support throughout my graduate studies. He has gone above and beyond the call of duty to ensure that I was not only able to complete my Ph.D., but also make it an enjoyable journey.

I would also like to thank Dr. Beau M. Ances and Dr. Lesley K. Fellows. Their vast knowledge in the field of neurology was extremely beneficial. Without their guidance and advice, my manuscripts would have minimal clinical impact and I would not have been able to adequately address all the scientific objectives that I proposed.

Further thanks must go to the various neurologists and scientists that used their expertise to enhance my dissertation. Specifically, I thank Dr. Mahsa Dadar, Dr. Josefina Maranzano, Dr. Susan Scott, Dr. Nancy E. Mayo, Dr. Richard W. Price, Dr. Dieter Meyerhoff, Dr. Henrik Zetterberg and Dr. Dietmar Fuchs. I would like to extend a special thanks to Dr. Serena Spudich for graciously providing me with all the data to complete the study in Chapter 5 and providing outstanding guidance regarding the neuropathogenesis of HIV in early infection.

Lastly, many thanks to the Natural Sciences and Engineering Research Council of Canada and McGill University for funding my doctoral studies.

## Table of Contents

## List of Figures

## List of Tables

## Chapter 1: Introduction

In July 1981, the words "HIV" and "AIDS" were unknown, but doctors in the United States already had their first look at the mysterious disease as forty-one homosexual men, one by one, were diagnosed with a rare and rapidly fatal form of cancer, known as Karposi's sarcoma. This diagnosis perplexed physicians as Karposi's sarcoma primarily affects individuals over the age of 50, while the individuals who were dying at the time had a mean age of 39[1]. These individuals also had severe defects to their immune system, leaving them vulnerable to other rare cancers and infections. Unbeknownst to the world, this would mark the beginning of the HIV/AIDS epidemic.

By 1982, a cumulative total of 270 individuals had reported with severe immune deficiency, 121 of whom had died from various cancers and infection[2]. To define those that exhibited this particular defect in their immune system, the Centers for Disease Control and Prevention introduced the term *acquired immune deficiency syndrome* (AIDS). However, the cause of AIDS was still completely unknown. It was not until 1984 that three research groups independently recovered a unique retrovirus – a single-stranded ribonucleic acid (RNA) virus that targets host cells – from several individuals with AIDS. All three research groups reported that the retrovirus had the ability to attack the human immune system and cause severe immune dysfunction[3]. In 1986, this retrovirus was determined to be the cause of AIDS and is now known as the human immunodeficiency virus (HIV)[3].

Since the discovery of HIV, extraordinary scientific efforts have advanced the understanding of the disease. Presently, HIV infection is characterized as a disease that results in the progressive failure of the immune system allowing life-threatening opportunistic infections and cancers, such as Karposi's sarcoma, to thrive, while late and more severe symptoms caused by the virus are referred to as AIDS[3]. The virus cripples the immune system by infecting, attacking and destroying CD4 T-cells, macrophages and microglia; cells vital for immune function[3]. Without treatment, the average survival time after initial infection was 8 to 10 years[4].

While there is currently no cure for HIV, a multi-drug regimen known as combination anti-retroviral therapy (cART) was introduced in 1996 as a means to control viral replication. This treatment regimen has been a resounding success in treating HIV as it slows the progression of the disease, reduces viral loads to undetectable levels and significantly improves immune function[4]. The advent of cART has reduced HIV-related morbidity and mortality, transforming HIV from a

fatal disease to a chronic manageable condition, allowing people living with HIV to have near normal life expectancies[5].

HIV also negatively impacts the central nervous system (CNS) producing a range of cognitive and motor symptoms, including impaired short-term memory, and reduced concentration and motor coordination, that are collectively referred to as HIV-associated neurocognitive disorders (HAND)[6]. These symptoms often occur together with behavioural changes, such as changes to personality and apathy, and social withdrawal, while more severe forms of HAND lead to a nearly vegetative and mute state[6].

Although the introduction of cART has resulted in a significant decline in severe forms of HAND, mild to moderate forms still remain prevalent, affecting up to 56% of people living with HIV, despite cART, good immune function and undetectable viral loads[7]. The etiology of this mild, but quality of life limiting cognitive impairment remains elusive with several proposed mechanisms, including: permanent and irreversible brain injury prior to treatment initiation, ongoing brain injury despite effective viral control, and cerebral small vessel disease (CSVD)[8]. Given that cART has allowed people living with HIV to approach near normal life expectancies, HAND may become a severe problem in the future. A clearer understanding of the mechanisms that may cause HAND is therefore critical.

Thus, the overall aim of this dissertation was to fully characterize the existence and extent of brain injury and cognitive deficit in people living with HIV using magnetic resonance imaging (MRI) and comprehensive neuropsychological assessments. The series of investigations reported reveals clues into the potential mechanisms underlying HAND in the era of effective HIV treatment, opening the door for novel treatment strategies that can focus on improving brain health and cognitive function.

## 1.1. Scientific Objectives

The scientific objectives of this dissertation were twofold. The first scientific objective was to investigate the underlying neuromechanisms of HAND. The specific aims were to:

1) Cross-sectionally examine a cohort of HIV+ individuals to assess the existence of cognitive deficits and the spatial extent of brain injury compared to a demographically similar control group.

2) Longitudinally monitor brain structure and cognitive function over time in a group of well-treated HIV+ individuals and demographically similar controls to determine whether greater-than-age related brain atrophy and cognitive decline occur in people living with HIV.

3) Longitudinally map brain structure and cognitive function over time in a group of newly infected HIV+ individuals, before and after treatment initiation, to assess the effect HIV has on the brain soon after initial infection, and the impact treatment has on these changes.

Recent evidence has suggested that HIV may alter the risk of developing CSVD. Given that CSVD is one of the most common causes of to vascular cognitive impairment in general populations[9], some components of HAND may be driven by CSVD[10]. The second scientific objective explores the association of CSVD with brain structure and cognitive function, and its interaction with HIV. The specific aims were to:

1) Examine whether HIV+ individuals had more severe CSVD compared to demographically similar controls.

2) Evaluate the relationship between CSVD and standard clinical markers of HIV infection severity in the HIV+ group.

3) Assess the magnitude to which HIV infection and CSVD severity contribute to changes in brain structure and cognitive function.

4) Provide evidence of the longitudinal evolution of CSVD, to assess whether HIV is associated with greater rate of change in CSVD.

This is a manuscript-based dissertation, organized into eight chapters. Chapter 2 provides the background and an in-depth literature review into the relevant literature of HIV, MRI acquisition and processing, neuropsychological evaluation and statistical analysis. Chapter 7 delivers a comprehensive scholarly discussion on all the findings reported in the dissertation, while Chapter 8 summarizes the clinical implications of the dissertation and outlines future work that is warranted to further expand our understanding of HAND. Chapters 3-6 take the form of manuscripts that were either published or submitted for publication. They are summarized as followed:

**Chapter 3: Regionally Specific Brain Volumetric and Cortical Thickness Changes in HIV-Infected Patients in the cART Era.**

While several studies have examined the brain in people living with HIV, the effects that HIV has on the brain and cognition were unclear in well-treated individuals with good viral suppression. The study in Chapter 3 was a cross-sectional study that reported brain volume reductions and poorer cognitive function in a group of treated HIV+ participants compared to demographically similar controls. We concluded that despite the majority of HIV+ participants being on cART with good viral control, regionally specific brain volume reductions and cognitive difficulties remained prevalent.

**Chapter 4: Association of Brain Structure Changes and Cognitive Function with Combination Antiretroviral Therapy in HIV-Positive Individuals.**

Although we observed brain volume reductions and poorer cognitive function in a group of treated HIV+ participants, we could not elucidate the extent to which these observations reflect changes before cART or ongoing brain injury, despite cART. In this longitudinal study, we sought to determine whether treated HIV+ individuals with undetectable viral loads experienced progressive brain atrophy and cognitive decline over a two-year period compared to demographically similar controls. Similar to Chapter 3, we observed that the HIV+ group had smaller brain volumes and poorer cognitive function compared to the controls at all visits. However, the changes in brain volumes and cognitive function over time were similar between the groups. These results argue against an active, destructive process as the cause of the brain injury and, instead, supports the hypothesis that brain and cognitive changes occurring prior to cART initiation may be responsible for the cognitive impairment commonly found in people living with HIV. More importantly, these findings highlight the importance of adhering to cART and maintaining good viral control to prevent ongoing brain injury and cognitive decline.

**Chapter 5: Longitudinal Trajectories of Brain Volume and Cortical Thickness in Treated and Untreated Primary HIV Infection.**

The studies in Chapters 3 and 4 alluded to the possibility that irrecoverable brain changes that occur before starting cART may cause subsequent HAND. However, this hypothesis could not be verified as all the HIV+ participants included in the previous work had chronic HIV infection (>1 year after exposure). This led to the study in Chapter 5, which was a longitudinal study that aimed to map the natural course of structural brain changes occurring in early infection, prior to cART initiation, and the impact cART has on these changes. We observed that longer duration of untreated infection was correlated with greater brain atrophy and cortical thinning, while initiating

treatment halted these changes. These findings verified the hypothesis that brain changes occur early in HIV infection before cART initiation and worsen with the absence of treatment. This emphasizes the importance of starting cART early to mitigate the extent of the brain injury and cognitive deficits.

**Chapter 6: Association of Cerebral Small Vessel Disease with Brain Structure and Cognitive Function in HIV+ Individuals.**

Recent evidence has suggested that HIV alters the risk of developing cerebral small vessel disease, which is the most common cause of vascular cognitive impairment in the general population. This means that cerebral small vessel disease could be a key contributor of HAND. Despite the growing body of literature, it is not yet clear whether cerebral small vessel disease is more common in people living with HIV and, more importantly, the synergistic effects between cerebral small vessel disease and HIV on the brain and cognition in people living with HIV are not well-characterized. We observed that HIV+ participants did not have more severe cerebral small vessel disease compared to controls. However, worse cerebral small vessel disease was associated with reduced brain volumes and poorer cognitive function in all participants, regardless of HIV serostatus. These results suggest that HAND in the cART era may be a mix of injury caused by the virus before treatment initiation and subsequent cerebral small vessel disease. These findings argue that optimizing vascular health in people living with HIV, who are on stable cART and virologically suppressed, may be a useful route to improve brain health and protect against decline.

## 1.2. Contribution to Original Knowledge

Through a series of investigations presented in this dissertation, we have made several original contributions to the knowledge of brain atrophy and cognitive impairment in people living with HIV in the cART era, including:

1) Establishing the existence and spatial extent of brain injury in treated HIV+ individuals with good viral suppression.

2) Reporting that distinct neuromechanisms may underlie the injury found in the subcortical and cortical regions.

3) Showing that there is no ongoing brain atrophy and cognitive decline in treated HIV+ individuals with excellent viral control.

4) Emphasizing the importance of adhering to HIV treatment and maintaining undetectable viral loads to prevent ongoing brain injury and cognitive decline.

5) Demonstrating that brain injury occurs soon after initial exposure to the virus before starting treatment.

6) Reporting that brain injury worsens with the continued absence of treatment.

7) Highlighting the importance of starting HIV treatment early to mitigate brain injury and cognitive decline.

8) Reporting that brain changes occurring early in HIV infection leads to downstream cognitive difficulties.

9) Demonstrating that cerebral small vessel disease is not more common in people living with HIV compared to controls.

10) Showing that worse cerebral small vessel disease is associated with smaller brain volumes and cortical thickness and worse cognitive function.

11) Stressing the importance of improving vascular health to prevent the development of cerebral small vessel disease.

12) Reporting that HIV-associated cognitive impairment in the cART era may be a mixture of injury caused by early HIV infection and subsequent cerebral small vessel disease.

## 1.3. Contribution of Authors

I am the first author on the four manuscripts included in this dissertation. I was responsible for the design and conceptualization, data analysis, including processing MRI data, quality control, statistical analyses and interpretation of the results, and drafting and revising the manuscripts in all studies. The contributions of the co-authors included supervision of the studies, data collection, data processing, data analysis, interpreting the results and revising the manuscripts. The following list summarizes the contributions of the co-authors organized by manuscript:

**Chapter 3: Chapter 3: Regionally specific brain volumetric and cortical thickness changes in HIV-infected Patients in the cART era.**

Authors: Ryan Sanford, Ana Lucia Fernandez Cruz, Susan C. Scott, Nancy E. Mayo, Lesley K. Fellows, Beau M. Ances and D. Louis Collins

Study design and conceptualization: Ryan Sanford, Beau M. Ances and D. Louis Collins.
Data processing and analysis: Ryan Sanford, Ana Lucia Fernandez Cruz, Susan C. Scott, Nancy E. Mayo and D. Louis Collins.
Interpreting results: Ryan Sanford, Lesley K. Fellows, Beau M. Ances and D. Louis Collins.
Manuscript preparation and revision: Ryan Sanford, Lesley K. Fellows, Beau M. Ances and D. Louis Collins.

**Chapter 4: Association of Brain Structure Changes and Cognitive Function with Combination Antiretroviral Therapy in HIV-Positive Individuals.**

Authors: Ryan Sanford, Lesley K. Fellows, Beau M. Ances and D. Louis Collins

Study design and conceptualization: Ryan Sanford, Beau M. Ances and D. Louis Collins.
Data processing and analysis: Ryan Sanford and D. Louis Collins.
Interpreting results: Ryan Sanford, Lesley K. Fellows, Beau M. Ances and D. Louis Collins.
Manuscript preparation and revision: Ryan Sanford, Lesley K. Fellows, Beau M. Ances and D. Louis Collins.

**Chapter 5: Longitudinal Trajectories of Brain Volume and Cortical Thickness in Treated and Untreated Primary HIV Infection.**

Authors: Ryan Sanford, Beau M. Ances, Dieter J. Meyerhoff, Richard W. Price, Dietmar Fuchs, Henrik Zetterberg, Serena Spudich and D. Louis Collins

Study design and conceptualization: Ryan Sanford, Beau M. Ances and Serena Spudich.
Data processing and analysis: Ryan Sanford, Dietmar Fuchs, Henrik Zetterberg, Dietmar Fuchs and D. Louis Collins.
Interpreting results: Ryan Sanford, Beau M. Ances, Serena Spudich and D. Louis Collins.
Manuscript preparation and revision: Ryan Sanford, Beau M. Ances, Dieter J. Meyerhoff, Richard W. Price, Serena Spudich and D. Louis Collins.

**Chapter 6: Association of Cerebral Small Vessel Disease with Brain Structure and Cognitive Function in HIV+ Individuals.**

Authors: Ryan Sanford, Jeremy Strain, Mahsa Dadar, Josefina Maranzano, Susan C. Scott, Nancy E. Mayo, Lesley K. Fellows, Beau M. Ances and D. Louis Collins

Study design and conceptualization: Ryan Sanford, Beau M. Ances and D. Louis Collins.
Data processing and analysis: Ryan Sanford, Jeremy Strain, Mahsa Dadar, Josefina Maranzano, Susan C. Scott, Nancy E. Mayo and D. Louis Collins.
Interpreting results: Ryan Sanford, Mahsa Dadar, Lesley K. Fellows, Beau M. Ances and D. Louis Collins.
Manuscript preparation and revision: Ryan Sanford, Lesley K. Fellows, Beau M. Ances and D. Louis Collins.

# Chapter 2: Background and Literature Review

Chapter 2 provides the background information for the manuscripts presented in the dissertation. It comprises of a comprehensive set literature reviews that covers a range of topics, including HIV neuropathogenesis, MRI signal acquisition and processing, neuropsychological evaluations and statistical testing.

## 2.1. Human Immunodeficiency Virus

### 2.1.1. The Discovery of the Cause of AIDS

Scientific research rarely follows a straight path. Generally, it is filled with many unexcepted meanderings, with a mix of good and bad ideas as well as good and bad luck[11]. The discovery of HIV as the cause of AIDS was no exception. The search for the cause began in 1981 focusing on retroviruses as they were previously known to affect the human immune system, which is the hallmark AIDS consequence[3]. The first breakthrough came in 1983 by Barre-Sinoussi *et al.,* who recovered a retrovirus from an AIDS individual with persistent lymphadenopathy syndrome; a disease later discovered to be commonly associated with AIDS[3,12]. It was reported that this virus had similar properties to the human T-cell leukemia virus (HTLV); a previously discovered retrovirus that targets CD4 T-cells, an important component of the immune system, and causes a form of cancer known as T-cell lymphoma[13]. This conclusion was supported by Gallo *et al.,* who also isolated an HTLV-like virus from multiple AIDS-infected individuals[14]. The infection caused by the HTVL-like virus produced symptoms that were consistent with the AIDS symptoms that were known at the time, since it could be transmitted through the blood and specifically targeted CD4 T-cells[11]. This led many to conclude that the virus causing AIDS had to be some derivative of HTLV. However, an HTLV-like virus could not explain the characteristic loss of CD4 T-cells in individuals with AIDS since it does not kill T-cells, instead, it often immortalizes them into continuous growth[3]. Further investigations confirmed that this mysterious HTLV-like virus specifically infects and kills CD4 T-cells, a property that distinguishes it from HTLV[3,15]. This led researchers to name the virus lymphadenopathy-associated virus (LAV) since it was only extracted from subjects with persistent lymphadenopathy syndrome. This was the first major breakthrough in the search for the AIDS causing virus[3,15].

In early 1984, several other laboratories were simultaneously searching for the AIDS causing virus. Gallo *et al.* isolated another HTLV-like virus, later named HTLV-III, from peripheral blood mononuclear cells (PBMC) of adult and pediatric AIDS individuals, but without

persistent lymphadenopathy syndrome[16]. The investigators reported that HTLV-III infected CD4 T-cells and induced cell death, exactly like LAV. Levy *et al.* also extracted a retrovirus from individuals with and without AIDS-related symptoms. They named their virus the AIDS-associated retrovirus (ARV)[17]. ARV had similar properties as the previously isolated retroviruses, LAV and HTLV-III, where it grew substantially in PBMC and killed CD4 T-cells. Since ARV was found in individuals that did not exhibit AIDS-related symptoms or persistent lymphadenopathy syndrome, it suggested that the spread of the AIDS causing virus could be larger than initially expected[3].

By 1986, it was confirmed that the three prototype retroviruses discovered (LAV, HTLV-III and ARV) were in fact the same virus and the most likely cause of AIDS. This lead the International Committee on Taxonomy to recommend giving this AIDS causing virus a separate name, the human immunodeficiency virus (HIV)[18]. Subsequently, HIV was recovered from a variety of individuals with AIDS, AIDS-related diseases, neurologic syndromes, as well as several clinically healthy individuals. While this discovery, unfortunately, demonstrated the widespread impact HIV already had on the world, it finally gave researchers the opportunity to focus their attention on halting this menacing disease.

### 2.1.2. Structure of HIV

Following the discovery of HIV, the structure was thoroughly investigated using electron microscopy[3]. Unlike other retroviruses, HIV is roughly spherical in shape with a diameter of ~100 nm (Figure 2.1). Inside the virion, there is a cone-shaped core, known as the capsid, that encapsulates two copies of viral RNA along with various viral enzymes, including reverse transcriptase and integrase; components that are vital for viral replication[3]. Surrounding the capsid is the viral envelope composed of a lipid bilayer as well as a surface protein, glycoprotein (gp) 120, and a transmembrane protein, gp41. Together, these proteins form a glycoprotein complex, where three molecules of gp41 are anchored to the viral envelope forming a *stem*, which is then fused with three molecules of gp120 to form a *cap*. This glycoprotein complex is embedded throughout the viral envelope and is essential for targeting and infecting CD4 T-cells[3].

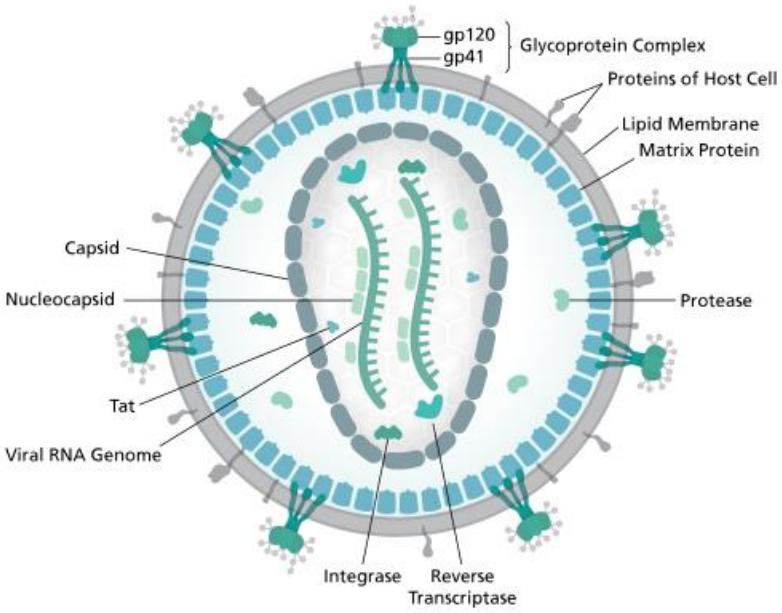


Figure 2.1: The structure of an HIV virion. (Image adapted from Thomas Splettstoesser (www.scistyle.com) [CC BY-SA 4.0 (https://creativecommons.org/licenses/by-sa/4.0)]).

### 2.1.3. HIV Replication Cycle

The main target of HIV is CD4 T-cells, also known as CD4 T-lymphocyte, which is a type of white blood cell that regulates the immune response to fight foreign pathogens. They are called CD4 T-cells because they express T-cell receptors and CD4 (cluster of differentiation 4) glycoproteins on their cell surface. The T-cell receptors enable the cell to recognize foreign antigens, while the CD4 glycoproteins communicate with other immune cells to initiate an immune response, if necessary. In addition, the surface of CD4 T-cells consists of multiple chemokine receptors, such as C-C chemokine receptor type 5 (CCR5) or C-X-C chemokine receptor type 4 (CXCR4), that bind to various signalling proteins to guide the CD4 T-cell to areas with potential foreign pathogens. Together, these surface components make the CD4 T-cell a vital asset for the immune system. If these cells were depleted, the immune system would fail to recognize and prevent the invasion and growth of foreign pathogens, allowing opportunistic infections, such as persistent lymphadenopathy syndrome, and cancers, such as Karposi's sarcoma, to thrive.

The entry of HIV into CD4 T-cells is through interactions between the glycoprotein complex and the CD4 and chemokine receptors (CCR5 or CXCR4)[19]. Other immune cells in the human body that have CD4 and chemokine receptors could also be infected by HIV, including macrophages and microglia in the CNS[19]. Initially, there is an interaction between gp120 and the CD4 receptor that initiates a conformational change to the glycoprotein complex. This enables

further interaction between the gp120 and a chemokine receptor, either CCR5 or CXCR4[3,20]. The gp120-chemokine interaction causes the distal tips of gp41 to be exposed, which pierces the host cell's membrane. The gp41 begins to undergo significant conformational change forming a hairpin-like structure that pulls the virus and host cell closer together mediating the fusion between the cells, allowing the viral capsid to be injected into the host cell[3,20].

Once inside the cell, the viral capsid is uncoated and releases the viral RNA and viral enzymes, most notably reverse transcriptase and integrase, into the cytoplasm[20]. The reverse transcriptase will reverse transcribe the viral RNA into double-stranded deoxyribonucleic acid (DNA). Since this process has an extremely high mutation rate (~1 error per 10,000 nucleotides), the virus can rapidly adapt to its host environment[21]. After reverse transcription, the viral DNA is actively transported to the host cell's nucleus using microtubule-based transport, where the viral enzyme integrase integrates the viral DNA into the host cell's chromosome[20]. At this point, the host cell is infected for the remainder of its life span[21].

Generally, the integrated viral DNA stays dormant and does not actively produce new viruses for an extended period of time. Viral transcription is activated when certain cellular transcription factors, such as NF-κβ, are present. Ironically, the role of NF-κβ is to regulate the immune function, where upregulation of NF-κβ activates the CD4 T-cells, meaning that the cells that are fighting the virus are also producing the most virus and are subsequently killed[21]. When viral transcription begins, the viral DNA integrated into the host cell's chromosome serves as a template for the mRNA to produce viral proteins and genomic RNA to be included in a newly-produced virion, exactly like the DNA central dogma[21]. Initially, viral transcription is slow and inefficient because the viral transactivator protein (Tat) and Rev, viral proteins required for effective transcription and transportation to the cytoplasm, respectively, are initially absent. However, when a mature viral mRNA is finally transcribed and exported to the cytoplasm, it is translated to produce Tat and Rev. This results in efficient synthesis and transportation of full-length mRNA and genomic viral RNA into the cytoplasm. The mRNA will also be translated to produce other viral proteins, such as Gag and Env, which are vital for packaging two genomic RNA into new virion particles[21].

The final stage of the viral replication cycle is the assembly and release of the virions from the infected host cell. The viral protein Env will pass through the endoplasmic reticulum and the Golgi complex to produce the viral envelope proteins, gp120 and gp41[21]. These are transported

to the host cell's plasma membrane, where gp41 anchors gp120 forming the glycoprotein complex. Simultaneously, the two genomic viral RNA and viral proteins accumulate near the plasma membrane. A newly-formed virion begins to form and buds off from the host cell[21]. However, the released HIV virion is in an immature and non-infectious state. Shortly after budding, the virion must undergo a maturation process that includes the formation of the capsid to surround the RNA. It is only after this maturation process in which a new HIV virion is activated and can infect new cells[21]. Figure 2.2 shows a simplified illustration of the entire replication.

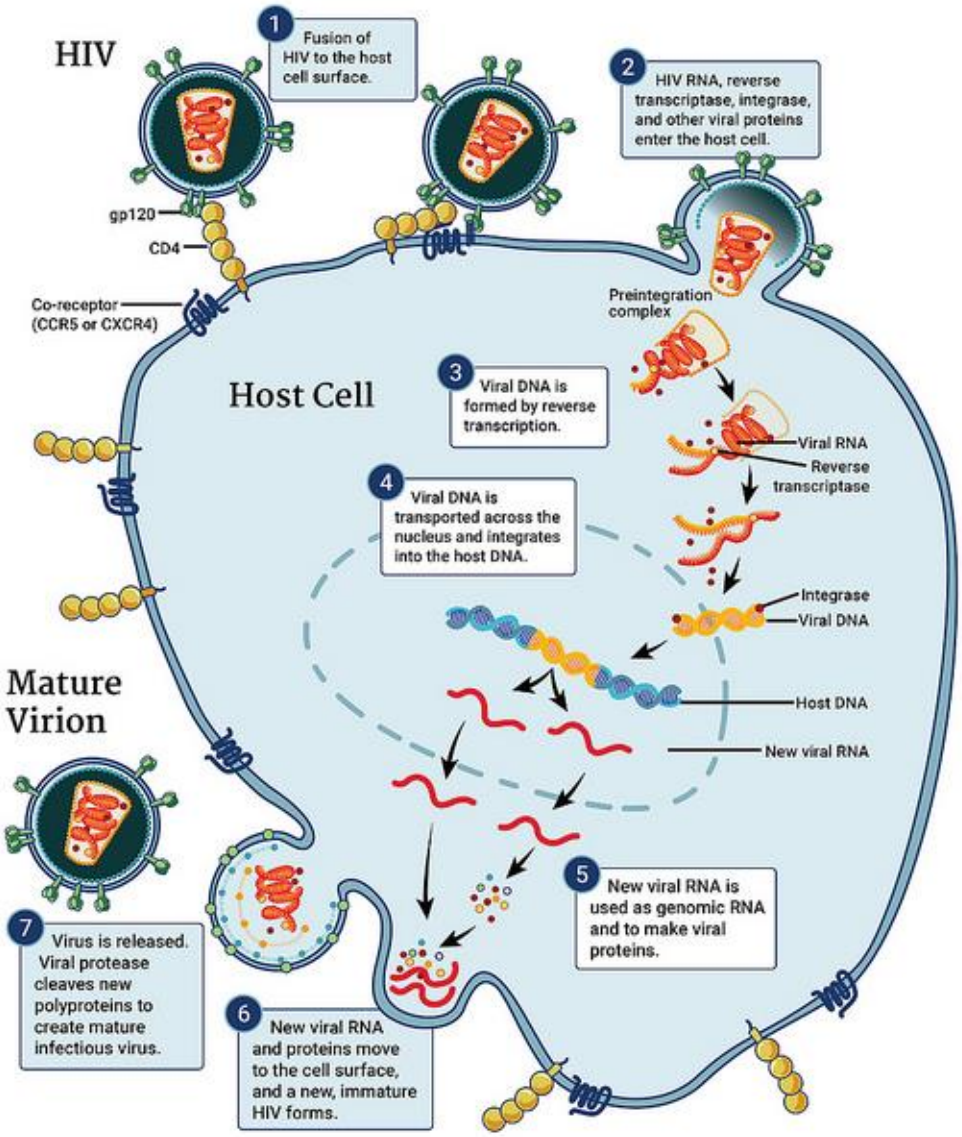


Figure 2.2: Brief overview of the HIV replication cycle. (Image taken from www.niaid.nih.gov/diseases-conditions/hiv-replication-cycle [CC BY-SA 4.0 (https://creativecommons.org/licenses/by-sa/4.0)]).

### 2.1.4. HIV Pathogenesis and Immune Dysfunction

The hallmark trait of HIV infection is the progressive depletion of CD4 T-cells leading to severe immune deficiency. CD4 T-cells can be eliminated directly through infection of the cell and indirectly from neighbouring infected cells, known as the bystander effect[22]. Cell death through direct mechanisms involve cells that are infected and actively producing viral proteins, such as gp120, Tat and Env[23]. Several *in vitro* experiments have shown that these viral proteins induce a cascade of cellular events that lead to mitochondrial dysfunction followed by apoptosis[23]. In addition, active production of new HIV virions can induce cell lysis by compromising the integrity of the plasma membrane through continuous budding of new HIV virions that reduce membrane integrity[23].

While it was evident that direct mechanisms contributed to the progressive elimination of CD4 T-cells, direct killing could not explain the massive CD4 T-cell loss commonly found in those with severe AIDS[22]. This led to the hypothesis that uninfected immune cells that surrounded infected cells (bystander cells) could also be killed by HIV[24]. The first evidence of this came from Finkel *et al.* who reported that the majority of cells undergoing apoptosis in the lymph nodes were not infected, but were in close proximity to infected cells[22,24]. While the mechanisms of bystander apoptosis are still not fully understood, it appears that the HIV envelope glycoprotein complex, comprised of gp120 and gp41, plays a critical role in the process[22]. Research has shown that gp120 and gp41 expressed on infected CD4 T-cell surfaces mediates fusion with nearby uninfected CD4 T-cells forming a giant multinucleated cell, or syncytia, that actively produce the virus before eventual death[6,23]. Partial fusion, or hemifusion, have also been reported to induce apoptosis in uninfected bystander cells[22,25]. In addition, studies have reported that inactivated HIV virions and viral proteins, such as Tat, released into extracellular spaces can induce cell death in nearby uninfected cells[23]. There is also evidence that suggests HIV suppresses the production of early precursors of CD4 T-cells, which could exacerbate the progressive loss of CD4 T-cells found in chronic infection as CD4 T-cells are not being replenished[3]. Taken together, the interplay of all these processes and mechanisms most likely contribute to the progressive elimination of CD4 T-cells, crippling the immune system leaving the body vulnerable to fatal infections and cancers.

### 2.1.5. Anti-Retroviral Therapy

The discovery of HIV and its replication cycle opened the door for researchers to develop novel treatment strategies focused on halting the virus. Zidovudine (AZT) was the first anti-retroviral treatment approved for HIV[26]. It is a nucleoside reverse transcriptase inhibitor (NRTI) that works by blocking nucleosides from being added to the coding strand, preventing the creation of viral DNA. Without the viral DNA, the HIV genome cannot be integrated into the host cell's genome eliminating the possibility of producing new HIV virions, and ultimately preventing toxic viral proteins from being produced and killing CD4 T-cells[26]. The use of AZT was immediately evaluated clinically and found to significantly improve CD4 T-cell counts and reduce viral loads. Furthermore, AZT was shown to slow the progression of the HIV infection, most likely prolonging life[27].

While hopes were high for AZT, the beneficial effects were of limited duration[28]. Given that the reverse transcriptase has a high mutation rate, HIV quickly became resistant to AZT[28]. To overcome this issue, additional NRTIs were developed and combined with AZT, known as dual therapy, which showed better outcomes compared to those on monotherapy (i.e. only AZT). Although the effects of the dual-NRTI combination were better than those on monotherapy, the effects were still of limited duration[28]. In 1996, a new class of anti-retroviral drug, protease inhibitor, namely indinavir, was introduced. This class of anti-retroviral drug works by selectively inhibiting viral proteins and enzymes, preventing the production and maturation of new HIV virions[29,30]. When indinavir was combined with the two NRTIs, the substantial beneficial effects of treatment became durable. This triple drug therapy, now known as combination anti-retroviral therapy (cART), was quickly incorporated into clinical practice and showed lasting benefits with an 80% decline in AIDS and death[31]. The resounding success of cART can be attributed to the combination of different anti-retroviral medications that selectively attacks a different part of the replication cycle. This reduces viral replication to minimal levels, increases CD4 T-cell counts to healthy levels, and the selective pressure that each anti-retroviral drug has on multiple viral genes reduces the likelihood that mutations will arise in the right combinations to render the virus resistant to all the drugs in a regimen[32].

With the advent of cART, HIV has been transformed from a fatal disease to a chronic manageable condition. This has dramatically changed the outlook for people living with HIV by allowing them to live to near normal life expectancy. As of 2018, a total of five anti-retroviral drug

classes exists (Table 2.1): NRTI, protease inhibitor, non-nucleoside transcriptase inhibitor, integrase inhibitor and fusion inhibitor. Typical cART regimens consist of two NRTIs along with one PI, non-nucleoside transcriptase inhibitor, integrase inhibitor or fusion inhibitor[33].

Table 2.1: Anti-retroviral drug classes and mechanism to prevent HIV replication.

| Anti-retroviral drug class | Mechanism to prevent HIV replication |
|---|---|
| Nucleoside reverse transcriptase inhibitor | Inhibits reverse transcription by preventing nucleosides from being incorporated into viral DNA chain[26]. |
| Non-nucleoside reverse transcriptase inhibitor | Inhibits reverse transcription by binding to the allosteric site of reverse transcriptase[34]. |
| Protease inhibitor | Blocks the viral proteases responsible for producing a mature virion after budding off the host cell[29,30]. |
| Integrase inhibitor | Inhibits the viral enzyme integrase preventing viral DNA from being integrated into the host cells genome[35]. |
| Fusion inhibitor | Prevents fusion and entry of HIV into the host cell by blocking the chemokine receptors, CCR5 and CXCR5, that are vital for viral entry[36]. |

## 2.2. Neuropathogenesis of HIV

Since the beginning of the HIV/AIDS epidemic, HIV-associated neurocognitive disorders (HAND) have been commonly observed in infected populations[37]. Similar to the pathogenesis in the periphery, neuronal injury can result from direct and indirect effects of the virus producing distinct neurological symptoms[32].

### 2.2.1. Invasion of the Brain by HIV

The CNS is separated from the rest of the body by the blood-brain barrier (BBB). The BBB is a selectively permeable continuous cellular layer consisting of brain microvascular endothelial cells that are linked together by tight junctions. This layer protects the brain by carefully regulating the cells that can access the CNS from the peripheral bloodstream[6].

Since HIV has been found in the CNS as early as eight days after initial infection[38], it is clear that HIV has found a way to overcome the tight junctions of the BBB (Figure 2.3). The method of invasion with the most compelling evidence is known as the trojan horse mechanism. Given that CD4 T-cells and some monocytes are the primary target of HIV and these cells can move across the BBB as part of normal immune surveillance, HIV is able to gain access to the CNS through infected immune cells[6]. Another means of HIV invasion is the possibility of the virus migrating between the tight junctions of the BBB[39]. Alternatively, HIV could access the CNS by moving across the endothelial cells through uptake on one side and release on the other side; a process known as transcytosis[6,39]. However, there is limited pathological evidence of HIV directly infecting endothelial cells and having the ability to pass through the tight junctions of the BBB making the latter two mechanisms unlikely to account for the virus invading the brain[6,39].

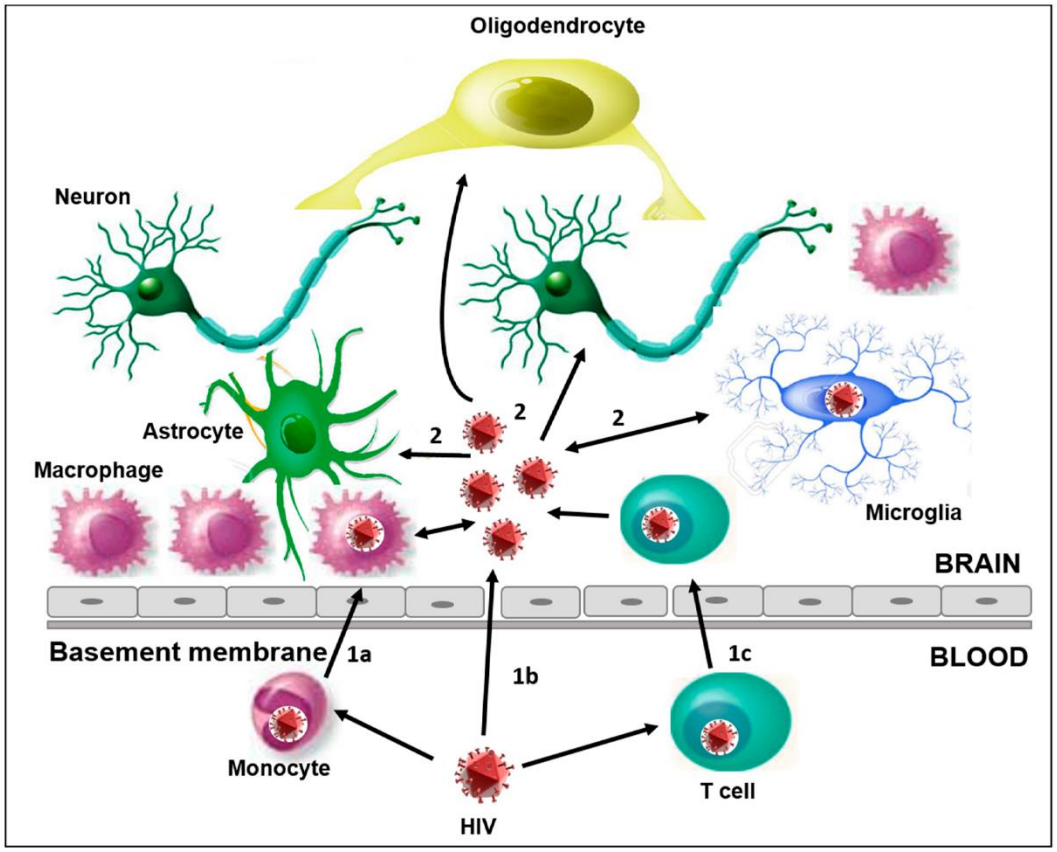


Figure 2.3: An illustration showing the possible mechanisms of HIV entry into the CNS as well as the cells in the brain that are affected by the virus. The trojan horse mechanism is shown in (1a) and (1c), where infected immune cells pass through the BBB, effectively bringing HIV into the CNS. There is also a possibility that HIV can pass through the tight junctions of the BBB (1b). (Image taken from "The Role of HIV Infection in Neurologic Injury" by Scutari et al., 2017[40]).

### 2.2.2. HIV Infection of Cells in the Brain

Once HIV passes through the BBB and is released into the CNS, HIV virions come into direct contact with cells in the brain (Figure 2.3). In particular, macrophages and microglia are the primary target of HIV as they have CD4 and CCR5 receptors making them ideal candidates to be infected and to become the main producer of new HIV virions in the CNS[6,39]. These cells constitute the resident immunocompetent cells of the brain and respond to all types of insults[6]. They play a key role in overall brain maintenance by scavenging for damaged neurons and destroying cellular debris and foreign substances[6].

Astrocytes, the most frequent cell type in the brain, are responsible for maintaining homeostasis in the CNS by regulating neurotransmitter levels, such as glutamate[6,39]. In addition, astrocytes help maintain the tight junctions of the BBB[6]. To some extent astrocytes appear to be infected by HIV, but are unlikely to actively produce new HIV virions[6]. The mechanisms of the viral entry into astrocytes remains unknown as they do not express detectable levels of cell-surface CD4 or the main HIV chemokine receptors required for viral entry[6,39].

Given that cognitive deficits are common in people living with HIV, it is not unreasonable to think that some neurons are infected by HIV. Indeed, there is significant evidence of neurodegeneration (i.e. death of neurons) and brain injury found in the brains of HIV-infected people[6]. However, there is no evidence that neurons are infected by HIV[6]. Similarly, oligodendrocytes, the lipid- and protein-rich membrane that enable fast axonal conduction, also do not appear to be infected by HIV[6]. Moreover, neurons and oligodendrocytes do not have CD4 nor chemokine receptors required for HIV access. This means that neurodegeneration in HIV is not caused through direct infection of the neurons, but through mechanisms related to macrophages, microglia and, to some extent, astrocytes.

### 2.2.3. Mechanisms of HIV-Related Neurodegeneration

Given that there is no evidence of neurons or oligodendrocytes being infected by HIV, other mechanisms must be involved to cause the neurodegeneration found in HIV-infected brains[6]. This led researchers to discover that infected macrophages and microglia, and possibly astrocytes, participate in HIV-related neurodegeneration. Similar to the mechanisms that cause immune dysfunction, neuronal injury can be caused by direct and indirect mechanisms (Figure 2.4)[6].

The HIV envelope protein gp120 has been shown in *in vitro* studies to directly contribute to neuronal death[6,39]. Through interactions with chemokine receptors at the cell-surface of neurons, gp120 can induce apoptosis. Neuronal death could also be induced through an interaction between gp120 and *N*-methyl-D-aspartate (NMDA) receptors, which increases intracellular $Ca^{2+}$ concentrations resulting in excitotoxic death[6,39]. Other viral proteins, such as Tat, Nef and Vpr, that are actively secreted by macrophages and microglia can be taken up by neurons[39]. They directly interact with ion channels on the neuronal surface to depolarize them causing an increase of $Ca^{2+}$ levels eventually leading to excitotoxic cell death[39].

Indirect mechanisms have also been implicated in the neurodegeneration process[6,39]. The presence of the virus in the brain results in the activation of both infected and uninfected immune cells, which amplifies neurotoxicity[6]. These activated immune cells synthesize quinolinic and arachidonic acids and nitric oxide, and increase production of cytokines, such as tumour-necrosis factor (TNF), all of which have neurotoxic effects on the brain[6]. Activated astrocytes increase the permeability of the BBB and promote the migration of more CD4 T-cells into the brain[6]. Furthermore, given that astrocytes regulate neurotransmitter levels, activated astrocytes will increase extracellular levels of glutamate while decreasing glutamate uptake causing excitotoxic death of neurons[6]. These neurodegeneration mechanisms most likely coexist, where the combination of direct and indirect effects causes significant brain injury, which disrupts cognitive function leading to HAND.

Although the mechanisms of neurodegeneration caused by HIV have been the primary focus in the literature, there is a growing body of evidence demonstrating that activated macrophages, microglia and astrocytes also have a neuroprotective effect[6,41,42]. These activated cells release β-chemokines and growth factors that promote $Ca^{2+}$ homeostasis in neurons, upregulate anti-apoptotic mechanisms and reduce gp120-mediated apoptosis, all of which promote neural survival[6,41,42]. Interestingly, while TNF has been shown to be neurotoxic to the brain, evidence has also suggested that TNF might also have a neuroprotective role by preventing accumulation of $Ca^{2+}$ inside neurons[43,44]. While these neuroprotective mechanisms may be helpful, it is obvious that they are not enough to protect the brain against clinically significant injury.

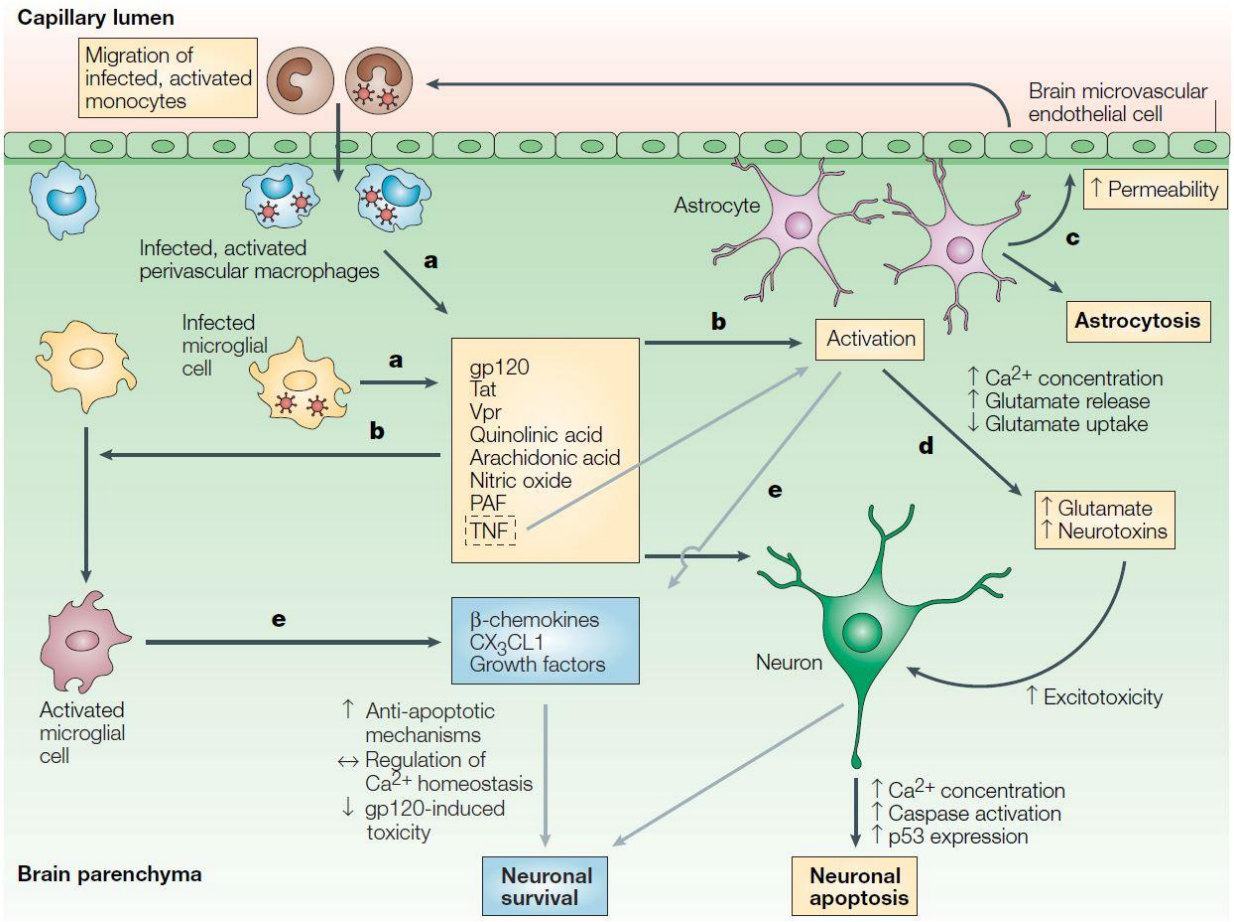


Figure 2.4: An illustration of the mechanisms of neurodegeneration caused by HIV, as well as neuroprotective pathways. (a) Infected and activated macrophages and microglia release neurotoxic factors into the CNS, such as gp120, quinolinic and arachidonic acid and TNF. (b) These factors activate astrocytes which (c) increases the permeability of the BBB and (d) manipulates the $Ca^{2+}$ and glutamate levels to cause excitotoxic cell death. (e) Activation of macrophages, microglia and astrocytes may also release factors that protects against cell death, promoting neuronal survival. (Image taken from "The Neuropathogenesis of AIDS" by Gonzàlez-Scarano and Martín-García[6]. Permission for reuse of figure granted by publishers.)

### 2.2.4. HIV-Associated Neurocognitive Disorders

According to the 2007 guidelines for HAND diagnosis[45], it is comprised of three distinct conditions (in order of increasing severity): asymptomatic neurocognitive impairment (ANI), mild neurocognitive disorder (MND) and HIV-associated dementia (HAD). These conditions are defined by performance on a battery of neuropsychological tests that cover at least five cognitive domains and by an assessment of activities of daily living[45]. The specific diagnostic criteria are listed in Table 2.2.

In HIV+ individuals with ANI or MND, a general neurological examination is often normal with the exception of mild difficulties in concentration and attention[32]. Affected individuals may have difficulties performing activities of daily living, such as grocery shopping, preparing meals

and everyday chores, as they tend to lose their train of thought for sequential mental and motor tasks[32]. Motor symptoms are often mild consisting of slowing of repetitive movements and balance problems[32]. The symptoms of HAND can often be distinguished from other dementias, such as Alzheimer's disease, because there is usually the absence of apraxia, agnosia and aphasia[32].

In HIV+ individuals with HAD, cognitive and motor dysfunctions are more distinct. Affected patients have severe impairment in activities of daily living such that everyday tasks can not be adequately completed. Motor abnormalities consists of slowed fine rapid movements, unsteady gait and loss of balance[32]. These symptoms often occur together with behavioural changes, such as personality changes and social withdrawal[6].

Table 2.2: Diagnostic criteria for HAND.

| **HAND Category** | **Criteria** |
|---|---|
| Asymptomatic Neurocognitive Impairment | • Defined by performance at least 1 standard deviation (SD) below the mean of demographically adjusted normative scores in at least two cognitive areas.<br>• No reported impairment of daily activities.<br>• Impairment not fully explained by comorbid conditions. |
| Mild Neurocognitive Disorder | • Defined by performance at least 1 SD below the mean of demographically adjusted normative scores in at least two cognitive areas.<br>• Self-reported impairment of daily activities.<br>• Impairment not fully explained by comorbid conditions. |
| HIV-Associated Dementia | • Defined by performance at least 2 SD below the mean of demographically |

| | |
|---|---|
| | adjusted normative scores in at least two cognitive areas.<br>• Marked difficulty in daily activities.<br>• Impairment not fully explained by comorbid conditions. |

## 2.3. Persistence of HAND in the cART Era

Since the introduction of cART, the prevalence of HAD has dropped significantly from 16% to 2% in people living with HIV[46]. However, milder forms of HAND (ANI and MND) remain frequent, affecting up to 56% of the HIV+ population, despite cART; a rate similar to that of the pre-cART era[8,47]. Likewise, MRI studies continue to report clinically significant brain volume loss across several brain regions, including the caudate[5,48-50], thalamus[49-51], globus pallidus[51], putamen[48,50,51], amygdala[5], hippocampus[50] and corpus callosum[5,51,52], in treated HIV+ individuals. This demonstrates that even with the introduction of cART the brain still appears to be negatively impacted by the presence of HIV.

Despite the growing body of literature, the reasons for the persistence of HAND remain elusive with several proposed mechanisms including: irreversible brain injury that occurs before starting cART; ongoing brain atrophy, despite cART; the presence of confounding comorbid conditions; and cerebral small vessel disease. Given that HAND is associated with poorer quality of life, poorer, clinical outcomes and higher mortality, it is imperative to elucidate the causes of HAND such that novel treatments focused on preventing and remediating the brain injury and cognitive deficits can be developed.

### 2.3.1. Brain Injury Before cART

There have been suggestions that irrecoverable brain injury occurring soon after initial infection, before starting treatment, may be responsible for the subsequent cognitive impairment that is common in people living with HIV[8,53]. The virus penetrates the CNS as early as eight days after initial systemic viral infection, infecting and activating local CNS immune cells[6,38]. These cells begin to release viral proteins and produce inflammatory factors resulting in prominent inflammation[38,54,55], immune activation[56-58], and BBB disruption[59], all of which facilitate neuronal injury and brain volume reductions[6,53,60,61]. If the infection remains

untreated, markers of immune status, inflammation and BBB permeability progressively worsen[54,57,59], possibly causing permanent and irreversible brain injury resulting in downstream cognitive impairment. This hypothesis has also received support from studies investigating chronic HIV+ individuals (defined as >1 year after exposure). These studies report that those who had more severe immunosuppression in early HIV infection, as indexed by the nadir CD4 T-cell count, had smaller brain volumes and poorer cognitive function[7,62-64]. However, several studies have refuted this explanation as HAND still appears to be frequent even in those with long standing aviremia from stable treatment[8,49,65].

**2.3.2. Ongoing Brain Injury**

Given that mild forms of HAND remain common despite cART, it is not unfathomable to think that there is an active, destructive process that causes progressive brain injury. Multiple longitudinal studies have provided evidence that supports this theory by reporting greater rates of brain atrophy in cortical and subcortical regions and greater rates of cognitive decline in HIV+ individuals compared to controls, despite the majority of participants being on treatment[49,66-69]. Ongoing brain injury may be a possibility as there have been reports that there are inadequate levels of cART in the CNS, leading to persistent viral replication and active inflammation. Even in those with effective viral control in the periphery may experience persistent CNS viral replication. For cART to be effective in the brain, it must be able to pass through the BBB a characteristic that depends on the anti-retroviral's chemical properties. This can be quantified using the CNS penetration effectiveness (CPE) score, where regimens with higher CPE scores have better CNS penetrance[70]. Several studies have shown that better penetrating cART regimens were associated with more suppressed CSF viral levels and improved neurocognitive outcomes[8,70,71]. Taken together, this suggests that the continued presence of HAND may reflect inadequate levels of cART in the CNS resulting in progressive brain injury and ultimately cognitive decline[8].

In contrast, there has been data suggesting that neurotoxicity brought on by certain anti-retrovirals may be the cause of the ongoing brain injury[72]. Several animal and *in vitro* studies have reported that older NRTIs, particularly AZT, were associated with increased mitochondrial dysfunction in the peripheral nerves[72]. While it is unknown if this effect is present in the human brain, indirect evidence from an MRI study reported that longer duration on cART was correlated with lower white matter and increased CSF volumes, even after adjusting for age and duration of

HIV infection[73]. Moreover, a longitudinal study investigating the cognitive function in HIV+ participants who voluntarily stopped cART, unexpectedly, found that cognitive performance improved following treatment discontinuation[74]. While these studies point to possible cART neurotoxicity, data describing its role in the neuropathogenesis of HAND remains sparse and warrants further investigations.

Although several studies have provided evidence for ongoing brain injury to be the reason that HAND remains common, other work has provided evidence that argues against this hypothesis. For instance, large multi-center studies have reported that only small subsets of HIV+ individuals actually experience deterioration in cognitive performance or HAND status[47,75,76]. Similarly, a longitudinal MRI study reported an absence of brain atrophy over two years in a well-treated HIV+ cohort[77]. *In vitro* studies with sensitive assays to detect CSF viral RNA have even demonstrated that CSF viral levels did not decline after receiving additional anti-retroviral drugs, suggesting that persistent viral replication in the CSF does not exist in the presence of cART[78,79]. These data in aggregate suggests that cART can prevent viral replication and chronic inflammation in the CSF; arguing against ongoing brain injury to be the cause of the persistence of HAND.

### 2.3.3. Presence of Confounding Comorbidities

Comorbid conditions, such as substance abuse and psychiatric illness, are numerous and complex in HIV populations[7]. These conditions are associated with cognitive difficulties and might explain the persistence of HAND in the cART era[8]. While the guidelines for HAND diagnosis explicitly states that a diagnosis can only be made if the cognitive deficits cannot be fully explained by a comorbid conditions (see Table 2.2)[45], it is often difficult to reliably determine whether the comorbidity was severe enough to cause the cognitive difficulties without the presence of HIV[7]. Recently, a study reported that one out of twenty-six participants was diagnosed with HAND. However, the authors reported an unexpectedly high screen failure rate that was largely attributed to substance abuse and psychiatric illnesses. This highlights the difficulty to isolate the effects solely caused by HIV on cognition[80]. Heaton *et al.* reported in their study that 15.4% of the HIV+ participants had confounding comorbidities, 83% of whom were diagnosed with some form of HAND[7]. This illustrates the possibility that cognitive difficulties experienced by some HIV+ individuals may actually be caused by a cofounding condition that is unrelated to HIV. However, Heaton *et al.* also reported that there was still a high

rate of HAND at 32.7% in the non-confounded group[7]. Overall, this suggested that confounding comorbidities were unlikely to explain the continued persistence of HAND, but it should not diminish the importance of accounting for possible confounding conditions.

### 2.3.4. Cerebral Small Vessel Disease

Cerebral small vessel disease (CSVD) is the term used to describe abnormalities related to the small blood vessels in the brain. It is the most common cause of vascular impairment in the general population and a major contributor to mixed dementia (i.e. cognitive impairment with multiple causes)[81]. Signs of CSVD are commonly observed on MRI in the form of white matter hyperintensities (WMH), which are lesions (i.e. dead tissue caused by hypoperfusion) found in the deep white matter that appear hyperintense in $T_2$-weighted images. To assess the severity of CSVD many clinical studies use the total volume of WMH as an indirect measure[81-84].

Recent evidence has suggested that people living with HIV have an increased risk of developing CSVD as the virus itself may affect the pathogenic process of CSVD through a process known as HIV-associated vasculopathy[83,85]. Similar to the mechanisms that cripple the immune system and cause neuronal injury, HIV and its associated viral enzymes can directly and indirectly damage the blood vessel walls provoking vascular changes, potentially accelerating the progression of CSVD[85,86]. Interestingly, even some cART regimens have been reported to increase factors commonly linked to CSVD, such as hypertension, dyslipidemia and diabetes[83,87]. Given that CSVD is the most common cause of vascular cognitive impairment and HIV+ individuals may have more severe CSVD, this could mean that some cases of HAND in the cART era may be driven by vascular components.

## 2.4. Role of Advanced MRI Processing Tools for HAND

While the introduction of cART has transformed HIV, there remains a large number of HIV+ individuals with clinically symptomatic cognitive impairment[7,37]. To advance our understanding of the biological underpinnings of HAND, the neuropathogenesis must be further examined. Typically, the severity and extent of the disease has been measured based on abnormal performance on neuropsychological tests. However, this approach offers limited specificity and sensitivity, and cannot distinguish between static and active brain injury[88]. To address this issue, several HIV-associated cells in the CSF have been investigated as possible markers to monitor CNS injury and disease progression. These markers can be broadly grouped into one of three categories: viral, immune-related and neural injury-related[88].

Viral markers refer to quantitative measures associated with the virus. The most common viral marker is the CSF viral load, which quantifies the amount of virus present in the CSF[88]. Before cART, high viral loads were associated with increased neuroinflammation, neuronal injury and worse cognitive function[6,7]. However, since cART has reduced CSF viral loads to undetectable levels, viral markers have become diagnostically unspecific as HIV+ individuals may have long standing CSF aviremia but still exhibit cognitive deficits[65,88]. Although CSF viral markers are no longer useful for monitoring CNS injury, they are still commonly used to assess the effectiveness of cART in the CNS and detect CSF viral escape (i.e. cART no longer prevents viral replication)[88].

Given that HIV+ individuals with long standing CSF aviremia still experience cognitive difficulties, it has been suggested that there may be a genetically distinct variant of HIV that may be responsible for the neurodegeneration[6,65,88]. This theory has received support from studies that have used phylogenetic reconstructions to show that HIV in the CSF is compartmentalized from HIV in the blood, that is, the virus in the CSF is genetically different from the virus in the blood[6,88]. Moreover, the degree of divergence from the virus in the blood was associated with the degree of HAND impairment[89]. This indicated that there may be a unique neurotropic genotype in HIV that causes neuronal injury. Although this approach has potential to explain HAND, additional research is warranted as a unique genetic sequence linked to HAND has yet to be discovered.

Immunological markers have been viewed as a possible indicator of CNS injury because the mechanisms of HIV-related neurodegeneration are largely driven by immunopathologic processes. Since these processes often involve activated macrophages and microglia, activation markers released from these immune cells have been identified as possible biomarkers[88]. For instance, neopterin and monocyte chemoattractant protein-1 (MCP-1) are by-products released by activated macrophages. These markers were shown to correlate with the degree of HAND impairment before cART was introduced[56,88,90]. Furthermore, neurotoxic metabolites released from activated macrophages and microglia, including quinolinic and arachidonic acid, have also been found to correlate with HAND[6]. These immune markers are particularly useful as they can differentiate HAND from other neurodegenerative diseases that are not driven by immunopathological processes, such as Alzheimer's disease[88]. However, the success of cART has significantly reduced the amount of immune activation in the CNS, which has rendered these

markers to undetectable levels. Similar to viral markers, immune-related markers are now diagnostically unspecific and rarely used to track disease progression.

In many neurologic diseases, such as Alzheimer's and Parkinson's disease, brain-specific markers of neurodegeneration have been utilized to track disease progression with reasonable success[88]. Typically, these markers are by-products of neuronal breakdown[60,88]. For example, neurofilament light chain is a structural component of axons, which means that high levels of this marker indicate that there is increased neuronal injury. Neurofilament light chain was reported to be elevated in HIV+ individuals and correlated with immune activation and inflammation suggesting the presence of neuronal injury[60]. However, this approach is non-specific to HIV as it is difficult to determine the origin of the neuronal injury. This makes it difficult to establish whether the neuronal injury is associated with HIV or a confounding process.

Despite their theoretical potential, a single HIV-associated marker in the CSF does not appear to be insufficient to meet all the needs required to understand the mechanisms underlying HAND. Another tool that has become an integral component of the clinical assessment of individuals with suspected neurodegenerative diseases is structural MRI as MRI-based measures of brain volume and atrophy are regarded as valid and sensitive markers of disease state and progression[91]. In addition, clinically meaningful lesions can be seen on MRI, which can be used as a means to track the progression of a disease[81-84].

Over the past decade there has been a revolution in the techniques used to investigate the brain from structural MRI. For instance, advanced MRI analysis techniques, such as tensor-based morphometry, voxel-based morphometry and cortical thickness extraction, that are sensitive to subtle brain changes have been developed[92]. These approaches are useful for examining regional brain morphometry as they do not require *a priori* anatomical hypotheses and they have been extensively used to examine other neurodegenerative diseases, including, but not limited to, Alzheimer's disease[93-95], Parkinson's disease[96], multiple sclerosis[97], and Huntington's disease[98]. It is also advantageous to use these methods together since they provide complimentary information: while tensor- and voxel-based morphometry are best suited to detect spatially localized volume changes in subcortical regions[49], cortical modeling is well-suited extracting cortical morphometric measures (i.e. thickness)[99].

Although several studies have used MRI to explore underpinnings of HAND[5,49,51,53,54,62,67,73,77,83,100-103], novel MRI analysis techniques that can discover

unpredicted brain differences and improve the statistical power have rarely been used. Given that the underlying mechanisms of HAND are still unclear, and the current literature is littered with conflicting reports, it is evident that additional investigations with advanced MRI techniques are required to advance our understanding of HAND in order to open doors to novel treatment strategies focused on remediating these brain and cognitive changes.

## 2.5. MRI Signal Acquisition

MRI is a medical imaging technique used to investigate the anatomy of the human body. It is non-invasive and does not expose the body to harmful radiation, making it a popular choice to use for diagnosis and staging of diseases. To capture images of the brain, MRI scanners use strong magnetic fields, commonly 1.5T or 3T, radio frequencies (RF), receiving coils and gradient coils[104]. The signal that is used to create the image originates from hydrogen atoms in tissues containing water molecules. These hydrogen atoms, at any given moment, are randomly spinning, or precessing, around their own axis with magnetic moments – a quantity representing the magnetic strength and orientation – pointing in random directions[104]. When a strong magnetic field is applied, such as the one produced by an MRI scanner, a small percentage of the magnetic moments of the hydrogen atoms align with the magnetic field. At this point, however, no signal has been created. To generate a signal the hydrogen atoms are sent, or tipped, to an excited state by an RF pulse emitted from the scanner, which is applied perpendicular to the scanner's magnetic field. This causes the hydrogen atom's magnetic moments to tip towards the perpendicular plane. Shortly after the RF pulse is turned off, the precessing hydrogen atoms will return to their equilibrium state by realigning their magnetic moment with the initial magnetic field produced by the scanner[104]. It is during this return to equilibrium state that the precessing hydrogen atoms emit an RF signal in the perpendicular plane that is captured by receiving coils. The return to the equilibrium state is typically analyzed in terms of two separate relaxation processes, each with their own time constants, namely $T_1$ and $T_2$. The $T_1$ time constant, or spin-lattice relaxation time, is the time it takes a hydrogen atom to return to approximately 63% of its equilibrium state[104]. This time constant creates the $T_1$-weighted image, which is commonly used to obtain general morphological information about the brain. The $T_2$ time constant, or spin-spin relaxation time, is the time it takes for the RF signal in the perpendicular plane to decay to 37% of its original value[104]. This gives rise to the $T_2$-weighted image, which is useful for detecting white matter lesions. Both $T_1$ and $T_2$-weighted scans have very good contrast between the tissue types in the

brain (white matter, gray matter and CSF) because the $t_1$ and $t_2$ time constants across these tissues significantly differ due to the local environment, which influences the relaxation times.

Finally, to spatially encode the origin of the RF signal from the hydrogen atoms, MRI scanners include gradient coils that vary the magnetic field linearly across the subject in the three directions of space (x, y, z). This causes hydrogen atoms at different spatial locations to precess at slightly different frequencies. In essence, the different precessing frequencies encode the signal's origin, enabling the scanner to know where the signal is coming from[104]. Since the RF signal acquired is in the frequency domain, known as the *k*-space, the Fourier transform of the RF signal must be calculated to create the image that we see (Figure 2.5)[104].

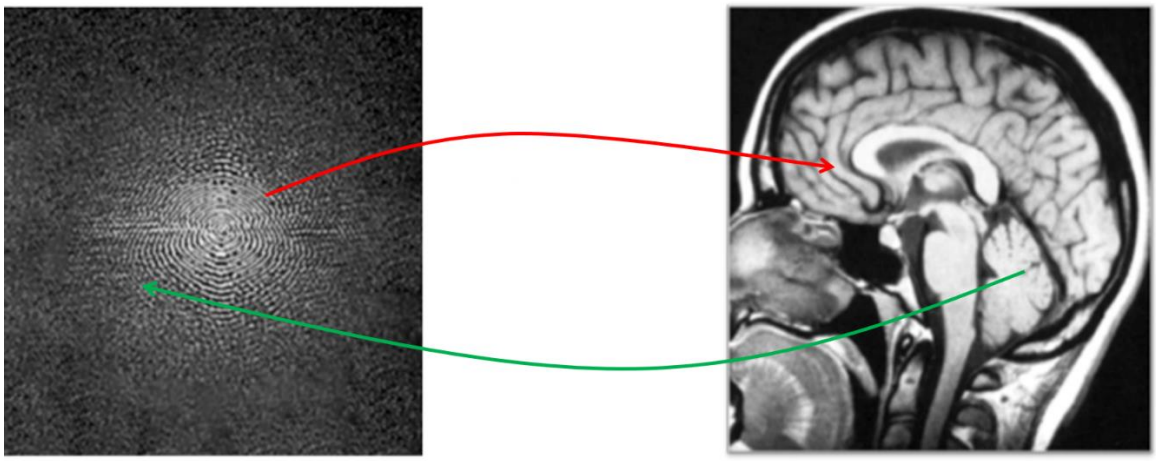

Figure 2.5: The RF signal acquired from the body is mapped to a *k*-space (left). Each point in the *k*-space contains information about the spatial frequency and phase of the signal. The image that we see (right) is created by computing the Fourier transform. The arrows represent corresponding points (arbitrarily chosen) between the *k*-space and the image space (red arrow) and the image space and *k*-space (green arrow).

## 2.6. Processing MRI Data

Structural MRI is ideal for examining neurodegenerative diseases because it offers high image resolution and good contrast between the tissue types, which is ideal for measuring brain volume and atrophy extracted from the MRI. Such measurements are regarded as valid markers of disease state and progression in many neurodegenerative diseases[105]. However, measuring brain volumes requires accurate and reliable delineation of the structures and tissues within the brain. In early MRI studies, the brain volumes were extracted by human experts (e.g. neuroanatomist) who manually outlined specific structures in each slice of a scan[91]. Although this approach produced accurate measurements, it was very time-consuming, especially in studies with large number of subjects, and vulnerable to operator error and bias[91]. These issues have since been resolved with

the development of fully-automatic MRI processing pipelines. These processing pipelines can produce accurate and reliable brain volumetric information from large amounts of data with minimal human intervention in short periods of time. This development has allowed researchers to conduct large, well-powered studies, which have been vital in furthering our knowledge of brain structure and function in health and disease. Generally, an MRI processing pipeline consists of several unique processing steps that are applied to the MRI data in sequential order. Each processing step manipulates the MRI data with goal of obtaining the most accurate volume information. The following sections provide an in-depth overview of the most fundamental components of typical MRI processing pipelines and how they improve brain volume measurements.

### 2.6.1. Intensity Non-Uniformity Correction

The MR signal captured from homogeneous tissue is rarely uniform, instead, it tends to vary smoothly across the image (Figure 2.6). This is known as intensity non-uniformity and occurs due to several reasons, including poor transmit and receive RF coil uniformity, gradient driven eddy currents and the fact that the subject is not entirely within the scanners field of view[106]. While these intensity variations have little impact on human visual diagnosis, the performance of fully-automatic MRI processing pipelines can be significantly affected, particularly the steps that rely on the absolute intensity information[106]. For example, two voxels in different spatial locations may be in the same tissue class (e.g. gray matter) but due to the non-uniform intensity they can have very different intensity values. As a result, a tissue classification method (i.e. identifying gray matter, white matter and CSF) will classify these two voxels into two different tissue classes, even though they actually belong to the same tissue class.

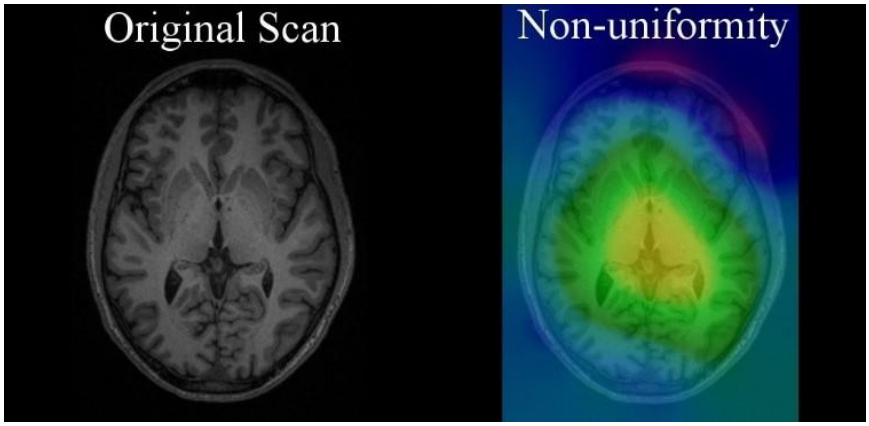


Figure 2.6: Example of an intensity non-uniformity in an MRI. Notice that the gray matter in the frontal lobe is noticeably darker than the gray matter in the insula. If this non-uniformity is not removed, tissue classification could wrongly classify these two voxels as different tissue types.

Initially, researchers attempted to remove the non-uniformity by measuring the static uniformity in the scanner with a second RF coil. With the RF signal from the hydrogen atoms and the static uniformity signal, researchers demonstrated that the non-uniformity signal can be modeled and removed using the Bloch equations[107,108]. However, this approach requires long scan times and additional scanner hardware, which is not always available, especially in the hospital, making it impractical for clinical use[106].

As an alternative, post-processing methods have been proposed that sought to compensate for non-uniformity *after* acquisition. For example, Wells *et al.* used an expectation-maximization approach to iteratively classify brain tissue and estimate the non-uniformity field[109]. While this approach showed promising results, it could not be scaled to different MRI scanners as the classifier must be retrained for different scanning parameters, which requires training data with similar scanning parameters[106]. Sled *et al.* proposed to develop a tool to remove non-uniformity without extended scanning time, additional scanning hardware, pre-training, *a priori* knowledge or data preprocessing[106]. Their method, named nonparametric non-uniform intensity normalization (N3), used an iterative, nonparametric approach to remove the non-uniformity and estimate the true distribution of the signal originating from the tissue[106]. First, they assumed that the non-uniform field was smooth and slowly varying, and multiplicative to the true underlying signal. Following these assumptions, the estimated non-uniformity field acts as a low-pass filter that removes the high frequency components of the true signal. Thus, the optimization criteria for N3 was to iteratively search a constrained solution space for a smooth, low frequency field that maximizes the high frequency content[106]. This approach proved to be very good at

removing the non-uniform field and quickly established itself as the standard in the field of MRI processing. It has been widely used as the first step for pre-processing MRI data[110]. However, given that N3 was developed during a time in which 1.5T scanners were predominately used, it was not optimized for 3T scanners. Although N3 provides reasonable estimates of the non-uniform field in higher field scanners, the performance is often sub-optimal[110]. To address this issue, Tustison *et al.* created N4ITK, which improves upon N3 by modifying the iterative optimization process to a hierarchical optimization scheme that significantly improves convergence and improves performance on higher field MRI scanners[110].

### 2.6.2. Image Volume Registration

A mandatory component of all MRI processing pipelines is image registration, which is the process of spatially transforming a source image volume such that corresponding brain structures are aligned with a target image volume[111]. Registering a target image volume to a common space helps to communicate and compare data across studies, to segment and classify data using *a priori* information from reference atlases and to find patterns in the data[112]. While several different registration methods exist in the current literature[112], all registration approaches consist of three fundamental components: spatial transform, similarity metric and optimization procedure. The diagram shown in  2.7 illustrates a typical registration procedure.

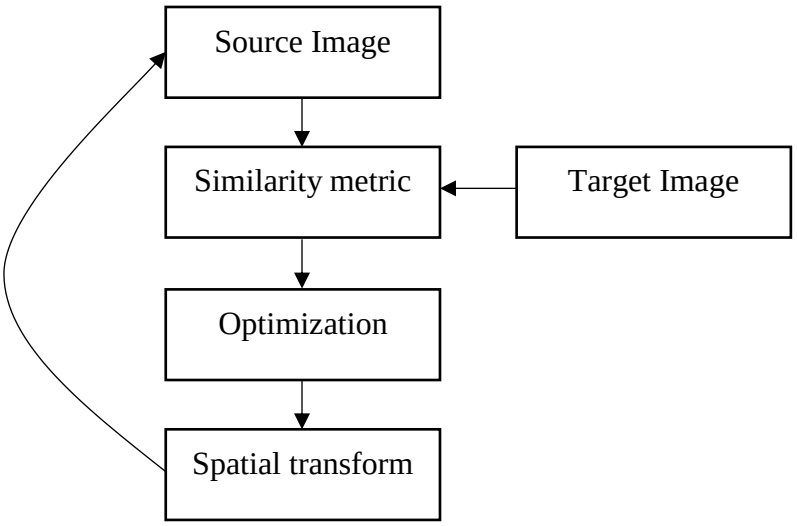


Figure 2.7: Diagram of a typical registration procedure. The algorithm will iterate through these steps until convergence is reached. After convergence, the source image should be aligned with the target image.

#### 2.6.2.1. Spatial Transform

During registration, the source image must be transformed to align with a target image. This transformation is defined by a spatial transform. There are different forms of spatial transformations that are differentiated based on the number of independent directions, or degrees of freedom (DOF), that a source image can be moved or deformed. These spatial transforms can be classified into two broad categories: linear and non-linear (also known as deformable registration). Linear registration translates, rotates, scales and/or shears the source image such that it is aligned with the target image[111]. However, linear registration cannot achieve point-to-point correspondence (i.e. align corresponding brain structures between two images). Instead, non-linear registration is used to achieve detailed registrations typically through b-splines, radial basis functions and non-linear dense transformations, or deformation fields[51,112]. The deformation fields can viewed as a discrete vector field that specifies the transformation required to achieve optimal alignment at every voxel location or local neighbourhood[113,114].

Determining the best spatial transform to use is dependent on the purpose of the image registration (Table 2.3). To register within-subject data (e.g. $T_1$-weighted to $T_2$-weighted MRI registration in the same subject), a linear spatial transform with 6 DOF (translations and rotations in x, y and z directions) should be used. This is also known as a rigid-body transform as the source image is not scaled, sheared nor deformed. However, a rigid-body transform is insufficient for between-subject registration because it cannot account for the differences in brain size and shape. Instead, a 9 or 12 DOF linear affine transform (translation, rotation, scale and/or shear in the x, y

and z directions) should be used to register data between subjects[111]. This form of registration will affinely deform (i.e. scale and/or shear) the source brain such that the brain size and shape match the target brain.

While a linear affine transform accounts for overall variations in brain size, position and orientation, it is still inadequate for detailed between-subject registration, which is required for future processing steps and statistical analysis, as it cannot achieve point-to-point mapping for corresponding brain structures, especially in the cerebral cortex across individuals with varying anatomy. For good quality between-subject alignment, non-linear registration, or deformable registration, should be used since it warps local brain areas in the source image such that a point-to-point mapping of corresponding brain structures is achieved with the target image[112]. Depending on the deformation method, this could involve millions of DOF all of which must be optimized. Typically, the linear affine transform (9 or 12 DOF) is used as a starting point for the non-linear registration to maximize performance and to avoid local optimums.

The brains across individuals are highly variable. For instance, the pattern of cortical folds may be unique to an individual. This means that achieving a point-to-point correspondence may not be possible, making the non-linear registration problem ill-posed[112]. To alleviate this issue, certain constraints are typically applied to non-linear registrations algorithms to force the resultant deformation field to exhibit special properties. Such properties include inverse consistency, topology preservation and diffeomorphism[115].

Despite common intuition, the majority of registration methods are not inverse consistent, that is, interchanging the source and target images may not result in forward and backward transforms that are the inverse of one another[115]. To tackle this shortcoming, inverse consistent methods aim to constrain the forward and backward transformations to be inverse mappings of one another. This is achieved by penalizing large differences between the forward transform and the inverse of the backward transform[115]. By imposing inverse consistency, the spatial transform and its inverse can be used to map data to and from a common reference space without biasing towards a particular transform.

Since non-linear registration methods require several million DOF to be optimized, the space of possible solutions (i.e. all possible spatial transforms) is very large. This means it is possible for transformations to apply anatomically impossible deformations to the brain, such as compressing or crossing two distinct points, which compromises the brain topology in the source

image[115]. This makes topology preservation a vital property for deformation fields. Brain topology is typically preserved by forcing the deformation field to be smooth and continuous. Generally, this is imposed by checking if the Jacobian determinant of the deformation field in local areas is greater than zero[115]. However, calculating the Jacobian determinant requires that the deformation field be differentiable at all points. By enforcing diffeomorphic deformation fields, this ensures that the spatial transform and its inverse are differentiable[115]. Together, imposing diffeomorphism and topology preservation, the resulting deformation field are smooth and continuous, which results in anatomically possible deformation.

Table 2.3: A summary of the suggested spatial transform to use depending on the purpose.

| **Spatial transform** | **Degrees of freedom** | **Purpose** |
|---|---|---|
| Rigid-body transform | 6 (3 translations and rotations). | Within-subject registration. |
| Affine transform | 9 (3 translations, rotations and scale). | Between-subject registration and initializing non-linear registration. |
| Affine transform | 12 (3 translations, rotations, scale and shear). | Between-subject registration and initializing non-linear registration. |
| Non-linear | Depends on the methodology. | Between-subject registration. |

#### 2.6.2.2. Similarity Metric

Regardless of the registration type or spatial transform, a similarity metric is mandatory as it provides a quantifiable measure that reflects the degree to which two images are aligned as the transformation parameters are changed[116]. Similarity metrics can be broadly classified as landmark-based, segmentation-based or voxel-based[117]. Landmark-based registration consists of aligning two images based on corresponding user-defined anatomical points on both images. While this method tends to be accurate, it is dependent on the user's accuracy in defining corresponding landmarks in the two images making it time-consuming and subject to operator error and bias. Segmentation-based registration aligns two images by matching corresponding

anatomical segmentations[116]. However, this approach requires both images to be segmented, which may be difficult in some modalities (e.g. ultrasound). Furthermore, since the registration accuracy is directly dependent on the segmentation accuracy, poor segmentations will result in poor registrations. Here, we focus on voxel-based similarity metrics that align two images by measuring the similarity between corresponding voxels with the assumption that optimally aligned images will give rise to maximum similarity. The advantage of voxel-based methods is that calculating the similarity is straightforward, without any user intervention or anatomical segmentations[117].

The most commonly used voxel-based similarity metrics are sum of squared differences, cross-correlation and mutual information. While all these metrics measure the similarity between voxel pairs, they each have different underlying assumptions that make them useful in some situations and unsuitable for others. Sum of squared differences assumes that the intensities between the corresponding structures are identical, that is, a lower sum of squared difference indicates better alignment[118]. Similarly, cross-correlation assumes that there is a linear correlation between the intensities of corresponding structures in both images[118]. Thus, a larger cross-correlation value indicates better alignment between the two images[118]. Typically, sum of squared differences and cross-correlation are the similarity metric of choice for unimodal registration (e.g. $T_1$-weighted MRI to $T_1$-weighted MRI or FDG PET to FDG PET) and non-linear registration methods since they adapt naturally to situations where intensities vary in local areas[119]. However, a disadvantage is that they assume corresponding voxel intensities are identical or have a linear relationship. This generally holds true for unimodal registration, which is why they achieve very good registration accuracies, but this intensity constraint is rarely satisfied in multimodal registration (e.g. $T_1$-weighted MRI to FDG PET registration)[116].

Mutual information is a basic concept from information theory that measures the amount of information one image contains about another[116]. In theory, larger mutual information between two images means better alignment. Unlike sum of squared differences and cross-correlation, mutual information has proven to be a robust and reliable similarity metric for multimodal registration as it does not make any strong assumptions about the underlying image intensities of corresponding structures[116]. Instead, mutual information understands that while image intensities corresponding to the same structure may be different across modalities, they are not independent quantities but are statistically related since the distribution of intensities should

be similar[116]. Mutual information takes advantage of the knowledge that one modality provides information about an underlying structure in the other modality. By maximizing the amount of information one modality provides about the other modality results in geometrically aligned images[116]. Interestingly, the mutual information similarity metric has also achieved state-of-the-art performance in unimodal registration[116]. However, given that mutual information relies on the global distribution of voxel intensities, this poses a problem for non-linear registration since local deformations may not significantly impact the global distribution of voxels resulting in negligible changes to the mutual information criterion, which is why almost all non-linear registration methods choose to use sum of squared differences or cross-correlation as the similarity metric[116].

#### 2.6.2.3. Optimization Procedure

The registration problem is often framed as an optimization problem, where the goal is to find the set of transformation parameters that optimizes a similarity metric. The underlying assumption is that optimizing the similarity metric would result in optimal alignment between two images. Registration failures often occur when the optimization strategy falls into a local optimal, failing to reach a global optimum[117]. Moreover, the speed of the registration is largely dependent on the optimization method[120].

Various optimization strategies have been introduced for image registration, which can be broadly classified as gradient- and non-gradient-based methods. Gradient-based methods require the differentiation of the similarity metric to find the optimal transformation parameters. The most straightforward method that uses the gradient information is gradient descent[120]. This involves taking small steps in the direction of the steepest gradient until an optimum (i.e. when the gradient is zero) is reached. This strategy is generally slow as it requires several small steps to reach the optimal, which can be especially slow if the solution space consists of long and narrow valleys[120]. To overcome this issue, the conjugate-gradient descent method was developed, which determines the direction of descent to be conjugate of the previous step, as oppose to the direction of steepest descent. This strategy does not require as many steps as gradient descent to reach the optimum[120].

Non-gradient-based methods do not require differentiation, instead, these approaches require the similarity metric to be a continuous function. Powell's method is an example of a non-gradient-based approach that finds the optimum of an $N$-dimensional function $f$ by repeatedly

minimizing *f* one dimension at a time along the set of *N* dimensions. The order of dimensions to minimize *f* influences the optimization performance and registration robustness[120]. Maes *et al.* reported for a rigid-body transformation (6 DOF; translation and rotation in the x, y and z directions) that translations in the x and y direction along with rotations in the z direction, followed by translations in the z direction and rotation in the x and y direction was the most optimal order of dimensions for registration[120]. Similar to Powell's method, the Simplex method does not require differentiation of the similarity metric, but unlike Powell's method it does not find the optimal solution by minimizing *f* one dimension at a time. Instead, this method is initialized with *N+1* points, defining a non-degenerate simplex in an *N*-dimension parameter space[120]. This simplex is then deformed iteratively by reflection, expansion or contraction steps such that the vertices of the simplex moves towards the optimum of *f*. In their experiments, Maes *et al.* reported that when using mutual information as the similarity metric, Powell's method performed the fastest while achieving accurate registration results[120].

Regardless of the optimization method, registration speed can be furthered improved by implementing an iterative multi-resolution approach[117,120,121]. This optimization procedure starts by estimating an initial registration transform between the images at a lower resolution, which reduces the likelihood of reaching a local optimum. Then, using the optimal low resolution transformation parameters as a starting point, the transformation parameters are refined at higher resolutions[117]. This strategy generally increases registration speed by 3-fold, while achieving optimal alignment without loss in precision or robustness compared to the single-resolution strategy[117,120]. However, appropriate down sampling factors must be determined experimentally because image resolutions that are too low may not provide a good starting point for the higher resolution registration. This could make the multi-resolution strategy slower than single-resolution and deteriorate registration robustness[117].

### 2.6.3. Brain Extraction

Raw, unprocessed MRI scans of the head include tissues outside of the brain, such as the skull, dura and eye fat[122]. Although these tissues do not impact manual visual radiological inspection and diagnosis and generally are not of significant interest when investigating neurodegenerative diseases, failing to remove the tissues external to the brain can sometimes negatively impact the outcome of some subsequent image processing steps, such as brain structure

segmentation, tissue classification and cortical thickness extraction. For example, failure to remove the dura may result in erroneous overestimation of the cortical thickness[122].

One of the first brain extraction (or skull stripping) method developed that produced robust results was the Brain Extraction Tool (BET)[123]. By using computational deformable surfaces, BET extracted the brain by initializing an ellipsoid mesh at the center of the brain and then iteratively deforming and expanding the mesh until the gray matter-CSF boundary was reached[123]. Although BET was robust and did not require any preprocessing, the intensity non-uniformity significantly affected the final output as BET solely relied on the voxel intensities to separate brain and non-brain tissue. This means that non-uniformity removal is almost always required before using BET. Unfortunately, even with the non-uniform field removed, brain extraction with BET is further complicated because it does not follow a gold standard to define what is brain and non-brain tissue[122]. This means that BET produces highly variable brain masks across subjects, that is, some areas are considered as brain tissue in one subject, while the same area may not be considered as brain tissue in another subject. To address this issue, Eskildsen *et al.* proposed a definition of brain and non-brain tissue. Here, they defined brain tissue as: all cerebral and cerebellar white and gray matter, CSF in all ventricles and the cerebellar cistern, CSF in the deep sulci and along the surface of the brain, and the brainstem[122]. Meanwhile, non-brain tissue was defined as: skull, skin, muscles, fat, dura mater, bone, bone marrow, and exterior blood vessels and nerves[122]. They implemented their definition of the brain by using nonlocal patch-based segmentation approach, namely Brain Extraction based on nonlocal Segmentation technique (BEaST), that labeled each voxel as brain or non-brain based on the similarity of its surrounding neighbourhood with patches from a set of manually segmented training library image volumes[122]. The sum of squared differences was used to estimate the similarity between the patches in the training and test set. In essence, lower sum of squared differences indicates that the test patch is similar to the patch in the training set, and the test patch should be assigned the same label as the training patch. This approach iterates across $n$ training patches to obtain $n$ labels. Majority vote (i.e. the mode of $n$ labels) is then used to fuse the $n$ label estimates into one unifying label (i.e. brain or non-brain). Given that sum of squared differences relies on the intensities being the same, all MRI data must undergo non-uniformity removal and intensity normalization. Moreover, the test data must be linearly registered (9 or 12 DOF) to a standard anatomical space such that the training and test patches come from similar brain areas[122]. While the patch-based

segmentation approach produces accurate brain extractions, computing similarities between all test patches and *n* training patches is computationally heavy. Therefore, to decrease the computational burden a few strategies were implemented. First, *N* MRIs were selected from the training set, where $N <$ training set size, that were most similar to the test MRI. This was followed by selecting the most informative patches for comparison by comparing the mean and variance of the patches, where patches that have similar mean and variance should, in theory, be the most informative as they should represent similar brain areas[122]. These steps effectively reduce the number of training patches, while eliminating useless patch comparisons by removing uninformative data. BEaST was reported to significantly outperform BET and other publicly available methods, by achieving state-of-the-art brain extraction results, while implementing the new gold standard definition of brain and non-brain tissue (Figure 2.8)[122].

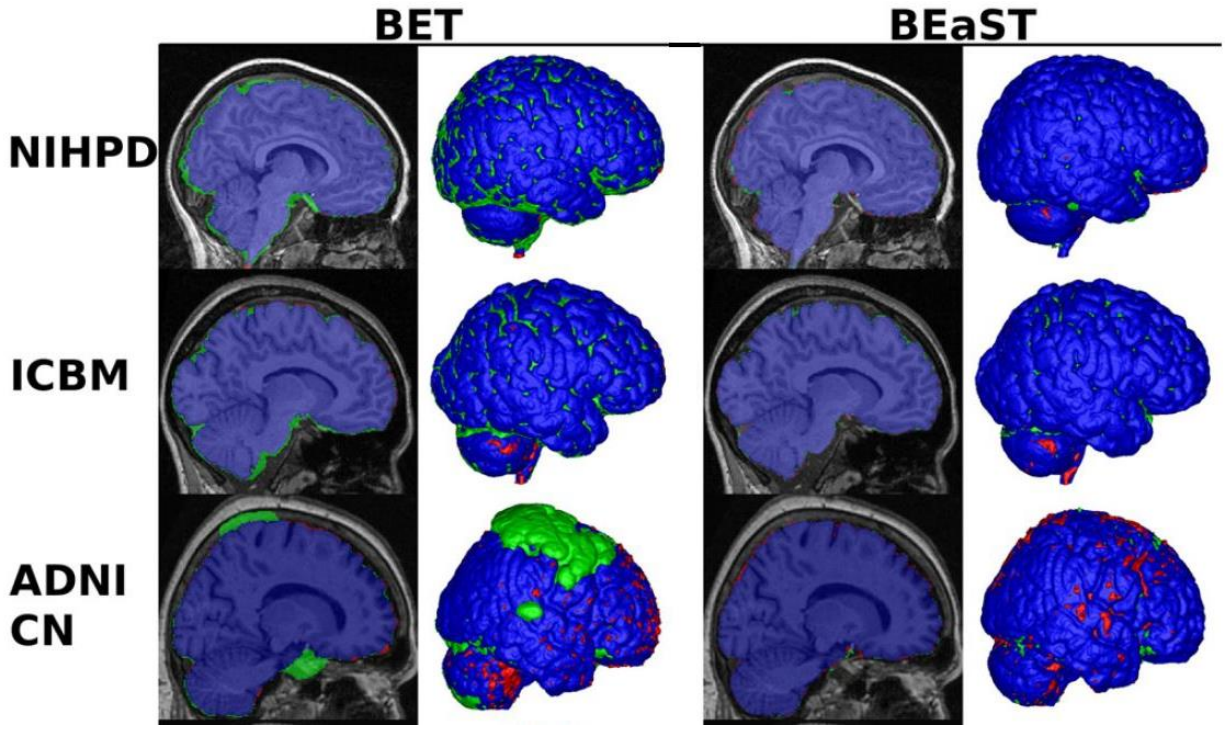


Figure 2.8: A visual comparison of brain extractions produced by BET and BEaST on publicly available datasets. Blue voxels indicate overlapping voxels with gold standard (i.e. correctly identified brains), green voxels are false positives and red voxels are false negatives. Notice that BEaST has significantly less errors compared to BET. (Image adapted from "BEaST: Brain extraction based on nonlocal segmentation technique" by Eskildsen *et al*.[122]. Permission for reuse of figure granted by publishers.)

In the past few years, deep learning, a subfield of machine learning, has had enormous success in the field of computer vision. For example, every year ImageNet – a large visual database designed for visual object recognition software – runs a contest where software programs compete to classify and detect objects in images. When the contest started in 2010 the best classification error rates were

approximately 25%, that is, the classifier would correctly detect and identify an object in the image 75% of the time. These methods typically used classic machine learning algorithm with hand-crafted features to optimize performance. However, in 2012 a deep convolutional neural network (CNN), a common deep learning algorithm today, achieved a 16% classification error rate; a rate that beat the closest competitor by almost 10%[124]. This result demonstrated the immense potential of deep learning, leading to an explosion of computer vision applications, including image segmentation, being tackled by deep learning.

Deep learning-based approaches can achieve state-of-the-art performance because they have a large capacity to automatically learn multiple levels of feature representation and abstractions that are most optimal for a given task[125]. Recently, deep learning has been applied to medical images, most notably for brain extraction. Kleesiek *et al.* implemented a deep CNN, similar to the one used in the 2012 ImageNet competition, to extract the brain[126]. On three publicly available datasets, Kleesiek *et al.* demonstrated that their deep CNN outperformed BEaST and BET, in regards to the brain extraction accuracy and in processing time on multiple publicly available datasets[126]. Notably, they demonstrated that their approach performed the best on a challenging dataset that contained brain tumours[126]. This is worth noting since clinical data often contains abnormal pathology that could degrade the brain extraction process highlighting the potential that deep learning-based approaches have in MRI processing pipelines.

### 2.6.4. Brain Structure Segmentation and Tissue Classification

In computer vision, image segmentation is the process of dividing an image into a set of semantically meaningful, homogeneous and non-overlapping regions that share similar attributes, such as intensity, shape and location[127]. In fact, brain extraction is a form of segmentation, where the goal is to segment the whole brain. Similarly, brain structure segmentation involves delineating specific brain structures (e.g. thalamus) or classifying the healthy tissues within the brain (white matter, gray matter or CSF) (Figure 2.9). These segmentations allow structural volume, tissue density and cortical thickness to be measured. Such measurements are considered valid markers of disease state and progression and could be leveraged to predict treatment outcomes[91,105].

In general, brain segmentation is a non-trivial task because the brain significantly varies across individuals and, even after preprocessing, MRI data is often imperfect and can be corrupted with noise and/or movement artifacts[127]. Nonetheless, several brain segmentation techniques

have been developed. The most common approaches can be broadly categorized into the two groups: intensity-based approach or atlas-based approach.

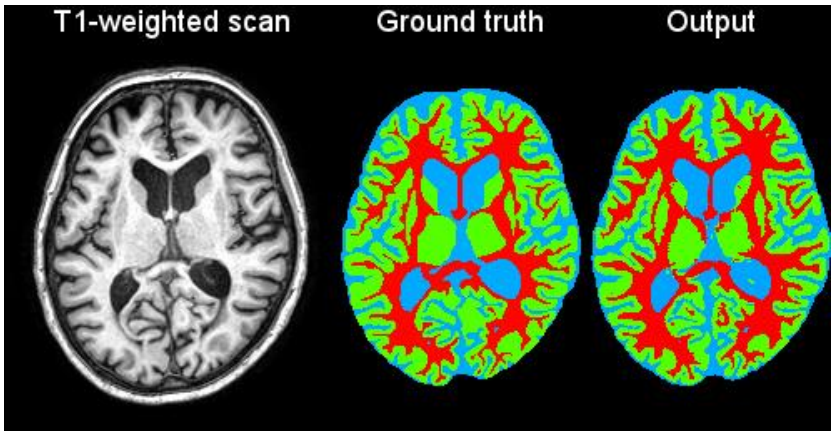


Figure 2.9: The tissues of the brain (white matter (red), gray matter (green) and CSF (blue)) are segmented using a deep learning algorithm (fully convolutional network) based on the $T_1$-weighted scan (left). Ideally, the output segmentation (right) should match the ground truth (middle).

#### 2.6.4.1. Intensity-Based Approach

Intensity-based methods for brain segmentation take advantage of voxel intensities to differentiate and identify areas of the brain. The simplest, but least effective, intensity-based approach is thresholding, where desired classes are separated by a cut-off value[127]. Segmentation is achieved by grouping all voxels that lie within defined intensity thresholds. Thresholding is fast and computationally efficient, but it is neither accurate nor reliable because it cannot account for the fact that the intensity profiles of different brain structures and tissue classes tend to overlap (Figure 2.10)[127]. This means that thresholding methods cannot provide the detailed segmentations that are required for studying the brain.

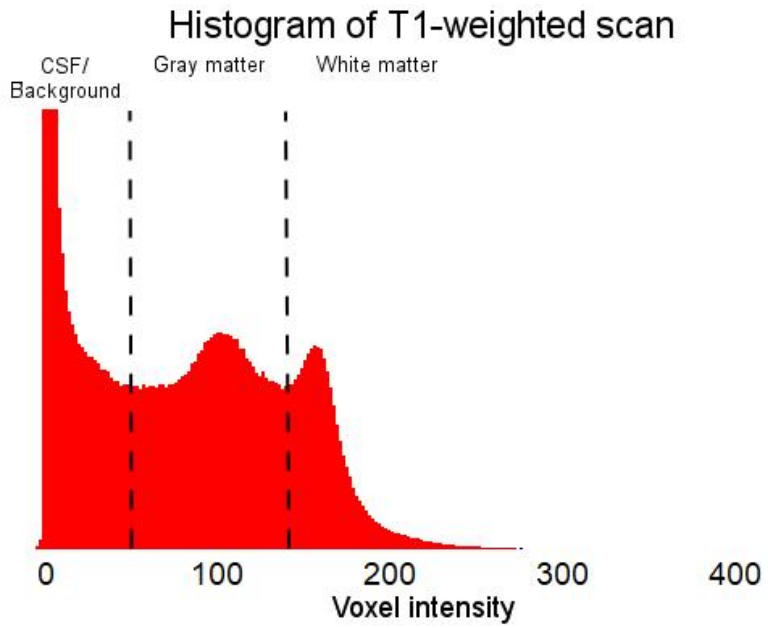


Figure 2.10: Histogram of the voxel intensities from the $T_1$-weighted scan in Figure 2.9. Notice that the intensity profiles across all tissue types have substantial overlap with each other. This makes it difficult to define a threshold for optimal performance.

Given that thresholding is a sub-optimal approach for brain segmentation, many have used the intensity information as features in machine learning-based classifiers. These classifiers can be divided into two distinct groups: supervised and unsupervised learning. Supervised classification approaches must be trained on manually segmented (see middle image in Figure 2.9) training data such that they can learn the underlying data representation and distributions. It is only after training is complete that a supervised learning method can be applied to new data. While supervised-based approaches are consistently at the forefront of the computer vision field, the requirement of gold standard training data is a large disadvantage as it is not always available. This issue is particularly noticeable with MRI data as manually segmenting large amounts of MRI data is a time-consuming process that typically requires multiple experts. Moreover, it is assumed that the training data is representative of the test data, which is not always the case and difficult to verify. This is a large issue with MRI data since different scanners and scanning parameters can produce significantly different intensity ranges. Nonetheless, several attempts have used supervised learning methods to segment the structure and tissues of the brain[127]. For instance, a commonly used supervised learning approach for brain segmentation has been the naïve Bayes classifier[127]. This technique takes advantage of the Bayesian framework to estimate a label for each voxel given the MRI data. The model is trained by finding optimal model parameters that maximize the posterior distribution of Bayes rules based on the training data. After training, classification of new data is made by

assigning each voxel a label that has the highest posterior probability based on the learned model[127].

In contrast to supervised learning, unsupervised learning approaches can classify new data without training data, making it a highly desirable choice when training data is sparse or completely absent. These methods use the available MRI data to train themselves by iterating between two general steps: data clustering and estimating the properties of each class[127]. An example of this approach is called Gaussian Mixture Modeling (GMM), which has been widely used for tissue classification. GMM assumes that the input data can be represented by *k* Gaussian distributions, where *k* is the number of classes (e.g. number of tissue classes)[127]. Each Gaussian distribution is characterized using the mean, variance and magnitude. These parameters are learned during unsupervised training through an approach known as the expectation-maximization (EM) algorithm. This is method that iterates between an expectation step (E-step) and a maximization step (M-step) until convergence is reached. The E-step clusters voxels into the appropriate Gaussian clusters based on the intensities and the current estimate of the model parameters (mean, variance and magnitude). The M-step estimates the model parameters given the updated voxel classifications [127]. Once the EM algorithm converges, each data point should be grouped into a unique Gaussian cluster that corresponds to the different classes.

Shortcomings of both the naïve Bayes classifier and GMM is that they treat each voxel independently, that is, it does not consider the intensity information surrounding a given voxel. Generally, the structures of the human brain follow a characteristic spatial pattern and this knowledge could enhance brain segmentation and tissue classification performance. For example, the hippocampus and amygdala are both gray matter structures with almost identical intensity profiles. Thus, using intensity information alone to differentiate these structures is difficult, if not impossible. Rather than relying solely on intensities, one could take advantage of the spatial information, where it is well-known that the amygdala is always anterior and superior to the hippocampus[128]. Similarly, tissues in the brain are commonly clustered together, where each tissue type is most likely to be surrounded by the same tissue. Therefore, modeling this spatial and contextual information, along with intensity information, could significantly improve the segmentation accuracy and reliability.

Spatial information can be modeled using Markov random fields or Conditional random fields[129]. These are graphical models that compute the probability of labeling each voxel a certain label, given the current estimate of the labels surrounding the voxel of interest. By tuning various hyper-parameters, these graphical models force voxel labels to be similar, or dissimilar, to

neighbouring voxels. The resulting segmentations are usually smooth and continuous. These are desirable properties as it eliminates spurious outputs in random locations that are unlikely occur in normal appearing anatomy (e.g. single white matter tissue surrounded by CSF)[130,131].

Since deep learning is a form of machine learning and could use the intensity information as input features, they can also be grouped as an intensity-based approach. Based on deep learning's success in the ImageNet competition and with brain extraction, it is expected that deep learning-based approaches for brain segmentation and tissue classification should also achieve state-of-the-art performance. Recently, Wachinger *et al.* developed a deep CNN to segment 25 brain structures[125]. The architecture incorporated spatial information by including the spatial location of the brain regions into the CNN, as well as using a Conditional random field as a form of post-processing to ensure smooth, continuous segmentations[125]. The authors reported that the deep CNN significantly outperformed three publicly available methods, including the popular FreeSurfer[125]. For tissue classification, Chen *et al.* developed a deep CNN with skip connections to facilitate propagation of the gradient through the network[132]. The authors tested their architecture against a well-known benchmark (MRBrainS13[133]) and reported that it outperformed 37 other methods. Despite the promising results from implementations by Wachinger *et al.* and Chen *et al*. these deep networks require significant computational power and large amounts of training data to achieve good performance, which is not always available. Even so, future brain segmentation and tissue classification approaches should consider using deep learning as it has the potential to provide accurate and reliable segmentations that are required for clinical studies. Moreover, it most likely has the capability to achieve good performance even in the presence of scanning artifacts and abnormal pathology.

#### 2.6.4.2. Atlas-Based Approach

A brain atlas is a collection of high-resolution MRIs of healthy or diseased brains in which the brain structures are meticulously segmented by experts. Brain atlases are commonly used as a reference space, sometimes referred to as the stereotaxic space, for image registration and facilitates data analysis and reporting of findings from neuroimaging experiments[134]. A commonly used brain atlas is the International Consortium for Brain Mapping (ICBM152) template, which was developed using MRI data from 152 healthy adults[135]. The single ICBM152 brain atlas was created by averaging the 152 MRIs through several non-linear registration iterations[136]. The ICBM152 brain atlas includes tissue probability maps, as well as a fully-segmented structural atlas (Figure 2.11).

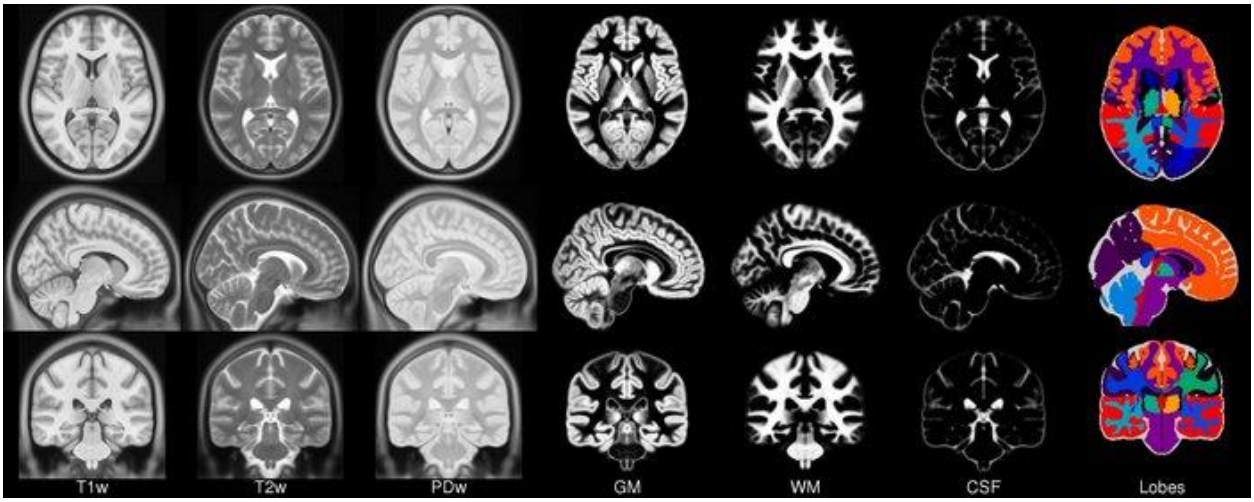


Figure 2.11: ICBM152 brain atlas along with tissue probability maps and anatomical atlas[135].

Given that brain atlases contain significant amount of information about brain anatomy, they can be used as *a priori* information to segment new MRI data. In atlas-based segmentation, the segmentation problem is posed as a registration problem, that is, non-linear registration is used to compute a transformation that maps new MRI data to the brain atlas[137]. Since non-linear registration aims to achieve one-to-one correspondence across the brain structures, the inverse of the computed transform can be used to map the labels from the brain atlas to the new MRI data resulting in a fully segmented brain[138]. The main advantage of the atlas-based approach is the possibility to segment any structure available in the atlas without any additional computational costs[127]. This is in stark contrast to machine learning-based approaches as segmenting additional structures requires re-training the model with the new label, which comes at the expense of increased computational costs. However, since the segmentation accuracies are directly dependent on the quality of the registration, it is often difficult to achieve detailed segmentations since registration quality for fine structures may be insufficient.

The segmentation accuracy could also be affected by anatomical variability because a single brain atlas may not generalize well to all individuals in a study[137]. For instance, a brain atlas created from healthy individuals may not be ideal for individuals with a neurological disease and severe atrophy[127]. To address this issue, anatomical template libraries have been created that include several anatomical atlases from a variety of healthy and diseased individuals[137]. Here, new MRI data is non-linearly registered to $N$ anatomical templates in the library and the labels are mapped back to the individual's MRI. This results in $N$ segmentations for the

individual's MRI[137]. Label fusion techniques are then used to combine the *N* segmentations into a single consistent label set[137]. The most common label fusion technique is majority vote, where the mode label at each voxel location is chosen as the final label[137]. This approach, known as multi-atlas label fusion segmentation, has been demonstrated to produce superior segmentation accuracies across several brain regions compared to using a single atlas[128,137], but requires significant computational effort as *N* non-linear registrations are required. This problem can be alleviated by selecting the *n*, where $n<N$, most appropriate atlases from the library using the mutual information to assess the similarity between the new MRI data and atlases in the library[139]. The main advantage of this technique is that using the most similar atlases improves the registration quality and thus improves segmentations.

### 2.6.5. Lesion Segmentation

The goal of brain segmentation and tissue classification is to delineate specific brain structures and tissue types such that the volume, tissue density and cortical thickness measurements could be obtained. However, when studying neurodegenerative diseases sometimes it is more meaningful to quantify the lesions that are caused by the disease (Figure 2.12). A brain lesion is non-specific term used to describe any type of abnormal, or unhealthy, tissue in the brain. These lesions could arise from several different factors, such as CSVD, multiple sclerosis, or ischemic stroke, all of which can be captured and quantified through MRI. Measuring these lesions, often quantified by the volume or number of lesions, can provide a surrogate marker of disease severity that could reveal clues about the neuromechanisms that underlie the disease. The lesion burden has also been shown to correlate well with cognitive deficits making it useful for monitoring disease progression and treatment outcomes[140]. For example, the volume of WMH, lesions caused by CSVD, were reported to be correlated with cognitive decline in individuals with Parkinson's disease[141]. Furthermore, the quantification of lesions is often used as a marker in clinical studies to assess the effectiveness of new treatment strategies. For instance, since the underlying pathology of multiple sclerosis consists of attacks on myelin that lead to lesions in gray and white matter areas, tracking the lesion burden is a common strategy to determine whether treatment is reducing the myelin attacks[142].

Accurate lesion segmentation is a challenging task because the heterogeneous appearance of lesions, including large variability in location, size, shape and frequency, makes it difficult to devise a robust segmentation strategy[140]. Early lesion segmentation methods posed the task as

a form of outlier detection, where tissues with intensity profiles that fall outside an expected range are considered to be lesions[143]. One implementation used an atlas-based approach by registering the MRI data to a healthy brain atlas. Any large deviations in tissue appearance between the MRI data and atlas was labeled as a lesion[143]. However, in many cases the presence of lesions can cause structural deformations (e.g. brain tumours), which could negatively impact registration quality that will ultimately affect the accuracy of the lesion segmentation[140].

Currently, almost all lesion segmentation methods use some form of supervised learning[140]. Geremia *et al.* used the voxel intensities to train a Random Forest classifier to segment multiple sclerosis lesions[144]. Zikic *et al.* followed a similar approach but included tissue probability maps as a form of prior information[145]. The Random Forest classifier has also been used to segment brain tumours[146]. Here, Tustison *et al.* trained a Random Forest classifier with voxel intensities and then incorporated spatial information with a Markov random field. This ensured that the lesion segmentations were smooth and continuous[146]. More recently, Dadar *et al.* used a set of informative features to identify WMH of presumed vascular origin[147,148]. The feature set included voxel intensity, spatial probability (i.e. the probability that a voxel at a given spatial location will be a lesion based on training data), intensity probability (i.e. the probability that a voxel with a given intensity is a lesion based on training data) and average intensity of healthy tissue at each voxel[147]. This feature set was used as an input into a Random Forest classier and the output was thresholded to create a binary lesion map[148]. While all the aforementioned approaches have been very successful in their own domains, their modeling capabilities are limited because they can only segment one type of lesion (e.g. brain tumour or WMH). This highlights the need to develop a generalizable approach that could segment all types of lesions, regardless of the origin, without significant modifications to the implementation.

With deep learning's immense modeling capacity and ability to automatically learn highly discriminative features, it appears to have the potential to accurately segment lesions, regardless of the lesion's origin[140]. Deep learning-based approaches have produced state-of-the-art results across several different lesion types, including brain tumour[149], ischemic stroke[150], multiple sclerosis lesions[151,152]. However, similar to classical machine learning approaches, specific deep learning solutions may not generalize well to other lesion types. For instance, a method trained to segment WMH of presumed vascular origin may produce sub-optimal lesion segmentations from multiple sclerosis data. In an attempt to address this limitation, Kamnitsas *et*

*al.* aimed to take full advantage of the power of deep learning and develop a robust, generalizable deep CNN that could segment a variety of lesions with minimal modifications to the model[140]. Their approach involved parallel convolutional pathways with multi-scale processing, allowing both local and contextual information to be efficiently incorporated into the model[140]. The authors demonstrated that their architecture could achieve state-of-the-art performance in three different lesion segmentation tasks (traumatic brain injury, brain tumour and ischemic stroke) without any major changes to the network architecture[140]. While this is promising result, a major disadvantage that plagues the development of a generalizable lesion segmentation solution is the requirement of training data and retraining of the network for every type of lesion, which requires significant time, effort and resources to acquire. Thus, before a generalizable segmentation method can be created, it is imperative that more training data become available.

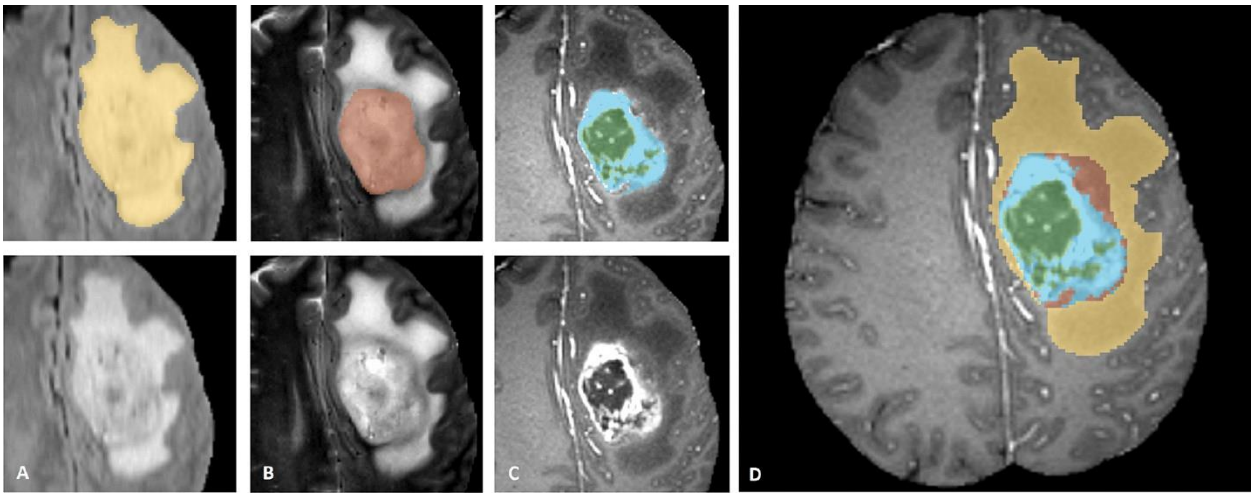


Figure 2.12: Example of a large brain tumour (bottom row) accompanied by the manual segmentations (top row) of different components of the tumour (edema (yellow), non-enhancing solid core (red), necrotic/cystic core (green), enhancing core(blue)). Notice that different modalities show the different components of the tumour better than others. A) The whole tumour visible in FLAIR. B) The solid core visible in $T_2$-weighted scan. C) The necrotic (green) and enhancing (blue) visible in $T_1$-weighted contrast enhanced scan. D) All components combined. (Image taken from "The Multimodal Brain Tumor Image Segmentation Benchmark (BRATS)" by Menze *et al.*[153]).

### 2.6.6. Tensor-Based Morphometry

Since measures of brain volume are considered to be valid markers of disease state and progression, it is common for researchers to analyze and compare volumes from different brain regions by disease status (i.e. diseased versus controls). However, this approach requires prior anatomical hypotheses in regard to the brain regions that are most likely to be affected by the disease. These hypothesis-driven studies cannot discover unpredicted volume differences, and

when statistical power is low, null findings may not provide additional information as the likelihood of type I error increases.

An alternative approach is tensor-based morphometry (TBM), which was developed to detect subtle structural abnormalities across the whole brain without the requirement of an anatomical hypothesis. This technique produces estimates of brain volume at the voxel level across the whole brain. These voxel-wise volume estimates are generated from the deformation field obtained from non-linearly registering the MRI data to a brain atlas (Figure 2.13). Since the deformation field can be viewed as a discrete vector field, which specifies the transform required to achieve optimal alignment at every voxel location or local neighbourhood, the volume change relative to the brain atlas can also be extracted[113,114]. This volume information is obtained by taking the Jacobian determinant of the deformation field[113,114]. By definition, the Jacobian determinant of a deformation is the volume of a unit-cube after an image has been deformed. This means that if a deformation field exists at every voxel, volume information at the voxel level can be calculated[114]. A Jacobian determinant value greater than one implies that the local area was enlarged to match the template (i.e. local volumetric expansion), while a determinant value less than one is associated with local shrinkage[154]. Given that the MRI data being analyzed is aligned to the same brain atlas, statistical models can be applied on a voxel-wise basis to identify structural abnormalities across the whole brain without an anatomical hypothesis. While TBM improves the power of detecting regionally specific volumetric differences, the power is limited by the accuracy of the registration[114].

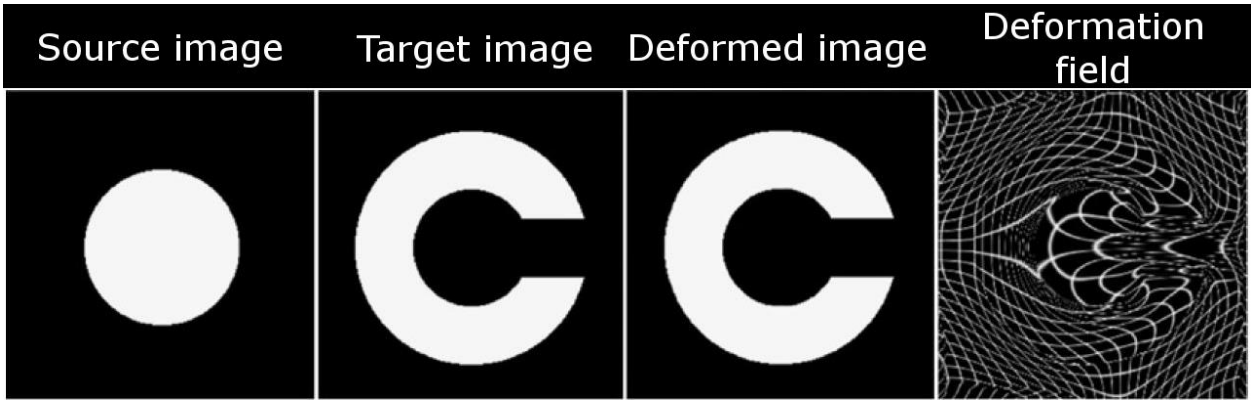


Figure 2.13: A simple example of tensor-based morphometry. The source image (circle) is deformed such that there is a pixel-to-pixel correspondence with the target image (C). The resulting deformation field specifies the deformation required at each local area to achieve optimal alignment. Notice the area of the cubes in the deformation field have expanded or contracted, depending on the transformation required. The amount of expansion or contraction can be quantified with the Jacobian determinant. (Image adapted from "3D pattern of brain atrophy in HIV/AIDS visualized using tensor-based morphometry" by Chiang *et al.*, 2007 [51]. Permission for reuse of figure granted by publishers.)

### 2.6.7. Voxel-Based Morphometry

Similar to TBM, voxel-based morphometry (VBM) is an approach used to detect brain abnormalities at the voxel-level without any prior hypotheses[113]. These techniques differ slightly as TBM focuses on differences in brain structure and shape, whereas VBM focuses on differences in the local concentration of brain tissue after brain structure and shape differences have been discounted[113]. Generally, VBM and TBM are used in tandem as they focus on different, but complimentary, measures of the brain.

Generating VBM brain maps involves non-linear registration to a common anatomical space, classifying the tissue as gray matter, white matter or CSF, and smoothing. The goal of non-linear registration is to correct for global brain volume and shape differences[114]. Following tissue classification, the segmented tissue maps are smoothed with an isotropic Gaussian kernel resulting in the tissue density maps (Figure 2.14). It should be noted that the term "tissue density" does not refer to the cell packing density, instead, these maps reflect the average concentration of each respective tissue at every voxel location[114]. In addition, smoothing with a Gaussian kernel makes the data more normally distributed, increasing the validity for parametric statistical tests[113]. As with TBM, statistical models can be applied on a voxel-wise basis to analyze and compare tissue concentrations.

An additional step could also be incorporated into the VBM procedure in order to preserve tissue volumes that may have been distorted through the non-linear registration process. This involves multiplying, or modulating, voxel values by the Jacobian determinant of the deformation field. In effect, this modulation step tests for regional differences in absolute amount of tissue, as oppose to local tissue concentration tissue[114,155].

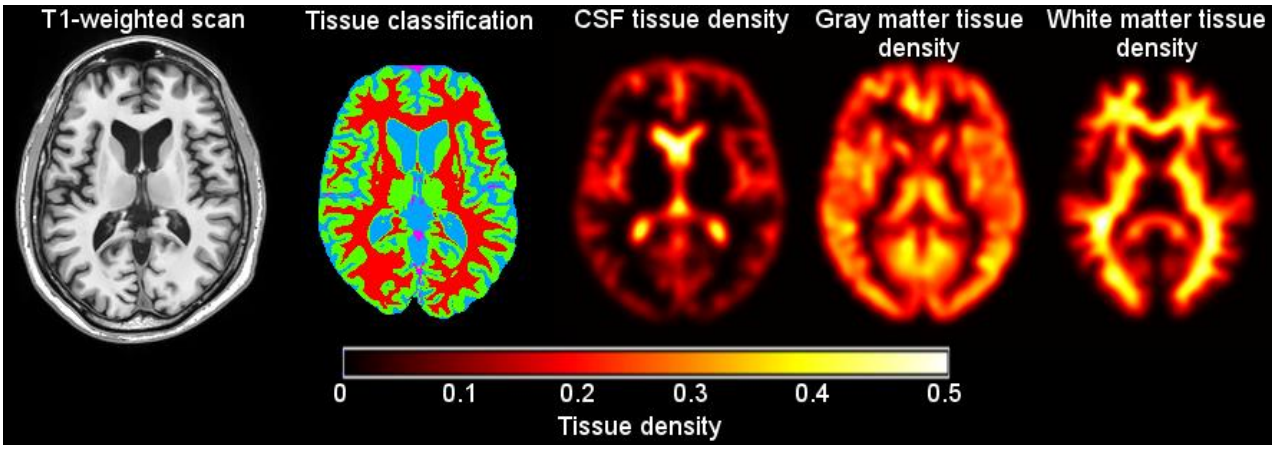


Figure 2.14: Example of VBM maps. The T1-weighted scan (leftmost) is segmented by tissue type (second image from the left; white matter (red), gray matter (green) and CSF (blue)). Each tissue type is smoothed with an isotropic Gaussian kernel (8 mm full width half maximum in the example) resulting in the tissue density maps. Higher tissue density indicates greater concentration of the tissue.

### 2.6.8. Cortical Thickness Extraction

The cerebral cortex is a highly folded sheet of gray matter that forms the outer layer of the brain and plays a vital role in most higher-level cognitive functions, including memory, attention, language, perception and consciousness. The thickness of the cerebral cortex, defined as the distance from the white-gray matter boundary to the nearest pial surface, varies by cortical region and is affected in multiple neurodegenerative diseases and disorders. For example, in those with Alzheimer's disease significant cortical thickness reductions in areas associated with memory have been observed[156]. This demonstrates that the cortical thickness, similar to brain volumes, could be viewed as a valid marker of disease stage and progression.

Like brain segmentation and tissue classification, extracting the cerebral cortex for cortical thickness measurements is a non-trivial task as the cortex is highly convoluted and the cortical folding patterns across individuals are highly variable[157]. This task is further complicated since the cortical boundaries are often obscured or partly missing because of noise and partial volume effects originating from MRI acquisition[157,158]. This problem is most pronounced in tightly folded sulci, where the CSF is almost undetectable as the distance between opposing sulci banks are smaller than the MRI resolution[157,159].

Early techniques for cortical extraction would use a bottom-up approach (i.e. edge detection) to detect the boundaries of the cerebral cortex without any constraints. An example of this approach is the "Marching Cubes" algorithm, which fits a polygonal mesh onto the boundaries of the cerebral cortex using the intensity information[160]. However, this approach produced sub-

optimal results since it could not account for partial volume effects causing tightly folded sulci to be fused together. Furthermore, it did not impose any constraints regarding the surface topology often leading to extracted cortices that had anatomically impossible self-intersecting sulci[157,159].

With the deficiencies of a bottom-up approach, top-down methods that use model-based constraints to restrict the space of possible solutions must be incorporated. Most notably, Dale *et al.* implemented a technique that first identifies the white-gray matter surface through tissue classification and then expands a deformable surface towards the pial surface[161]. While this approach provided superior results relative to the unconstrained "Marching Cubes" algorithm, it could not preserve the cortical topology[157,159]. To address this deficit, MacDonald *et al.* used a coupled surface approach, where inner and outer surfaces were simultaneously deformed to fit the white-gray matter boundary and pial surface, respectively[157]. This implementation used topology-preservation constraints to prevent self-intersecting sulci and ensured topological correctness by deforming a surface that was topologically equivalent to a sphere. In addition, constraints were used to force the cortical thickness values to lie within an anatomically-plausible range[157]. However, by imposing such thickness constraints, it introduced a bias to populations that have thickness values that fall outside the defined range[159]. For example, this approach would not be ideal for those with advanced Alzheimer's disease because they may have cortices that are thinner than the defined range. Kim *et al.* proposed a modification to the method by MacDonald *et al.*, by eliminating the thickness constraint. Instead, they used partial volume information to correctly classify cortical CSF and then expanded a deformable surface with topology-preservation constraints from the white matter surface to the previously identified cortical CSF[159]. While this method showed promising results, the process of expanding the deformable surface is computationally expensive[158]. This led to the introduction of Generalized Gradient Vector Flow as a solution to quickly and accurately extract the cortical surface[158]. Eskildsen and Østergaard implemented a cortical extraction method that first identified the white matter surface, similar to Dale *et al.* [161], and then used the Generalized Gradient Vector Flow to quickly expand a surface towards the pial surface, which was identified using gray matter and CSF tissue classification[158]. This method was shown to be fast, robust and produced accurate cortical thickness estimates (Figure 2.15)[158].

Similar to TBM and VBM, the extracted cortical surface can be registered to a standard cortical template through a non-linear surface-based registration. This surface-based registration scheme uses sulci and gyri depth maps the drive the non-linear deformation field. By aligning the depth maps, it improves the chances that corresponding vertices will be in similar positions within a cortical fold[162]. After non-linear registration, statistical models can be applied on a vertex-wise basis to identify regionally specific cortical thickness differences by disease status and correlations with variables of interest.

Figure 2.15: Left: Example of a cortical surface extracted from the ICBM152 template by FACE. Right: The cortical thickness is defined as the 3D distance from the inner surface (black) and the corresponding outer surface (white). (Image taken from "Active Surface Approach for Extraction of the Human Cerebral Cortex from MRI" by Eskildsen and Østergaard[158]. Permission for reuse of figure granted by publishers.)

## 2.7. Neuropsychological Evaluation

While measures of brain volume, tissue density, cortical thickness and lesion burden correlate well with cognition, these measures cannot be used to directly assess cognitive function. Instead, cognitive function is evaluated by performance on a neuropsychological assessment[163]. This approach is typically used to examine the cognitive consequences of a neurodegenerative disease and is almost always required to diagnose the presence of cognitive impairment, such as HAND[45]. A neuropsychological assessment is usually performed through a battery approach, which consists of multiple cognitive tests that assess different areas of cognitive ability[163]. These cognitive areas include memory and learning, language, processing speed, executive function, motor and attention. A list of standard neuropsychological tests recommended to judge

cognitive impairment and the cognitive domain that they predominantly test can be found in Table 2.4. The performance on each test provides a measure of functioning in the respective cognitive area, which, in turn, could be attributed to the function of general brain areas (e.g. poor executive function could indicate frontal lobe dysfunction). The scores across multiple tests can be combined (e.g. averaged) to provide a measure of global cognitive function.

Table 2.4: Neuropsychological tests commonly used administered to test for HAND.

| **Neuropsychological tests in cognitive domains** | **Test description** |
|---|---|
| **Memory and learning** | |
| • Hopkins Verbal Learning Test – Revised immediate recall | Immediately recall 12 words, 4 words each from three semantic categories[164]. |
| • Hopkins Verbal Learning Test – Revised delayed recall | Recall 12 words, 4 words each from three semantic categories after an extended period of time (e.g. after completing other tasks) [164]. |
| **Language fluency** | |
| • Category fluency | Produce as many words as possible in a given category (e.g. animals) in an allotted time frame[165]. |
| • Action fluency | Produce as many verbs as possible in an allotted time frame [166]. |
| • Letter fluency (FAS test) | Produce as many words that start with a given letter (e.g. F, A, S) in an allotted time frame [167]. |
| **Speed of information processing** | |
| • Trail making test – Part A | Connect a set of dots with numbers in incremental order as quickly and accurately as possible[168]. |

| | |
|---|---|
| • WAIS-III Digit Symbol Substitution | Given a set of digit-symbol pairs, write down the corresponding symbol under digits in a test set[169]. |
| • WAIS-III Symbol Search | Check whether two given symbols on one side match a set of five test symbols on the other side[169]. |
| **Executive function** | |
| • Trails making test – Part B | Similar to Part A except targets are numbers and letters. Dots must be connected in alternating order (e.g. 1, A, 2, B, etc.)[168]. |
| • Stroop Color and Word Test | Naming the colour the word is printed in (e.g. Green; correct answer is red)[170]. |
| **Attention and working memory** | |
| • Letter-Number Sequencing | When given a sequence of randomly ordered letters and numbers orally, produce the correct order of letters followed by numbers (e.g. given GFH432; correct answer is FGH234)[169]. |
| **Motor** | |
| • Groove Pegboard Test | Insert pegs into a pegboard as quickly as possible. This test is performed with both dominant and non-dominant hands[171]. |
| • Timed Gait Test | Time to walk a defined distance[172]. |

A critical concept of neuropsychological assessment is normative data[163]. Generally, this involves taking into account an individual's demographic information, such as age, sex, education and race, as these factors could significantly impact an individuals performance on neuropsychological tests, regardless of neurological severity[163]. For example, the Timed Gait Test is commonly used to assess motor dysfunction of lower extremities and gait abnormalities[172]. An elderly individual with no motor dysfunction or history of neurological disease may perform poorly on this task merely because of their age. To account for these

demographic factors, the test scores are usually normalized (e.g. *Z*-score) based on the performance of a group of healthy individuals with similar demographics on the same test[163]. Normalization of the test scores allows for the determination of whether the individual performed as would be expected, given their demographic factors, or poorer than expected[163].

When performance is poorer than expected it is common to assume that a cognitive deficit exists. However, this judgement process is complicated by the existence of performance variations, even in healthy individuals. This means that it is important to consider a few factors to distinguish normal variations from clinically meaningful variations[163]. Variations in performance may arise from the normative data as it is assumed that the normative data is representative of the sample under study, which is difficult to verify and most likely does not always hold true[75]. The reliability of the test should also be considered since less reliable tests tend to produce more variable scores[163]. Finally, a definition is required to separate normal variations from clinically meaningful variations. A widely accepted definition is performance that is one standard deviation below the normative mean is considered to be a clinically meaningful deficit. For example in HAND diagnosis (see Table 2.2 for the detailed diagnostic criteria), a person living with HIV is diagnosed with ANI/MND if they perform more than one standard deviation below the normative mean in two or more cognitive domains[45]. While HAD, the most severe form of HAND, is defined as performance that is two or more standard deviations below the normative mean in two or more cognitive domains[45]. These thresholds were chosen based on the experience and views of several neuropsychologists and neurologists who interact with impaired and unimpaired HIV+ individuals daily[45].

Although normalizing neuropsychological test scores with normative data is common practice, this approach has limitations. First, the available norms may not be appropriate for all individuals studied. Second, to obtain a measure of overall cognitive function, the test scores across multiple domains are usually averaged. However, averaging can reduce informative variance, posing potential difficulties in its use for statistical analysis[173]. To overcome these limitations, an alternative approach, Rasch Measurement Theory, can be used to summarize the neuropsychological test scores to yield a measure of global cognitive ability without the need for normative data. This approach uses item response theory to determine the extent to which a set of items (e.g. neuropsychological tests) and responses to those items reflect a single latent construct (i.e. cognitive ability)[173]. Rasch analysis arranges items and participant responses on the same

scale (logits) such that items that most participants pass are considered easy items and participants who fail to pass them are considered to have less cognitive ability. Similarly, items that few participants pass are harder items, and participants who pass them have more cognitive ability[173]. The result is an estimate of each person's cognitive ability that can be treated as a continuous ruler-like measure. This approach also accommodates missing data, allowing them to be applied on all available neuropsychological test scores. Since the Rasch approach generates a continuous measure of cognitive ability, it is more suitable for parametric statistical testing and may be more practical for testing brain structure–function relationships[173].

## 2.8. Statistical Analysis

Once data, such as brain volume, lesion load and/or cognitive function, has been acquired from study participants, rigorous statistical analyses are required to test research hypotheses such that appropriate conclusions can be drawn. It is vital to choose the appropriate statistical approach for hypothesis testing because incorrect analyses could return false and misleading results, which could have serious consequences. While the existence of several different statistical approaches makes it difficult to determine the appropriate one to use, the choice is largely dependent on the research question and the data type (e.g. continuous or discrete)[174].

### 2.8.1. Statistical Methods for Group Comparisons

Cohort studies (i.e. diseased and control group) are designed to estimate the impact a disease (e.g. HIV) has on a population relative to a demographically similar control group. In these studies, it is common to hypothesize that certain measures in a diseased population differs from that in a control population (e.g. brain volumes are reduced in people living with HIV compared to controls). Testing this hypothesis requires a statistical method that can compare the means of the measure of interest. Typically, a *t*-test can be used when the variable of interest is continuous and follows a normal distribution, while the Wilcoxon's rank sum test is a non-parametric test used for continuous variables that are not normally distributed. If the variable of interest is discrete, or categorical (e.g. gender), then the chi-square ($\chi^2$) test or Fisher's exact test is most appropriate[174]. These methods are also commonly used to verify whether the control group has been drawn from the same population (i.e. demographically similar) as the diseased group to avoid confounding factors that may bias the results and conclusions.

### 2.8.2. Statistical Methods to Test for Associations

In research studies, to assess if there is a possible connection between two or more variables, it is essential to examine their association or relationship[174]. For instance, the connection between tobacco smoking and mortality was concluded when a strong positive correlation was found between these two variables[175]. A popular statistical method to test the association between variables is the linear regression, which estimates a linear model that best explains the relationship between a response (or dependent) variable and one or more explanatory (or independent) variables with the given data. A linear regression assumes that there is a linear relationship between the dependent and independent variable, each data point in the model is independent of each other, and the response variable is continuous following a normal distribution curve[174]. If the response variable is discrete or not normally distributed, a generalized linear model (GLM) should be used. Generally, linear regression or GLM include several explanatory variables in the model to prevent spurious correlations from arising, which can occur when two or more variables that are not actually related, are wrongly inferred to be related because of a coincidence or the presence of an unseen confounding factor[174]. For example, in studies investigating brain volumes in HIV+ individuals, it was common to hypothesize that longer duration of HIV infection is associated with more brain volume reductions[5,53,62,67,102]. This hypothesis can be tested with a linear regression analysis, where the brain volume is modeled as the response variable and the duration of HIV infection as the explanatory variable. However, longer duration of HIV infection also tends to be correlated with older age[32] and it is well-known that brain volume decreases with increasing age[91]. This means that ageing is a confounding factor that must be included in the model to avoid capturing ageing effects with longer duration of HIV infection. It is important to note that while linear models examine associations and relationships between variables of interest, strong correlations do not imply causation. Disentangling the cause-and-effect relationship requires carefully designed longitudinal studies.

#### 2.8.2.1. Linear Mixed-Effects Modeling

When using linear regression or GLM it is assumed that each data point is independent of one another. This assumption usually holds true for cross-sectional studies that observe data from a population at one time point. However, for longitudinal studies that involve repeated measures from the same population this assumption is violated (e.g. multiple MRI scans from the same subject). While linear regression and GLM could be used in data with repeated measures, it is not

recommended as these methods cannot account for within-subject correlations. Instead, studies with repeated measures should analyze the data with mixed-effects models[176].

A typical linear regression model consists of one or more explanatory variables, which are also known as fixed effects because they are variables that are fixed across individuals. However, fixed effects cannot account for variables that vary across individuals. This can only be accounted for through random effects, which is why mixed-effects models are ideal for longitudinal data because it can account for within-subject variations by modeling both fixed and random effects (hence, the name *mixed-effects* model). In essence, adding random effects to the model resolves the non-independence issue by assuming that each individual has a unique baseline and/or slope, which are commonly referred to as random intercepts and slopes, respectively. This means that each individual will have their own functional relation between the dependent and independent variable (Figure 2.16)[176].

The random effects are assumed to follow a multivariate normal distribution with zero mean and some variance, σ, that must be estimated along with the weights (also know as βeta) parameters for the fixed effects[177]. Unlike the linear regression model, which can be solved with a closed form solution, namely Ordinary Least Squares, mixed-effects models must be estimated by maximizing the log-likelihood function using the EM algorithm[177]. Given that model estimation is an optimization problem, the model can fail to converge if the model structure is too complex and/or if there is insufficient amount of data to explain the complexity[177].

An advantage of using mixed-effects models for longitudinal data analysis is that each subject does not have to have the same number of repeated measures (i.e. thus accounting for missing data points)[176]. The model accounts for this by weighting the parameter estimations based the number of observations. Essentially, the random slope and intercept estimation for subjects with few observations will be similar to the overall group average, whereas the random slope and intercept estimates in subjects with many observations will rely more on the subjects data[176].

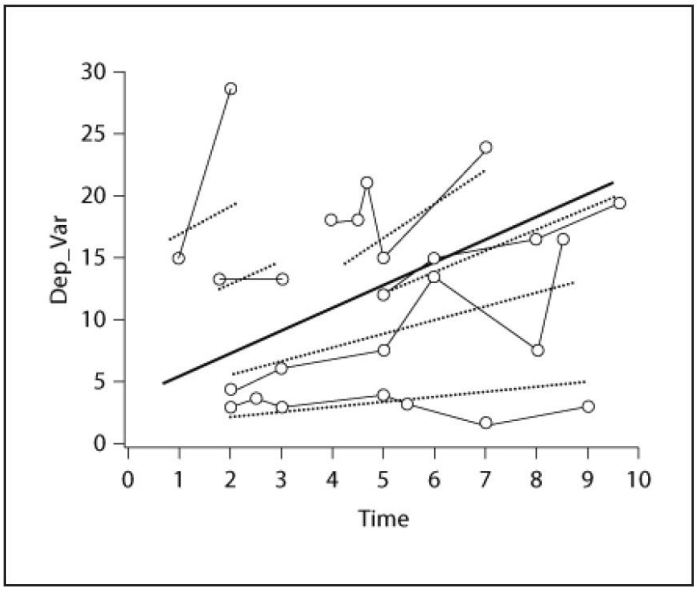


Figure 2.16: Illustration of a linear mixed-effects model. Data points are indicated by circles with a thin solid line connecting data points from the same subject. Thick solid line is the estimated overall effect between Dep_Var and Time. The dotted straight lines are the regression lines characterized by the random slope and intercept. (Image was taken article entitled, "An Overview of Longitudinal Data Analysis Methods for Neurological Research" by J.J. Locascio and A. Atri[176]).

### 2.8.3. Statistical Significance Testing

Regardless of the statistical approach, statistical significance testing is required to determine if a variable is significantly different between the groups, or if a significant relationship exists between two or more variables. More precisely, statistical significance determines if the results are unlikely to have occurred by chance, given a null hypothesis. Here, a null hypothesis is defined as a general hypothesis that states there is no difference between two groups, or no relationship between two or more variables. Contrary to the null hypothesis is the alternative hypothesis (e.g. there is a statistical difference between the two groups). In statistical significance testing, a defined significance level, α, is the probability of incorrectly rejecting a null hypothesis when it is true, while the *p*-value is the probability of obtaining an extreme result, given that the null hypotheses were true. This means that when the *p*-value is less than α the result is considered to be statistically significant because there is sufficient evidence to reject the null hypothesis and accept the alternative hypothesis. For example, when comparing the brain volumes between an HIV+ and control group, the null hypothesis would state that the brain volumes are similar while the alternative hypothesis would state that the brain volumes are different. This hypothesis can be tested using a *t*-test. Assuming a significance level α of 0.05, and the *t*-test reports that the means of the brain volumes are different with a *p*-value of 0.01, then it can be concluded that the brain

volumes between the HIV+ and control group are significantly different. This means that the probability of incorrectly rejecting the null hypothesis is very unlikely, that is, there is a low probability (i.e. one time out of 100) that this is an extreme result occurring by chance and it is generally safe to conclude that the effect reflects the characteristics of the whole population. Typically, the significance level, α, is set to 0.05 (or 5%), but this can vary depending on the field of study, data available and research question.

### 2.8.4. Effect Size

While significance testing indicates whether results are statistically significant, it gives no indication regarding the clinical significance of the results as it does not indicate the magnitude of the effect. This is important to consider, especially for studies in medicine, since statistical significance does not necessarily mean that the effect has practical importance in real life. For instance, brain volumes may be significantly smaller in HIV+ individuals compared to a control group, but the magnitude of this difference may be negligible. A common approach to quantify the clinical significance is with the effect size, which provides the magnitude of the effect (e.g. magnitude of the brain volume difference)[174]. It is useful to report effect sizes when the variables under study have intrinsic meaning (e.g. reporting brain volumes in $cm^3$) to improve the interpretability and understanding[178]. If the variables do not have an intrinsic meaning (e.g. tissue concentration), standardized measures of effect, such as the correlation coefficient or Cohen's *d*, are typically used[178]. The effect size is also used to plan studies by determining the minimal sample size required to observe a statistically significant effect of a desired magnitude[179]. This approach is most prominent in planning clinical trials as it is important to ensure that the study has enough participants to capture a clinically meaningful effect, if it is present[179].

### 2.8.5. Multiple Comparison Correction

Analyzing whole brain TBM, VBM and cortical thickness maps usually involves mass statistical testing in which a separate hypothesis test (e.g. *t*-test) is performed on every voxel or cortical vertex[180]. In a typical whole brain voxel-wise analysis, upwards of 1,000,000 independent tests could be performed. Based on simple probability with only random data, the standard significance level, α, of 0.05 would result in 50,000 significant effects due to chance alone. This illustrates that such approaches are highly susceptible to false-positive errors. Failure to control the number of false-positives could lead to impressive, but incorrect, results[180]. To

ensure that the false-positive rates are controlled, multiple comparison correction must be performed[180].

The simplest approach to reduce the number of false-positive errors is to define a stricter significance level (e.g. $\alpha = 0.001$). This approach does not solve the multiple comparisons issue, it simply reduces the number of possible false-positive errors in the results. However, there is no optimal procedure to define the significance level making this approach somewhat arbitrary.

Bonferroni's correction is a well-known approach to account for multiple comparison correction[181]. It compensates for the multiple tests by defining a significance level at $\alpha/m$, where $m$ is the number of independent tests performed. For instance, with $\alpha$ of 0.05 and 1,000,000 voxels, Bonferroni's method would require a test to have $p < 0.00000005$ to be considered statistically significant. While this approach most likely eliminates almost all false-positive errors, it comes at the cost of increasing the probability of producing false-negatives (i.e. removes true positive results). Given the stringent nature of this approach, it is not often used in practice.

Random Field Theory was developed as an extension of Bonferroni's method for medical image analysis[182]. Instead of assuming that all points in the volume are independent, it assumes that blocks of voxels, or resolution elements (resels), are independent. This assumption translates well to MRI as data from one voxel generally correlates well with data from neighbouring voxels[182]. Given a significance level, $\alpha$, of 0.05, Random Field Theory states that there is only a 5% chance that the significant effects are false-positive[182].

The False Discovery Rate (FDR) was also developed for multiple comparisons correction in medical image analysis[183]. Unlike the previous approaches, FDR is less stringent. It states that of all the significant effects, 5%, on average, will be false positive[183]. The advantage of FDR is that it increases the sensitivity to significant effects, but comes at the cost of certainty[183].

Finally, an increasingly popular approach for multiple comparison correction is permutation testing[184]. This is a non-parametric approach used to determine the exact distribution of a particular statistical test by calculating all possible values of the test statistic by permuting the labels (e.g. disease or control) of the observed data. To calculate the statistical significance at 0.05, the test statistics are sorted and the test statistic at the fifth percentile from the top is chosen as the significant threshold[184]. Although permutation testing provides strong control over false-positive errors, it requires a statistical test to be repeated for all possible permutations of labels and observed data to estimate the underlying distribution. In many cases

this is not tractable as the sample size is too large, instead, the distribution can be approximated by taking a large number of permutations (e.g. 1000-10000 permutations)[184].

## Chapter 3: Regionally Specific Brain Volumetric and Cortical Thickness Changes in HIV-Infected Patients in the cART Era

Despite the growing body of work that have investigated the brain in people living with HIV[5,50,51,61,73,100-102,185-188], the existence and extent of the brain injury in HIV remains unclear. For example, increased putamen volume was detected in a group of HIV+ individuals compared to a control group[188], while other studies have reported decreased putamen volumes[48,51]. Discrepancies between the studies may arise due to the heterogeneity of both HIV+ (e.g. degree of infection and impairment severity) and control (e.g. poorly matched controls) groups, variations in the methods used to estimate brain volumes, and/or differences in the brain regions investigated.

In the following paper, we used TBM, VBM and cortical thickness extraction to characterize the brain volumes and neuropsychological testing to evaluate cognitive function in cohort of 125 treated HIV+ individuals and 62 demographically similar controls. We sought to: 1) compare the regional brain measures and cognitive function between the HIV+ and control group; and 2) assess the relationship between standard clinical measures of HIV disease severity, including current and nadir CD4, duration of HIV infection and viral loads, and brain volume measures and cognitive function.

We observed that the HIV+ group had significantly reduced cortical thickness and smaller subcortical volumes and poorer cognitive function compared to the control group. Moreover, subcortical brain volumes were associated with lower nadir CD4 cell counts in the HIV+ group. These results demonstrated that despite the majority of HIV+ participants being treated with good viral suppression significant brain atrophy and cognitive deficits were still evident. We also provided evidence that the brain changes and cognitive deficits may reflect damage that occurred in early infection before starting treatment.

# Regionally Specific Brain Volumetric and Cortical Thickness Changes in HIV-Infected Patients in the cART Era

Ryan Sanford[1], MSc, Ana Lucia Fernandez Cruz[1], MSc, Susan C. Scott[3], PhD, Nancy E. Mayo[3], PhD, Lesley K. Fellows[1] MD CM, DPhil, Beau M. Ances[2], MD, PhD and D. Louis Collins[2], PhD

[1] Montreal Neurological Institute, McGill University, 3801 University Street, Montréal, Québec, Canada H3A 2B4

[2] Department of Neurology, Washington University, Box 8111, 660 South Euclid, St. Louis, Missouri, USA 63110

[3] Division of Clinical Epidemiology, McGill University, Montreal, Quebec, Canada.

*Journal of Acquired Immune Deficiency Syndrome. 2017; 74(5):563-570.*

## 3.1 Abstract

**Background:** Cognitive impairment still occurs in a substantial subset of HIV-infected patients, despite effective viral suppression with highly active antiretroviral therapy (HAART). Structural brain changes may provide clues about the underlying pathophysiology. This study provides a detailed spatial characterization of the pattern and extent of brain volume changes associated with HIV, and relates these brain measures to cognitive ability and clinical variables.

**Methods:** Multiple novel neuroimaging techniques (deformation-based morphometry, voxel-based morphometry and cortical modeling) were used to assess regional brain volumes in 125 HIV-infected patients and 62 HIV-uninfected individuals. 90% of the HIV-infected patients were on stable HAART with a majority (75%) having plasma viral suppression. Brain volumetrics and cortical thickness estimates were compared between the HIV-infected and uninfected groups, and the relationships between these measures of brain volume and indices of current and past infection severity, central nervous system penetration of HAART, and cognitive performance were assessed.

**Results**: Regionally specific patterns of reduced thalamic and brainstem volumes, as well as reduced cortical thickness in the orbitofrontal cortex, cingulate gyrus, primary motor and sensory cortex, temporal, and frontal lobes were seen in HIV-infected patients compared to HIV-uninfected participants. Observed white matter loss and subcortical atrophy were associated with lower nadir CD4 cell counts, while reduction in cortical thickness was related to worse cognitive performance.

**Conclusion:** Our findings suggest that distinct mechanisms may underlie cortical and subcortical injury in people with HIV, and argues for the potential importance of early initiation of HAART to protect long term brain health.

## 3.2. Introduction

The introduction of highly active antiretroviral therapy (HAART) has successfully shifted HIV from a terminal illness to a manageable chronic condition. However, the prevalence of mild-to-moderate cognitive impairment due to HIV has not declined, with up to 40% of HIV-infected patients affected despite effective viral suppression and minimal comorbidities[7]. The underlying pathogenesis of brain dysfunction remains unclear with several proposed mechanisms, including: permanent damage prior to HAART initiation, ongoing brain injury from low level viral replication and immune activation despite effective viral control, presence of comorbid neurological or psychiatric conditions, and HAART neurotoxicity[8].

Neuroimaging studies in the HAART era have reported brain volume loss in various cortical and subcortical regions[71,189]. Despite a growing body of studies, the patterns and spatial distribution of brain injury remains unclear[92]. For example, increased putamen volume was detected in HIV-infected individuals compared to an age- and education-matched HIV-uninfected group[188], while other studies have reported decreased putamen volume[48,51]. Likewise, there is no clear consensus on the existence or extent of cortical effects in HIV, with some studies reporting significant cortical atrophy[50,62,102], while others have detected no cortical differences[5,186]. These inconsistencies could reflect heterogeneity of both HIV-infected (i.e. degree of infection and impairment severity) and HIV-uninfected (i.e. poorly matched controls) groups across studies, variations in the methods used to estimate brain volumes, and/or differences in the brain regions investigated. Much of this work has involved small samples, often necessitating region-of-interest designs that constrain their anatomical scope.

The present study aimed to provide a detailed spatial characterization of the pattern and extent of brain volume changes in a cohort of HIV-infected patients and a demographically-matched HIV-uninfected group. Multiple novel neuroimaging methods with complementary strengths (deformation-based morphometry (DBM), voxel-based morphometry (VBM) and cortical modeling) were applied to this large sample to assess the relationship between regionally specific brain volume estimates and HIV status, measures of current and past infection severity, treatment effects, and cognitive function.

## 3.3. Methods

### 3.3.1. Subjects

HIV-infected participants were recruited from the infectious disease clinic at Washington University in St. Louis (WUSTL), while HIV-uninfected participants with similar sociodemographic factors were recruited from the local community by leaflets. All participants provided written consent approved by the WUSTL Institutional Review Board. Participants were excluded from the study if they had a history of confounding neurological disorders including epilepsy, dementia or stroke, current or past opportunistic central nervous system infection, traumatic brain injury (loss of consciousness >30 minutes), major psychiatric disorders including schizophrenia, depression, bipolar disorder or obsessive-compulsive disorder, or active substance abuse and dependence diagnosis according to Diagnostic and Statistics Manual of Mental Disorders 4$^{th}$ edition criteria. Individuals with past substance use were not excluded. All participants who met these criteria, had laboratory evaluations (current plasma CD4 cell count and viral load), and completed magnetic resonance imaging (MRI) and neuropsychological tests were included in the analysis. This yielded a total of 133 HIV-infected and 66 HIV-uninfected participants. For all HIV-infected patients receiving HAART, a central nervous system penetration effectiveness (CPE) score was generated based on previous methods[70].

### 3.3.2. Neuropsychological evaluation

Ninety-eight HIV-infected and 47 HIV-uninfected participants completed an extensive neuropsychological assessment: Timed Gait, Grooved Pegboard (dominant and non-dominant), Hopkins Verbal Learning Test Revised, Trail-Making Tests A/B, Digit-Symbol, Stroop Colour and Words, Stroop Interference, Letter Number Sequencing, and Verbal Fluency. An additional 35 HIV-infected and 19 HIV-uninfected participants completed a briefer neuropsychological assessment (due to logistical reasons): Trail-Making Tests A/B, Hopkins Verbal Learning Test

Revised, and Digit-Symbol. Two approaches were taken to summarize overall test performance. The conventional method generates *Z*-scores from each test using demographic (age, gender, ethnicity, and education) adjusted normative means [37]. *Z*-scores from four tests available in the whole sample (Trail-Making Tests A/B, Hopkins Verbal Learning Test Revised, and Digit-Symbol) were averaged to generate a summary *Z*-score (NPZ-4). However, the NPZ-4 has limitations: the available norms may not be appropriate for all individuals studied, and averaging can reduce informative variance, posing potential difficulties in its use for statistical analysis [173]. An alternative approach, Rasch analysis, uses item-response theory to determine the extent to which a set of items (i.e. neuropsychological tests) and responses to those items reflect a single latent construct (i.e. cognitive ability)[173]. Rasch analysis arranges items and participant responses on the same scale (logits) such that items that most participants pass are considered easy items and participants who fail to pass them are considered to have less cognitive ability. Similarly, items that few participants pass are harder items and participants who pass them have more cognitive ability[173]. The result is an estimate of each person's cognitive ability that can be treated as a continuous ruler-like measure, and does not require demographic norms. This approach also accommodates missing data, allowing it to be applied on all available neuropsychological test scores for this sample (see section A.3.1. in Appendix for additional details and results). Since the Rasch approach generates a continuous ruler-like measure of cognitive ability, it is more suitable for parametric statistical testing and was therefore used to test brain structure-function relationships[173].

### 3.3.3. Magnetic resonance imaging acquisition and analyses

All participants underwent contemporaneous MRI using the same 3T Siemens Tim TRIO whole-body magnetic resonance scanner (Siemens AG, Erlangen, Germany) with a 12 channel transmit/receive head coil. The scanning protocol included $T_1$-weighted three-dimensional magnetization-prepared rapid acquisition gradient echo (MPRAGE) sequence [repetition time (TR)/echo time (TE)/inversion time (TI) = 2400/3.16/1000 ms, flip angle = 8˚, and voxel size = 1 $mm^3$], and a $T_2$-weighted SPC sequence [TR/TE=3200/460 ms, flip angle = 120˚, and voxel size = 1 $mm^3$]. The same scanning protocol was used for all participants. All acquired MRI were visually inspected at the scanner with an additional scan performed if significant movement or artifact was observed.

Pre-processing of all scans included denoising with optimized non-local means filtering[190], correction for intensity inhomogeneity[106], brain masking[122], and linear intensity scaling using histogram matching to the Montreal Neurological Institute (MNI) 152 average brain template. The resulting images were linearly registered to the MNI152 template using a nine-parameter affine transform to correct for variations in head size, position, and orientation[111]. Following these pre-processing steps, all MRI data was carefully inspected for significant structural brain abnormalities, white matter hyperintensities from the $T_2$-weighted images, and unacceptable image processing outcomes. This resulted in the removal of 8 HIV-infected and 4 HIV-uninfected participants from subsequent analysis, yielding a final total of 125 HIV-infected and 62 HIV-uninfected participants. Following visual quality control, the $T_1$-weighted data for all participants was available for VBM, DBM and cortical modeling as described below.

The use of VBM, DBM and cortical modeling is advantageous because they provide complementary information about brain volumes, that is, VBM and DBM are better suited to detect subcortical changes associated with tissue densities and anatomical size (i.e. volume), respectively, while cortical modeling can capture subtle cortical thickness changes. Combining these methods maximizes brain volume information, so regionally specific brain changes can be optimally detected in cortical and subcortical regions.

### 3.3.4. Voxel-based morphometry

VBM identifies local tissue density changes in gray matter (GM), white matter (WM), and cerebrospinal fluid (CSF) space[113]. The pre-processed $T_1$-weighted data was spatially normalized to the MNI152 space. An artificial neural network classifier categorized each voxel into one of three classes: GM, WM, and CSF [191]. Each tissue map was smoothed with an isotropic Gaussian kernel of 8 mm full width half maximum (FWHM). The resulting maps are considered to reflect local tissue densities[113].

### 3.3.5. Deformation-based morphometry

VBM enables one to identify the *location* of a morphological difference between groups, but it can be difficult to interpret the underlying cause of the difference (i.e. could be due to a change in tissue density or volume). DBM complements VBM because it estimates a surrogate of local brain volume relative to the MNI152 template, which allows for the underlying cause of difference to be interpreted[192]. It consists of spatially transforming each MRI non-linearly to

the MNI152 template and provides a deformation field[138]. To characterize volumetric growth and shrinkage, the voxel-wise Jacobian determinant of the deformation field was computed[192].

### 3.3.6. Cortical modeling

Both VBM and DBM are dependent on automated non-linear registration procedures to map each voxel of an individual's MRI to its corresponding location on an atlas brain. This procedure can sometimes fail when applied to the cortex due to wider inter-individual variability in cortical morphology, reducing its effectiveness to detect cortical volume differences. To overcome this limitation, cortical modeling provides a direct quantitative index of cortical thickness useful for detecting subtle cortical thickness differences[99]. Fast Accurate Cortical Extraction (FACE) was used to extract the cortical surface and measure the cortical thickness by deforming polygonal meshes to fit the gray-white matter and pial surface boundaries[158]. Thickness estimates were mapped to the MNI152 average cortical template using non-linear surface registration tools that are more effective than existing registration tools used for VBM and DBM[193]. This was followed by blurring each thickness map with a 20 mm surface-based kernel.

### 3.3.7. Statistical analyses

Voxel-wise general linear models (GLM) were used to compare whole brain maps for Jacobian determinants, tissue densities, and cortical thickness estimates between the HIV-infected and HIV-uninfected group. Additionally, a series of GLM were used to examine the relationship between brain maps and the following HIV-related factors within the HIV-infected group: nadir CD4, current CD4, current plasma viral load, viral suppression status (detectable versus undetectable), CPE score, treatment status (treated versus untreated), and cognitive function as summarized by Rasch analysis. For each model age, gender, ethnicity, and education were included as covariates to account for variance in brain volumes (see section A.3.2. in Appendix for additional details). All models controlled for multiple comparisons by using the standard false discovery rate (FDR) with a false-positive rate of 5%[183]. FDR accounts for multiple comparisons by controlling the number of false positives. It is applied to the uncorrected whole brain statistical maps, where surviving voxels are considered to be statistically significant. A false-positive rate of 5% implies that no more than 5% of all surviving voxels are false positives.

## 3.4. Results

### 3.4.1. Demographics

Table 3.1 summarizes cohort demographics, neuropsychological performance, and clinical characteristics. The majority (75%) of HIV-infected patients had effective viral suppression (<50 copies/mL), and 90% were currently receiving stable HAART. Although the two groups were demographically similar, HIV-infected patients performed significantly worse than HIV-uninfected subjects on neuropsychological testing, whether summarized by NPZ-4 or Rasch scoring ($p < 0.001$).

Table 3.1: Demographic, medical, neuropsychological, and laboratory values for all subjects.

| | **HIV+ (n=125)** | **HIV- (n=62)** | ***p* value** |
|---|---|---|---|
| **Demographics** | | | |
| Mean age (years old) | 47.2 ± 12.2 | 45.4 ± 11.9 | 0.10 |
| Sex (% Male) | 64 | 55 | 0.27 |
| Education (years) | 14.4 ± 2.6 | 14.5 ± 2.2 | 0.25 |
| Ethnicity | | | 0.31 |
| % African American | 67 | 62 | |
| % Caucasian | 33 | 38 | |
| **Clinical and Neuropsychological Characteristics** | | | |
| Duration of HIV infection (years) | 10.5 ± 7.8 | NA | NA |
| % receiving highly active antiretroviral therapy | 90 | NA | NA |
| Central Nervous System Penetration Effectiveness (CPE) Score | 6.70 ± 2.85 | NA | NA |
| Neuropsychological Performance (Rasch Score)[1] | 0.14 ± 1.19 | 1.16 ± 1.08 | **< 0.001** |
| Neuropsychological Performance (NPZ-4)[1] | -0.85 ± 1.27 | -0.14 ± 0.91 | **< 0.001** |
| **Laboratory** | | | |
| Median CD4 (cells/μL) (Quartiles) | 533 (267, 724) | NA | NA |
| Median nadir CD4 (cells/μL) (Quartiles) | 189 (40, 308) | NA | NA |
| Median Log Plasma Viral Load (copies/mL) (Quartiles) | 1.31 (1.30, 1.94) | NA | NA |
| % Virologically Suppressed (<50 copies/mL) | 75 | NA | NA |

[1] Higher scores indicate better performance on neuropsychological test

### 3.4.2. Neuropsychological performance

VBM and DBM analysis revealed that poorer neuropsychological performance in the HIV-infected group, as quantified by Rasch analysis, was strongly correlated with larger lateral ventricle volume ($p < 0.04$). Cortical modeling also revealed a strong relationship between poorer neuropsychological performance and cortical thickness reductions in the left lateral temporal pole, left inferior occipital, right lateral occipital and right inferior lateral frontal cortices in the HIV-infected group ($p < 0.03$) (Figure 3.1).

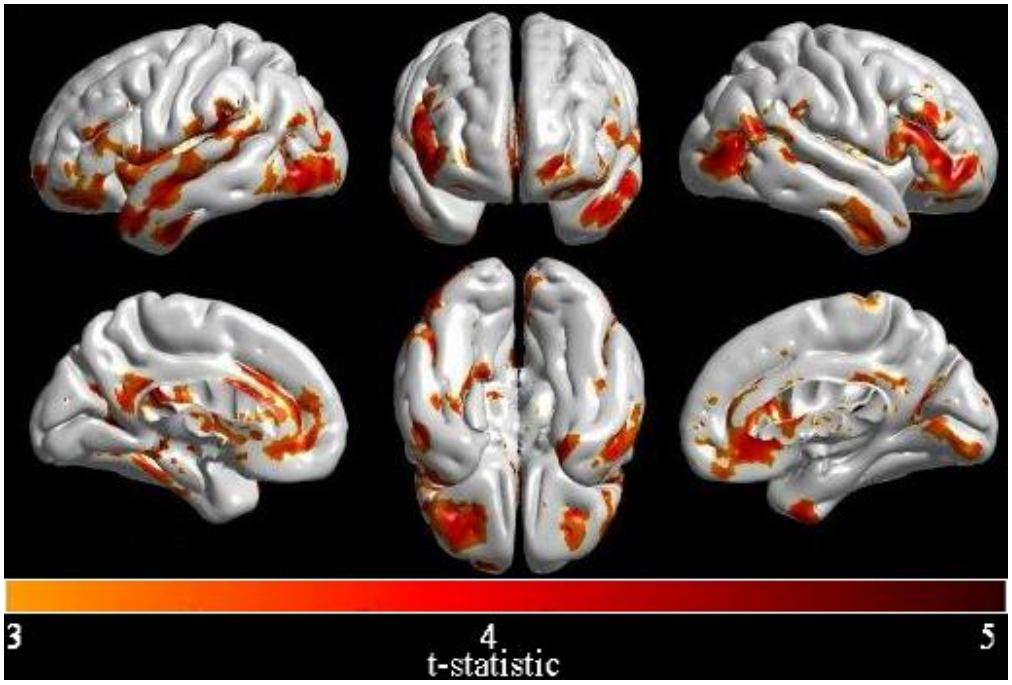


Figure 3.1: Cortical thickness reductions associated with lower neuropsychological performance in the left lateral temporal pole, left inferior occipital, right lateral occipital and right inferior lateral frontal cortices.

### 3.4.3. HIV-infected versus HIV-uninfected

VBM analysis demonstrated that HIV-infected patients had significant reductions in WM densities in the brainstem and thalamus compared to the HIV-uninfected group ($p < 0.03$) (Figure 3.2). No significant tissue density differences in the GM or CSF maps were detected. DBM analysis did not reveal significant volumetric differences between the HIV-infected and HIV-uninfected groups. However, regional patterns of brain volume loss were similar to those seen with VBM when a more lenient statistical threshold was utilized ($p < 0.1$). Cortical modeling revealed significant cortical thickness reductions in the HIV-infected group compared to the HIV-uninfected group ($p < 0.02$) (Figure 3.3). The most pronounced reductions were seen bilaterally in

the temporal and frontal lobes, and right primary motor and sensory cortex. On the medial surfaces, significant cortical thickness reductions were seen in the posterior cingulate, orbitofrontal cortex, and left anterior cingulate.

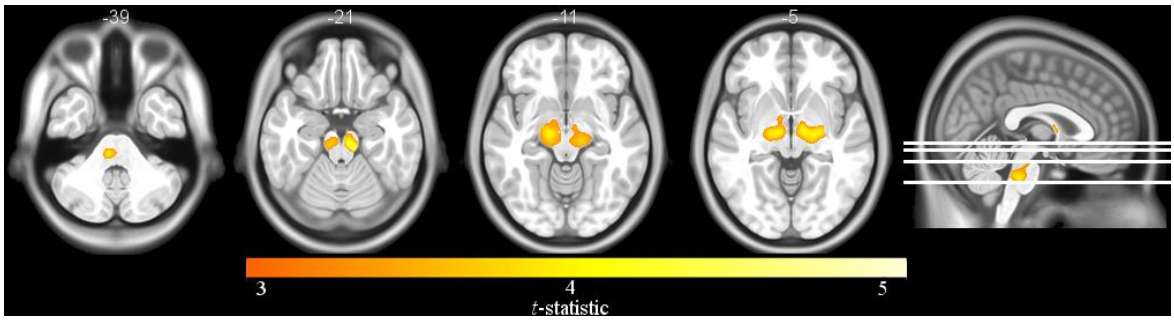


Figure 3.2: Voxel-based morphometry results highlighting WM volume reductions in the brainstem and thalamus of HIV+ patients.

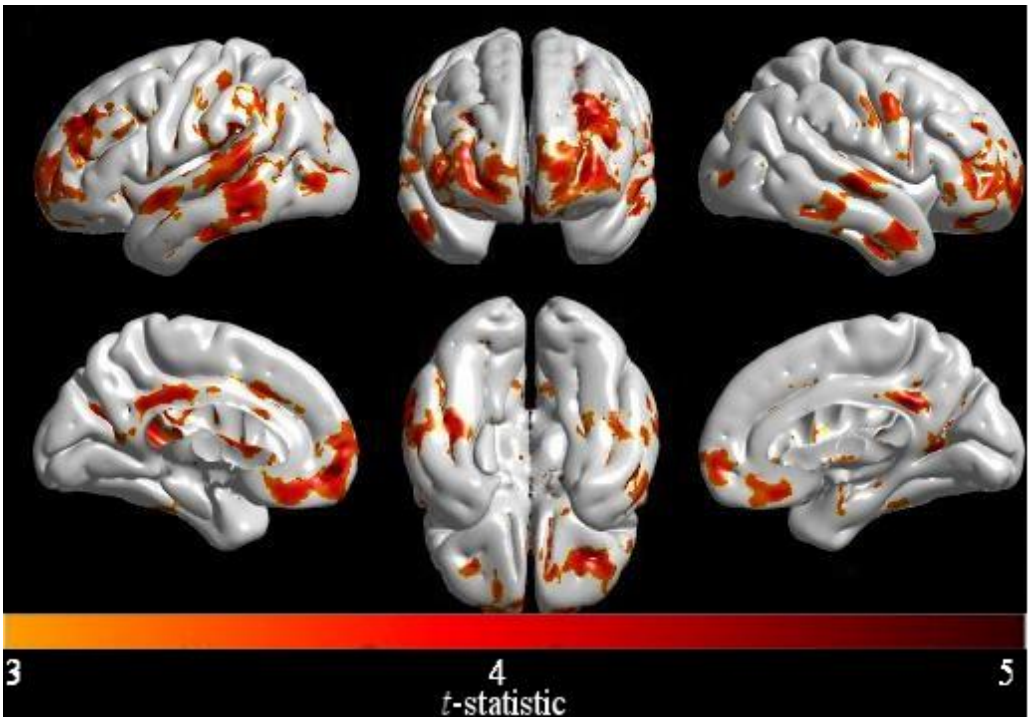


Figure 3.3: Significant cortical thickness reductions in HIV+ patients most pronounced in the lateral temporal and frontal lobes, as well as posterior cingulate, orbitofrontal cortex and left anterior cingulate.

### 3.4.4. Nadir CD4

VBM and DBM analysis revealed significant reductions in WM densities and volumes, respectively, in the brainstem, globus pallidus, internal capsule, caudate, and right frontal lobe associated with lower nadir CD4 ($p < 0.01$). Lower nadir CD4 was also significantly associated with greater CSF volume in the third ventricle (Figure 3.4A/B). In contrast, nadir CD4 was not significantly associated with changes in cortical thickness.

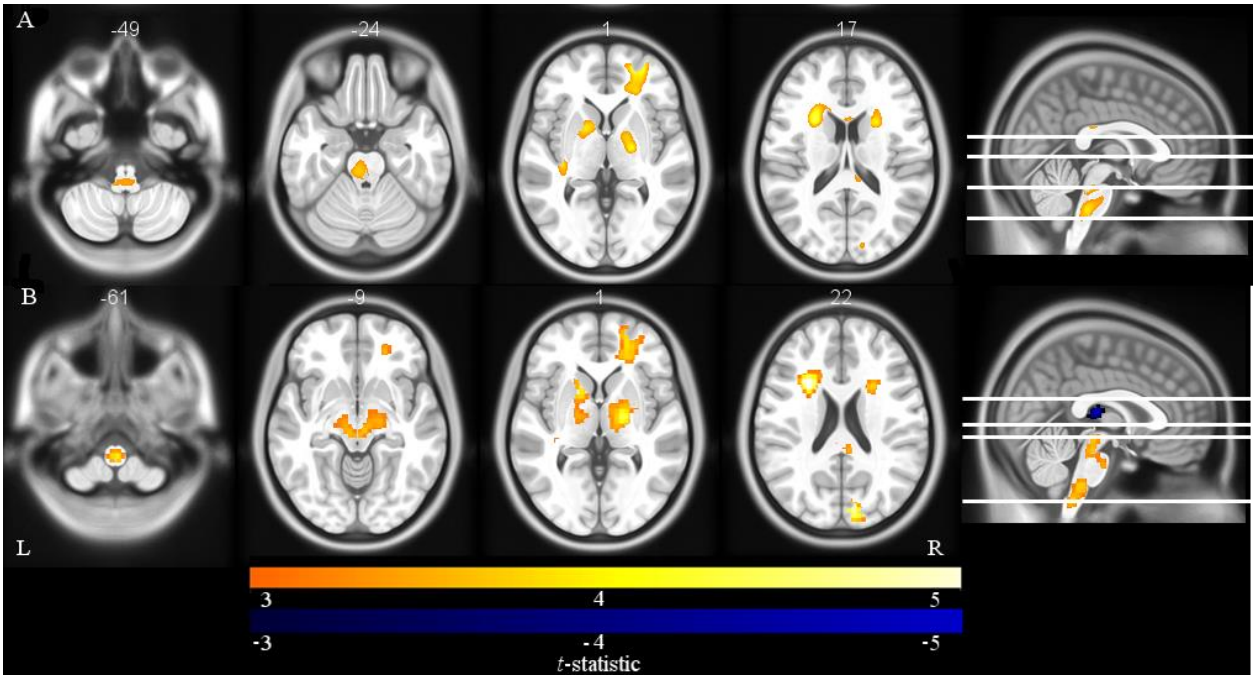


Figure 3.4: A) Voxel-based morphometry results highlighting significant WM volume reductions in brainstem, globus pallidus, internal capsule, caudate, and right frontal lobe associated with lower nadir CD4. B) Deformation-based morphometry results revealing the association of lower nadir CD4 with smaller volumes in the brainstem, thalamus, caudate, putamen, globus pallidus and right frontal lobe, and enlargement of the third ventricle.

### 3.4.5. Current CD4

There were no detectable volumetric or cortical thickness changes associated with current CD4. Additional analysis controlling for historical effects of HIV infection (i.e. nadir CD4) was performed. Similarly, no significant effects were observed.

### 3.4.6. Current Plasma Viral Load

Current viral loads and viral suppression status (detectable versus undetectable viral loads) were not significantly correlated with any brain volume or cortical thickness estimates.

### 3.4.7. Treatment Effects

No significant differences were observed for regional brain volume and cortical thickness estimates in treated and untreated HIV-infected participants. Moreover, no significant correlations were observed between CPE scores and brain volumetric measures.

## 3.5. Discussion

In this study, we took advantage of multiple neuroimaging methods to investigate the spatial distribution of cortical and subcortical volume loss in a group of HIV-infected individuals in the HAART era. We observed significant reductions in cortical thickness throughout the cortex

and WM tissue densities in subcortical structures, and worse cognitive performance in the HIV-infected cohort. HIV-infected patients with a history of more severe immunosuppression had significantly smaller subcortical volumes, but this variable was not related to cortical thickness reductions. In contrast, worse cognitive performance was associated with reduced regional cortical thickness but not subcortical volumes. The results presented provide a detailed characterization of the pattern and extent of brain injury in a diverse group of HIV-infected patients.

Patterns of reduced subcortical integrity were observed in HIV-infected patients compared to a demographically similar HIV-uninfected group. Most notably, VBM analysis revealed reductions in WM tissue density in the brainstem and thalamus. These results are consistent with several prior studies that have reported volume loss in similar regions[50,51,185-187], including diffusion tensor imaging studies that show loss of WM integrity in the thalamus and brainstem of HIV-infected patients[194,195]. The findings here support the hypothesis that subcortical structures are particularly vulnerable to the virus [32], and add spatial detail regarding the distribution of atrophy. Although DBM did not reveal any significant group differences, regional patterns of volumetric loss similar to those seen with VBM were evident at more lenient statistical thresholds. This argues that the observed subcortical differences primarily reflect reductions in WM tissue density rather than volumetric shrinkage, which implies that the underlying pathophysiology may particularly target WM. This also demonstrates the advantage of using VBM and DBM together[192].

While VBM and DBM have the potential to detect cortical volume changes, variability in cortical folding patterns may lead to suboptimal spatial normalization, reducing the statistical power to detect subtle cortical changes. Cortical modeling overcomes this limitation by smoothing highly variable cortical folds and utilizing cortical depth maps to optimally align homologous cortical regions. Cortical modeling revealed that HIV-infected patients had thinner cortices in the temporal and frontal lobes on both hemispheres, right primary motor and sensory cortex, posterior cingulate, orbitofrontal cortex, and left anterior cingulate cortex. The observed cortical thickness differences support findings from a limited number of cortical modeling studies suggesting that HIV infection can lead to significant cortical-based changes[100,101,196].

The HIV-infected group performed significantly worse than demographically similar HIV-uninfected individuals on neuropsychological tests, adding to the growing body of evidence that suggests HIV-related cognitive impairment remains frequent despite effective treatment and

minimal comorbidities[7]. Regional cortical thickness reductions were related to poorer neuropsychological performance in the left lateral temporal pole, left inferior occipital, right lateral occipital and right inferior lateral frontal cortices, effects that presumably reflect the regions engaged by the particular set of cognitive tests administered. In contrast, subcortical volume changes were not significantly related to overall performance. These differential results may reflect the fact that the neuropsychological tests that were administered primarily assess cortical-hemispheric functions and might be less sensitive to subcortical dysfunction, *a priori*.

To assess whether brain volume changes were influenced by variables related to the infection, brain volumes were correlated with nadir CD4, current CD4, viral load, and CPE measures within the HIV-infected group. VBM and DBM analysis revealed that HIV-infected patients with a history of more severe immunosuppression, indexed by nadir CD4, had significant reductions in WM density and smaller volumes in the brainstem, thalamus, caudate, putamen, globus pallidus, internal capsule and right frontal lobe, as well as greater enlargement of the third ventricle. This finding is consistent with the existing literature[49,50,62,64,73,197] supporting the theory that volume loss, in part, occurs during the time of untreated infection[5,48] suggesting that early initiation of HAART might be beneficial for long term brain integrity. Longitudinal data is required to determine whether these are static changes, arrested by HAART, or continue to develop despite HAART.

Interestingly cortical modeling did not reveal any cortical thickness reductions associated with the severity of immunosuppression. This confirms, in a much larger sample, the results of a prior cortical modeling study, which likewise found no relationship between the cortical thickness estimates and nadir CD4[101]. The differential results argues that the underlying pathogenesis of injury between subcortical and cortical structures may be different or progress at different rates in the presence of the virus[101,198]. In particular, cortical thinning may be secondary to subcortical dysfunction[196] possibly mediated by subcortical WM destruction[101]. However, the underlying pathophysiology of cortical thinning in HIV-infected patients remains unknown, and should be addressed in future work.

The association between brain volumes and nadir CD4 reported here add further weight to a considerable body of existing evidence. However, there is less consensus as to the relationship between other HIV-related factors (current CD4, viral load, and treatment status) and brain structural measures. Inconsistencies likely reflect differences in degree of infection severity in HIV

cohorts, as well as limitations of sample size and imaging analytic approaches, with most studies relying on a single method. Here, the large sample with wide variance in HIV-related variables, and the comprehensive approach to characterizing regional brain volumes are strengths that allow the brain volume relations with current CD4, viral load, and treatment status to be thoroughly explored.

Despite the power afforded by the large sample size, indices of current infection severity, including current CD4, viral load, and viral suppression status, were not associated with subcortical or cortical changes. While a few studies have reported that increasing viral loads were associated with decreased caudate, thalamus, frontal and parietal lobe volumes[49,62], accumulating reports in the HAART era have not detected such relationships[5,48,51,64,100,101] suggesting that the use of blood markers, particularly plasma viral loads, may not be sensitive enough to monitor brain injury once treatment is initiated. However, the current study may not have detected such relationships due to the small number of HIV-infected patients with detectable viral loads (n=31), with few patients (n=9) having high viral loads (>1000 copies/mL). Further studies are needed to clarify whether plasma viral load relates reliably to brain integrity in patients with poor control despite HAART.

The effects of HAART on brain integrity were assessed by comparing brain volume estimates in treated and untreated HIV-infected patients, and correlating with CPE scores. No significant differences, or correlations, with any volumetric measures were revealed. Although this finding is consistent with prior studies, and suggests that higher penetrating regimens do not significantly influence brain volumes[5,51,64,185], this study was not designed to determine the neuro-protective or toxic effects of HAART. The small untreated group (n=13) and limited number of regimens prescribed to most participants (average CPE Score = 6.70 ± 2.85) means that this sample is not well suited to address this question. Studies with larger variability of treatment regimens would be needed to fully test this hypothesis.

This study has limitations. First, causal inferences cannot be made based on cross-sectional data. Validation of these results and unraveling the underlying pathogenesis of brain dysfunction will require longitudinal studies that track brain volumes from primary to chronic HIV infection. Second, recent evidence has found that cardiovascular risk factors are elevated in HIV-infected patients, particularly those with longer infection and treatment duration, and were related to WM damage and cognitive deficits[199]. Unfortunately, data on cardiovascular risk factors were not

acquired in the present study, so the possibility of vascular injury causing the observed changes cannot be fully discounted. Further work is needed to establish the contribution of vascular injury to brain structure and function.

In conclusion, this study applied multiple advanced analytic approaches to explore the spatial distribution of changes on brain structure in HIV-infected patients in the HAART era. Significant volume reductions were detected in the HIV-infected group, primarily in subcortical WM, and these reductions were associated with previous episodes of immunosuppression. Regionally specific reductions in cortical thickness were also detected between HIV-infected and uninfected groups. However, the cortical thickness reductions were not predicted by nadir CD4. Collectively, the results reported here suggests that distinct mechanisms may underlie subcortical and cortical injury, and demonstrates that subcortical injury most likely occurs during the time of untreated infection suggesting that treatment with HAART as early as possible might mitigate brain injury. Longitudinal investigations to confirm these reports are warranted.

## 3.6. Chapter 3 Reference List


5. Ances BM, Orteg M, Vaida F, Heaps J, Paul R. Independent Effects of HIV, Aging and HAART on Brain Volumetric Measures. J Acquir Immune Defic Syndr **2012**; 59(5): 469-77.
7. Heaton RK, Clifford DB, Franklin DR, et al. HIV-associated neurocognitive disorders persist in the era of potent antiretroviral therapy: CHARTER Study. Neurology **2010**; 75(23): 2087-96.
8. Mothobi NZ, Brew BJ. Neurocognitive dysfunction in highly active antiretroviral therapy era. Curr Opin Infect Dis **2012**; 25(1): 4-9.
32. Ances BM, Ellis RJ. Dementia and Neurocognitive Disorders Due to HIV-1 Infection. Semin Neurol **2007**; 27(1): 86-92.
37. Heaton RK, Franklin DR, Ellis RJ, et al. HIV-associated neurocognitive disorders before and during the era of combination antiretroviral therapy: Differences in rates, nature and predictors. J Neurovirol **2011**; 17(1): 3-16.
48. Becker JT, Sanders J, Madsen SK, et al. Subcortical brain atrophy persists even in HAART-regulated HIV disease. Brain Imaging Behav **2011**; 5(2): 77-85.

49. Cardenas VA, Meyerhoff DJ, Studholme C, et al. Evidence for ongoing brain injury in human immunodeficiency virus-positive patients treated with antiretroviral therapy. J Neurovirol **2009**; 15(4): 324-33.
50. Kallianpur KJ, Shikuma C, Kirk GR, et al. Peripheral blood HIV DNA is associated with atrophy of cerebellar and subcortical gray matter. Neurology **2013**; 80(19): 1792-9.
51. Chiang M, Dutton RA, Hayashi KM, et al. 3D pattern of brain atrophy in HIV/AIDS visualized using tensor-based morphometry. Neuroimage **2007**; 34(1): 44-60.
61. Ragin AB, Du H, Ochs R, et al. Structural brain alterations can be detected early in HIV infection. Neurology **2012**; 79(24): 2328-34.
62. Cohen RA, Harezlak J, Schifitto G, et al. Effects of Nadir CD4 Count and Duration of HIV Infection on Brain Volumes in the HAART Era. J Neurovirol **2010**; 16(1): 25-32.
64. Hua X, Boyle CP, Harezlak J, et al. Disrupted cerebral metabolite levels and lower nadir CD4+ counts are linked to brain volume deficits in 210 HIV-infected patients on stable treatment. Neuroimage Clin **2013**; 3: 132-42.
70. Letendre S, Marquie-Beck J, Capparelli E, et al. Validation of CNS Penetration-Effectiveness Rank for Quantifying Antiretroviral Penetration into the Central Nervous System. Arch Neurol **2008**; 65(1): 65-70.
71. Holt JL, Kraft-Terry SD, Chang L. Neuroimaging studies of the aging HIV-1-infected brain. J Neurovirol **2012**; 18(4): 291-302.
73. Jernigan TL, Archibald SL, Fennema-Notestine C, et al. Clinical factors related to brain structure in HIV: the CHARTER study. J Neurovirol **2011**; 17(3): 248-57.
92. Thompson PM, Jahanshad N. Novel Neuroimaging Methods to Understand How HIV Affects the Brain. Curr HIV/AIDS Rep **2015**; 12(2): 289-98.
99. Lyttelton O, Boucher M, Robbins S, Evans AC. An unbiased iterative group registration template for cortical surface analysis. Neuroimage **2007**; 34(4): 1535-44.
100. Thompson PM, Dutton RA, Hayashi KM, et al. Thinning of the cerebral cortex visualized in HIV/AIDS reflects CD4+ T lymphocyte decline. Proc Natl Acad Sci USA **2005**; 102(43): 15647-52.
101. Kallianpur KJ, Kirk GR, Sailasuta N, et al. Regional Cortical Thinning Associated with Detectable Levels of HIV DNA. Cereb Cortex **2011**; 22(9): 2065-75.

102. Becker JT, Maruca V, Kingsley LA, et al. Factors affecting brain structure in men with HIV disease in the post-HAART era. Neuroradiology **2012**; 54(2): 113-21.
106. Sled JG, Zijdenbos AP, Evans AC. A nonparametric method for automatic correction of intensity nonuniformity in MRI data. IEEE Trans Med Imaging **1998**; 17(1): 87-97.
111. Collins DL, Neelin P, Peters TM, Evans AC. Automatic 3D intersubject registration of MR volumetric data in standardized Talairach space. J Comput Assist Tomogr **1994**; 18(2): 192-205.
113. Ashburner J, Friston KJ. Voxel-Based Morphometry - The Methods. Neuroimage **2000**; 11(6): 805-21.
122. Eskildsen SF, Coupe P, Fonov V, et al. BEaST: Brain Extraction based on nonlocal Segmentation Technique. Neuroimage **2012**; 59(3): 2362–73.
138. Collins DL, Holmes CJ, Peters TM, Evans AC. Automatic 3-D model-based neuroanatomical segmentation. Hum Brain Mapp **1995**; 3(3): 190-208.
158. Eskildsen SF, Østergaard LR. Active Surface Approach for Extraction of the Human Cerebral Cortex from MRI. Med Image Comput Comput Assist Interv **2006**; 9: 823-30.
173. Brouillette M, Mayo N, Fellows LK, et al. A better screening tool for HIV-associative neurocognitive disorders: is it what clinicians need? AIDS **2015**; 29: 895-902.
183. Genovese CR, Lazar NA, Nichols T. Thresholding of Statistical Maps in Functional Neuroimaging Using the False Discovery Rate. Neuroimage **2002**; 15(4): 870-8.
185. Küper M, Rabe K, Esser S, et al. Structural gray and white matter changes in patients with HIV. J Neurol **2011**; 258(6): 1066-75.
186. Janssen MAM, Meulenbroek O, Steens SCA, et al. Cognitive function, wellbeing and brain correlates in HIV-1 infected patients on long-term combination antiretroviral therapy. AIDS **2015**; 29(16): 2139-48.
187. Wade BSC, Valcour VG, Wendelken-Riegelhaupt L, et al. Mapping abnormal subcortical brain morphometry in an ederly HIV+ cohort. Neuroimage Clin **2015**; 9: 564-73.
188. Castelo JMB, Courtney MG, Melrose RJ, Stern CE. Putamen Hypertrophy in Nondemented Patients With Human Immunodeficiency Virus Infection and Cognitive Compromise. Arch Neurol **2007**; 64(9): 1275-80.
189. Ances BM, Hammoud DA. Neuroimaging of HIV Associated Neurocognitive Disorders (HAND). Curr Opin HIV AIDS **2014**; 9(6): 545-51.

190. Coupe P, Yger P, Prima S, Hellier P, Kervrann C, Barillot C. An optimized blockwise nonlocal means denoising filter for 3D magnetic resonance images. IEEE Trans Med Imaging **2008**; 27(4): 425-41.
191. Zijdenbos AP, Forghani R, Evans AC. Automatic 'pipeline' analysis of 3-D MRI data for clinical trials: application to multiple sclerosis. IEEE Trans Med Imaging **2002**; 21(10): 1280-91.
192. Ashburner J, Hutton C, Frackowiak R, Johnsrude I, Price C, Friston KJ. Identifying Global Anatomical Differences: Deformation-Based Morphometry Hum Brain Mapp **1998**; 6(5-6): 348-57.
193. Collins DL, Le Goualher G, Evans AC. Non-linear cerebral registration with sulcal constraints. In: Wells WM, Colchester A, Delp S. Medical Image Computing and Computer-Assisted Interventation — MICCAI'98: First International Conference Cambridge, MA, USA, October 11–13, 1998 Proceedings. Berlin: Springer, **1998**:974-84.
194. Nir TM, Jahanshad N, Busovaca E, et al. Mapping white matter integrity in elderly people with HIV. Hum Brain Mapp **2014**; 35(3): 975-92.
195. Wright PW, Vaida FF, Fernández RJ, et al. Cerebral white matter integrity during primary HIV infection. AIDS **2015**; 29(4): 433-42.
196. Plessis Sd, Vink M, Joska JA, et al. Prefrontal cortical thinning in HIV infection is associated with impaired striatal functioning. J Neural Transm **2016**; 123(6): 643-51.
197. Pfefferbaum A, Rosenbloom MJ, Sassoon SA, et al. Regional Brain Structural Dysmorphology in HIV Infection: Effects of AIDS, Alcoholism, and Age. Biol Psychiatry **2012**; 72(5): 361-70.
198. Moore DJ, Masliah E, Rippeth JD, et al. Cortical and subcortical neurodegeneration is associated with HIV neurocognitive impairment. AIDS **2006**; 20(6): 879-87.
199. Kuller LH, Lopez OL, Newman A, et al. Risk factors for dementia in the cardiovascular health cognition study. Neuroepidemiology **2003**; 22(1): 13-22.

## Chapter 4: Association of Brain Structure Changes and Cognitive Function with Combination Antiretroviral Therapy in HIV-Positive Individuals

The cross-sectional study in Chapter 3 established that reduced brain volumes and poorer cognitive function were still evident in people living with HIV, despite being on suppressive cART. However, causal inferences cannot be made with cross-sectional data, which makes it difficult to disentangle whether the brain changes occurred in early infection, before treatment initiation, or caused by an ongoing, destructive process in the CNS. In the current literature, multiple neuroimaging studies have provided evidence of an ongoing process to be the cause of the brain atrophy and cognitive decline in the cART era[49,66,67]. However, since these studies included HIV+ participants that had advanced disease and poor viral control, the findings that may not generalize-well to cART-treated individuals with good viral control, which is very common in the cART era.

In the following longitudinal study, we used multiple advanced MRI processing methods, TBM, VBM and cortical modeling, to assess whether detectable brain changes and cognitive decline occurs over two years in 48 cART-treated HIV+ individuals with good viral suppression compared to 31 demographically similar controls. We observed significant reductions in cortical thickness and subcortical volumes and poorer cognitive function in the HIV+ group compared to controls at baseline and follow-up visits. However, the rate of change in brain volume and cognitive function were similar between the groups over two years. These findings demonstrate that stable treatment with good viral suppression may prevent progressive of brain atrophy and cognitive decline, supporting the hypothesis that brain injury pre-dates treatment initiation suggesting a possible neurocognitive benefit from early treatment.

# Association of Brain Structure Changes and Cognitive Function with Combination Antiretroviral Therapy in HIV-Positive Individuals

Ryan Sanford[1], MEng; Lesley K. Fellows[1] MD CM, DPhil; Beau M. Ances[2], MD, PhD and D. Louis Collins[1] PhD

[1] Department of Neurology and Neurosurgery, Montreal Neurological Institute, McGill University, 3801 University Street, Montréal, Québec, Canada H3A 2B4

[2] Department of Neurology, Washington University, Box 8111, 660 South Euclid, St. Louis, Missouri, USA 63110

*JAMA Neurology. 2018; Volume: 74; Issue: 1.*

## 4.1. Abstract

**Importance:** Despite the introduction of combination antiretroviral therapy (cART), HIV-associated neurocognitive disorders continue to be a problem for treated HIV+ individuals. The cause of this impairment remains unclear.

**Objective:** To determine if detectable brain changes occurs over two years in cART-treated, aviremic HIV+ individuals.

**Design:** In this longitudinal case-control study, participants underwent neuroimaging and neuropsychological assessment approximately two years apart. Data were collected from October 2011 to March 2016.

**Setting:** Patient data were acquired at Washington University in St. Louis from ongoing studies conducted in the infectious disease clinic and AIDS Clinical Trial Unit. HIV- control participants were recruited from the St. Louis community and a research participant registry.

**Participants:** Forty-eight cART-treated, aviremic HIV+ individuals and 31 demographically-similar HIV- controls were included in the study.

**Main Outcomes and Measures:** Brain volumes were extracted with tensor- and voxel-based morphometry, and cortical modeling. Raw scores from neuropsychological tests quantified cognitive performance. Multivariable mixed-effects models assessed the effect of HIV serostatus

on brain volumes and cognitive performance, and determined if HIV serostatus affected how these measures changed over time. With HIV+ participants, linear regression models tested if brain volumes and cognitive performance were associated with measures of infection severity and duration of infection.

**Results:** The two groups were demographically similar (HIV+ age: 47±13, education: 13±3, sex: 52% male; HIV- age: 51±13, education: 14±2, sex: 48% male). HIV+ participants had poorer neuropsychological test scores compared to controls. Changes in neuropsychological scores over time were not significantly different between the groups for any test. Cortical thickness and subcortical volumes were smaller in HIV+ individuals compared to controls. However, changes in brain volume over time were similar between the groups. Sensitivity analysis demonstrated that this study was powered to detect differences in brain volume loss between the groups as small as 0.1%/year in subcortical regions and 0.01mm/year in cortical thickness. Lower nadir CD4 was related to smaller subcortical volumes, but not cortical thickness.

**Conclusions and Relevance:** These findings are consistent with the idea that cognitive and structural brain changes may occur early after seroconversion, and argue that maintaining aviremia with cART can prevent or minimize progressive brain injury.

## 4.2. Introduction

The introduction of combination antiretroviral therapy (cART) has transformed HIV from a fatal disease to a chronic condition. However, HIV-associated neurocognitive disorders (HAND) are still prevalent, affecting up to 40% of HIV+ individuals despite effective viral suppression[7]. The etiology of this mild, but quality-of-life limiting brain dysfunction remains unclear.

Recently, a few studies have reported that while HAND remains common, progressive worsening is uncommon, with only a small proportion of HIV+ individuals on stable treatment with good viral suppression showing cognitive decline as assessed with repeated neuropsychological testing over three to four years[47,75,76,200]. However, it is unclear whether effective viral suppression can mitigate the progression of brain atrophy. Previous neuroimaging studies have provided evidence for ongoing brain atrophy in HIV+ individuals with advanced disease and poor viral control[49,66,67], but those results may not generalize to cART-treated individuals who have viral suppression. A recent neuroimaging study reported no longitudinal changes in cortical thickness, deep gray matter volumes, or white matter integrity in cART-treated HIV+ individuals with undetectable viral loads over two years[77]. However, this study included

only 21 participants, had no HIV- comparison group, and extracted brain measures only from pre-defined regions of interest.

In this longitudinal study, we sought evidence of ongoing brain atrophy over two years using structural magnetic resonance imaging (MRI) and neuropsychological assessment in a larger sample of treated, virologically well-controlled HIV+ group, compared to demographically similar HIV- controls. We characterized brain volumes as seen on MRI by applying multiple advanced neuroimaging processing methods (tensor-based morphometry (TBM), voxel-based morphometry (VBM) and cortical modeling), and assessed cognitive function with a standard battery of neuropsychological tests.

## 4.3. Methods

### 4.3.1. Standard protocol approvals, registrations, and patient consents

Washington University in St. Louis (WUSTL) Institutional Review Board approved the study. Written informed consent was obtained from all participants.

### 4.3.2. Participants

HIV+ participants were selected from ongoing studies conducted in the infectious disease clinic and the AIDS Clinical Trial Unit at WUSTL from October 2011 to March 2016. Demographically similar HIV- control participants were recruited from the St. Louis community by leaflets and a research participant registry at WUSTL. Participants were not eligible to enter the studies at WUSTL if they had a history of confounding neurological disorders, current or past opportunistic central nervous system (CNS) infection, traumatic brain injury (loss of consciousness >30 minutes), major psychiatric disorders, or an active substance abuse and dependence diagnosis according to Diagnostic and Statistics Manual of Mental Disorders 4$^{th}$ edition criteria. The present study included HIV+ and HIV- participants who had completed two MRI and neuropsychological testing sessions at least 1.5 years apart. HIV+ participants were on stable cART with undetectable viral loads (<50 copies/ml) at baseline and follow-up visits. Participants were excluded if they had extensive white matter hyperintensities on $T_2$-weighted MRI as defined by an expert neurologist (B.M.A.). All participants who met these criteria were included in the analysis, yielding 48 HIV+ and 31 HIV- participants. A CONSORT diagram showing the participant selection process is provided in Figure 4.1. For all HIV+ participants, a CNS penetration effectiveness (CPE) score was generated based on previous methods[70].

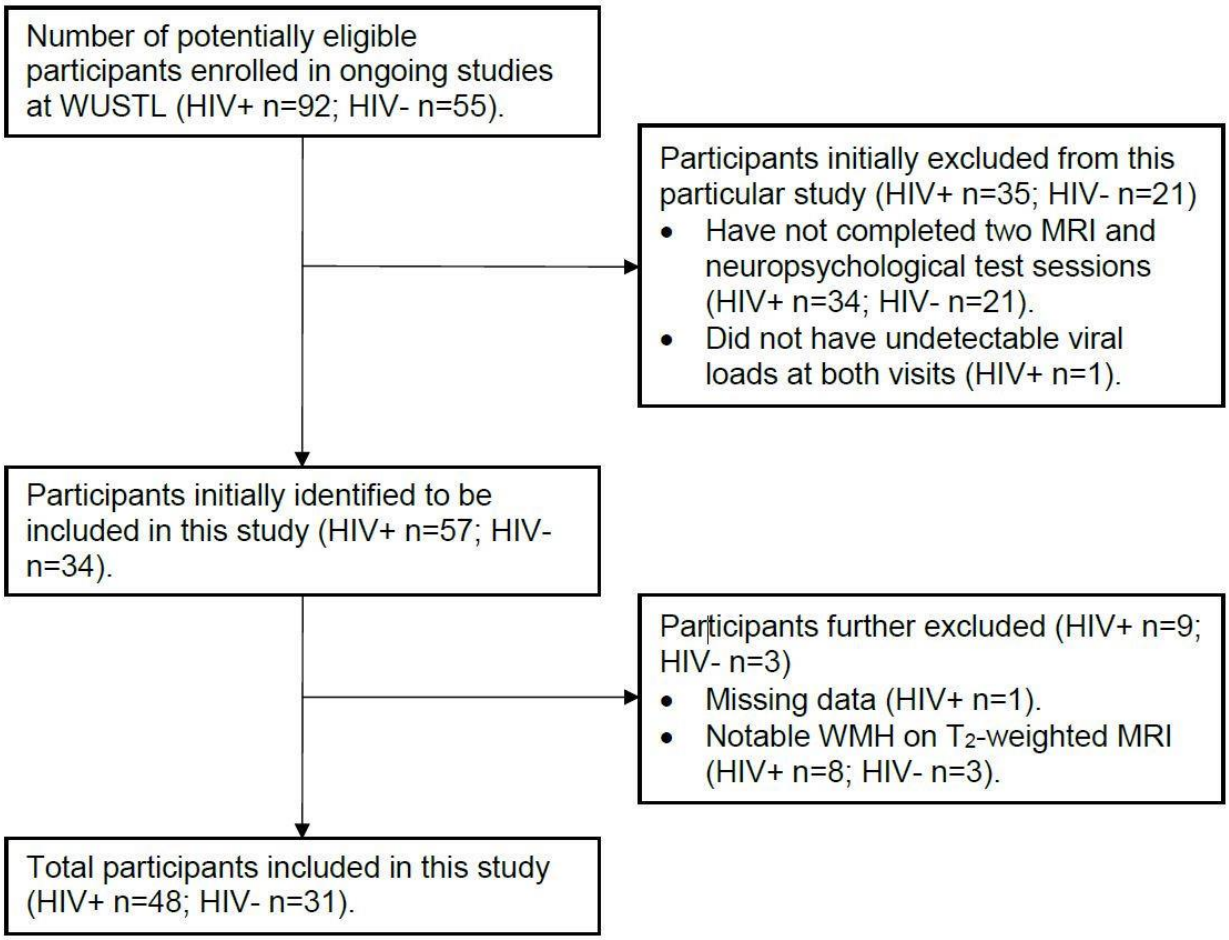


Figure 4.1: Study CONSORT diagram.

### 4.3.3. Neuropsychological testing

All participants underwent a neuropsychological assessment at both visits that consisted of eight standard tests recommended to assess HAND[45]: Trail Making Test Part A and B, Digit Symbol Substitution Task, Letter-Number Sequencing, Letter Fluency (FAS), Action (verb naming) Fluency, Hopkins Verbal Learning Test–Revised (HVLT-R) immediate and delayed recall. All participants also completed the Wide Range Achievement Test (WRAT-3) reading subtest to estimate premorbid intellectual ability[201]. Functional limitation in activities of daily living was not assessed.

### 4.3.4. MRI acquisition

All participants at both visits underwent MRI using the same 3T Siemens Tim TRIO whole-body magnetic resonance scanner with a 12-channel transmit/receive head coil at WUSTL. The scanning protocol included $T_1$-weighted three-dimensional magnetization-prepared rapid

acquisition gradient echo sequence [repetition time (TR)/echo time (TE)/inversion time (TI)=2400/3.16/1000ms; voxel=1.0mm$^3$], and $T_2$-weighted Fast Spin Echo sequence [TR/TE=3200/460ms; voxel=1.0mm$^3$].

#### 4.3.5. MRI processing

$T_1$-weighted data was processed using a longitudinal pipeline, as previously described[202]. Pre-processing included denoising[190], intensity inhomogeneity removal[106] and brain masking[122]. Images were linearly registered to the Montreal Neurological Institute ICBM152 template using a nine-parameter affine transform to correct for variations in head size and orientation[111]. To ensure the registrations to the ICBM152 space were consistent across all time points, a subject-specific template was created using an unbiased template creation approach[136]. This subject-specific template creation process yields nonlinear transformations that maps each visit to the ICBM152 space in a consistent manner reducing the intra-subject variability in brain volume measures across visits, increasing the statistical power to detect changes within-subject. [138,202].[203]. All data were carefully inspected for unacceptable processing outcomes. All data passed visual quality control, and were available for TBM, VBM, and cortical modeling.

#### 4.3.6. Tensor-based morphometry (TBM)

TBM provides a voxel-wise estimate of brain structure volume relative to the ICBM152 template. Structural volumes were calculated by taking the Jacobian determinant of the deformation field from the nonlinear transform[113].

#### 4.3.7. Voxel-based morphometry (VBM)

VBM provides a voxel-wise estimate of the amount of gray matter, white matter, and cerebrospinal fluid (CSF)[113]. Following spatial normalization to the ICBM152 space, each voxel was identified as gray matter, white matter, or CSF[203]. The tissue maps were then modulated by the Jacobian determinants of the nonlinear transform. Resulting modulated tissue maps were smoothed with an 8-mm FWHM Gaussian kernel.

#### 4.3.8. Cortical Modeling

Cortical modeling provides a quantitative measure of cortical thickness. Cortical thickness estimates were extracted with Fast Accurate Cortical Extraction by deforming polygonal meshes to fit the gray-white matter and pial surface boundaries[158]. Thickness estimates were mapped to

the ICBM152 average cortical template using an iterative feature-based registration algorithm[204], and blurred with a 20mm surface-based kernel.

#### 4.3.9. Statistical analysis

Multivariable mixed-effects models were used to assess neuropsychological test performance, while voxel-wise and vertex-wise mixed-effects models were used to assess regional brain volumes, estimated with TBM, VBM and cortical modeling, from all available data at both visits. To compare neuropsychological scores and brain volumes by HIV serostatus, and to determine if changes in these measures over two years were significantly different between the HIV+ and HIV- groups, a mixed-effects model included fixed effects for HIV serostatus, time (years from baseline visit), average age (mean of age at baseline and follow-up), sex, and HIV serostatus by time interaction, and a subject-specific random intercept. Within each group, independent mixed-effects frameworks modeled time, age and sex as fixed effects, along with subject-specific random intercepts, to test if significant changes in test scores and brain volumes occurred between visits. Within the HIV+ group, linear regressions were used to explore the relationship between neuropsychological scores and brain volumes with the following HIV-related factors: current and nadir CD4 cell counts, CPE score, and duration of infection. These models were only applied to baseline data. Additional linear regressions tested whether baseline current CD4 cell counts and CPE score predicted neuropsychological scores and brain volumes at follow-up. Statistical significance was set at a *P* value less than 0.05 for all models that assessed neuropsychological performance. Whole brain statistical maps were corrected for multiple comparisons using the standard false discovery rate with a false-positive rate of 5%[183]. (Additional information on model structures can be found in section A.4.1. in the Appendix).

### 4.4. Results

#### 4.4.1. Participants

Table 4.1 summarizes baseline demographic and clinical characteristics of study participants. The HIV+ and HIV- participants were comparable with respect to age, sex, education, ethnicity, and history of drug use. The HIV+ group tended to have lower WRAT-3 reading scores compared to HIV- controls, although these differences did not reach statistical significance after controlling for age, sex and education (-2.4 raw score, 95% Confidence interval (CI): -3.9 to -0.9; $p$=0.09). Both groups had similar time periods between visits (HIV+: 2.1±0.08 years; HIV-: 1.9±0.32 years). All HIV+ participants were on stable cART throughout the study period.

Table 4.1. Baseline demographic and clinical characteristics of study participants.

| | **HIV+ (n=48)** | **HIV- (n=31)** | ***p* value**[a] |
|---|---|---|---|
| Age [years, mean (SD)] | 47.7 (13.2) | 51.2 (12.9) | 0.25 |
| Sex [n (% male)] | 25 (52) | 15 (48) | 0.93 |
| Ethnicity [n (%)] | | | 0.12 |
| White | 15 (31) | 16 (52) | |
| African-American | 33 (69) | 15 (48) | |
| Education [years, mean (SD)] | 13.3 (3.4) | 14.5 (2.1) | 0.09 |
| WRAT-3 reading [mean (SD)] | 43.8 (8.9) | 48.1 (6.1) | 0.09 [b] |
| Current CD4 [cells/µl, median (IQR)] | 630 (486, 881) | NA | |
| Nadir CD4 [cells/µl, median (IQR)] [c] | 190 (57, 300) | NA | |
| Estimated Duration of HIV infection [years, median (IQR)] [d] | 13.5 (5.2, 20) | NA | |
| Hepatitis-C co-infection [n (%)] | 1 (2) | 0 (0) | 0.3 |
| CPE Score [median (range)] | 7.5 (5, 13) | NA | |
| Past Substance Use [n (%)] [d] | | | |
| Marijuana | 5 (10) | 3 (10) | 0.9 |
| Meth | 1 (2) | 1 (3) | 0.8 |
| Opiates | 1 (2) | 1 (3) | 0.8 |

[a] *p* value determined using Student's *t*-test (age and education) or chi-square test (sex, ethnicity, past substance use, and hepatitis-C co-infection), unless otherwise stated.

[b] *p* value computed from a linear regression model. WRAT-3 reading score was the dependent variable and HIV serostatus, age, sex and education were independent variables.

[c] 7 participants missing nadir CD4.

[d] Based on patient's self-report.

### 4.4.2. Neuropsychological performance

HIV+ participants had lower neuropsychological scores compared to HIV- participants on Trail Making Test Part A (5.9 sec, 95% CI: 1.5 to 10.3; $p$=0.01) and B (27.3 sec, 95% CI: 15.0 to 39.6; $p$<0.001), Digit Symbol Substitution Task (-12.5 marks, 95% CI: -18.9 to -6.0; $p$<0.001), Letter-Number Sequencing (-2.5 marks, 95% CI: -3.7 to -1.3; $p$<0.001), Letter Fluency (-6.6 words, 95% CI: -11.5 to -1.6; $p$=0.01) and HVLT-R immediate recall (-2.4 words, 95% CI: -4.4 to -0.4; $p$=0.05), after adjusting for age, sex and education (see Table S2 in section A.4.1. in Appendix). No differences in HVLT-R delayed recall or Action Fluency were observed.

The primary analysis compared changes in neuropsychological scores over time by HIV serostatus. Improvements in test scores were observed in Letter Fluency in HIV+ (1.4 words/year, 95% CI: 0.5 to 2.3; $p$=0.003) and HIV- participants (1.7 words/year, 95% CI: 0.2 to 3.3; $p$=0.02), and Digit Symbol Substitution Task in the HIV+ group (1.1 marks/year, 95% CI: 0.3 to 2.0; $p$=0.02). Only changes in Trail Making Test Part A scores differed between the groups (-1.9 sec/year, 95% CI: -3.8 to -0.02; $p$=0.03): the HIV+ group had greater improvements compared to HIV- individuals over time. No significant interactions between HIV serostatus and time were detected in other neuropsychological tests.

Neuropsychological scores did not correlate with current CD4, nadir CD4, CPE score or duration of infection. Additionally, baseline current CD4 and CPE scores did not predict neuropsychological performance at follow-up.

**4.4.3. Brain volumes**

Comparing brain volumes revealed reduced cortical thickness and smaller subcortical volumes in the HIV+ group compared to controls (Figure 4.2). Cortical thickness differences were detected in bilateral primary sensory and motor cortex, superior temporal gyrus and poles, middle and posterior cingulate cortex, and left frontal lobe (Figure 4.2A). TBM and VBM revealed significantly smaller subcortical volumes and reduced white matter volumes, respectively, in the thalamus, caudate, putamen, globus pallidus, brainstem, and midbrain of HIV+ participants (Figure 4.2B). Modeling brain volumes over time did not reveal significant differences in the changes in regional volume or cortical thickness between the groups. The changes in these brain volume estimates over time were similar between the groups.

Power calculations were done to aid in interpreting the absence of detectable differences in brain volume change. This analysis showed that differences in brain volume loss between the groups ranging from 0.1 to 6.0%/year (median (IQR): 0.90%/year (0.71, 1.12)) could have been detected, if present, when brain volumes were estimated with TBM or VBM (see Figure S2 in section A.4.2. in Appendix). Likewise, differences in cortical thickness changes between groups ranging from 0.01 to 0.5mm/year (median (IQR): 0.08mm/year (0.07, 0.1)) could have been detected, if present, using cortical modeling (see Figure S3 in section A.4.2. in Appendix).

Lower nadir CD4 counts were significantly correlated with reduced white matter volumes and smaller brain volumes in the putamen, globus pallidus, and thalamus, as revealed with VBM and TBM (Figure 4.3). In contrast, no correlations between nadir CD4 counts and cortical

thickness estimates were observed. The remaining HIV-related factors (current CD4, CPE score, and duration of infection) were not associated with any brain volume estimates. Baseline current CD4 and CPE score did not significantly predict brain volumes at follow-up.

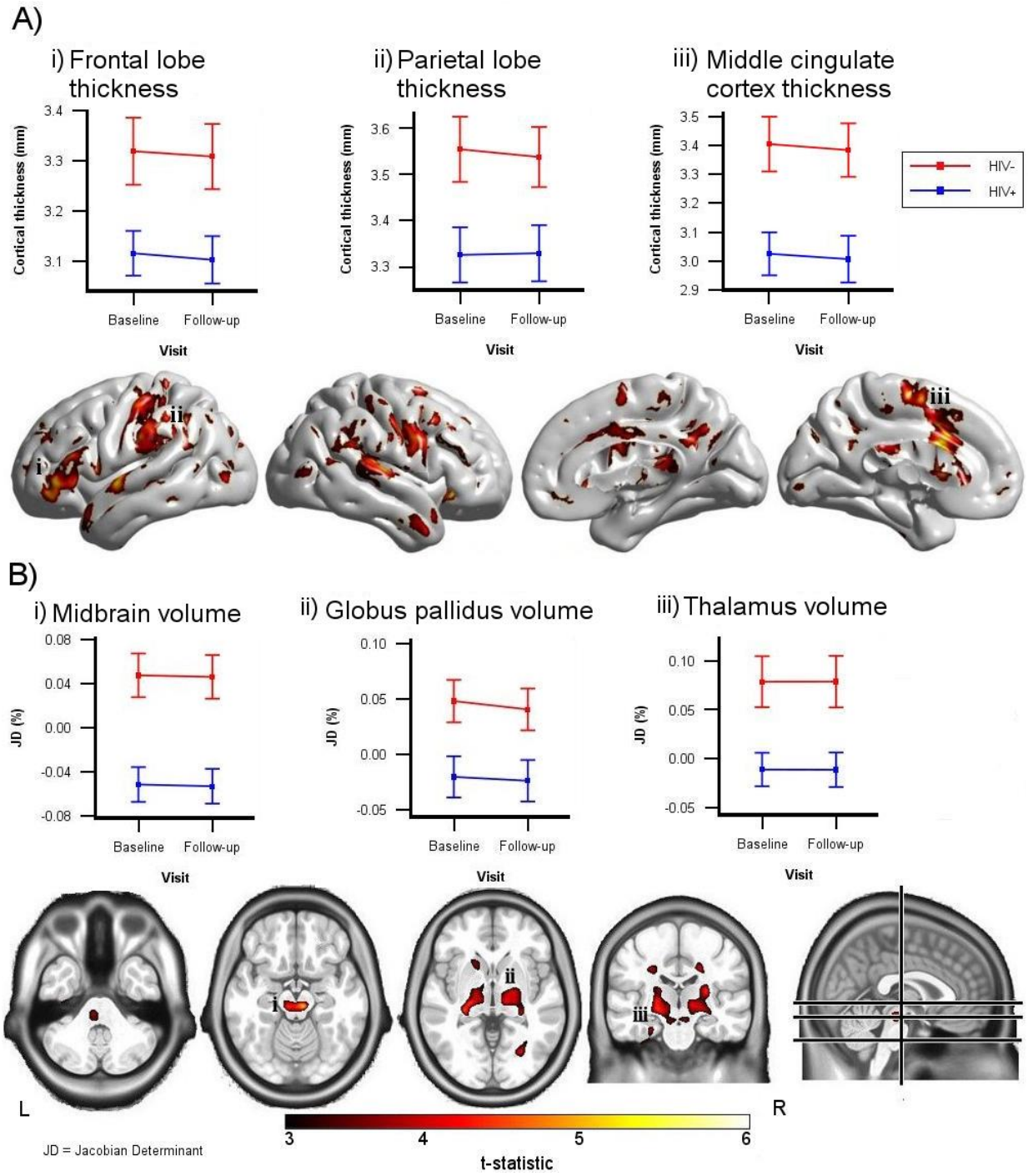


Figure 4.2: A) Upper row: Cortical thickness estimates at baseline and follow-up in the i) frontal lobe, ii) parietal lobe, and iii) middle cingulate cortex in HIV+ patients (blue) and HIV- control participants (red). Lower row: Visualization of cortical thickness reductions in the HIV+ group compared to HIV- controls. B) Upper row: Subcortical volume measures with TBM at baseline and

follow-up in the i) midbrain, ii) globus pallidus, and iii) thalamus in HIV+ patients (blue) and HIV- control participants (red). Lower Row: Visualization of subcortical volume reductions in HIV+ group compared to HIV- controls with TBM.

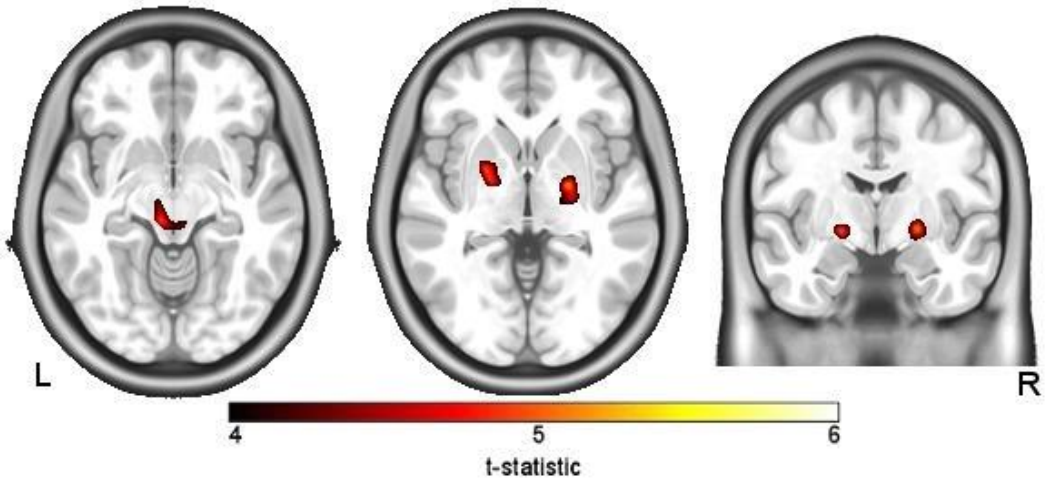


Figure 4.3: Smaller subcortical brain regions associated with lower nadir CD4.

## 4.5. Discussion

While HAND persists, recent studies have reported that neuropsychological performance does not deteriorate over spans of three to four years in the vast majority of cART-treated, aviremic HIV+ individuals[47,75,76]. Whether stable treatment and effective viral suppression also prevents progressive structural brain atrophy is unclear[49,66,67,77]. Here, we observed significant differences in cortical thickness, subcortical volumes and cognitive performance in HIV+ participants compared to demographically similar HIV- controls at both visits. However, the changes in cognition and brain volumes over two years were similar between the HIV+ and HIV- groups.

We applied multiple neuroimaging processing methods capable of detecting small changes in cortical thickness and subcortical volumes. Post hoc power analysis demonstrated that differences in annual brain volume loss between the groups as small as 0.1%/year in subcortical regions and 0.01 mm/year in the cortex could be detected, if present. Changes of greater magnitude were reported in an HIV+ group, 33% of whom had detectable viral loads, with 3.2% more volume loss detected in the temporal lobe compared to an HIV- group[49]. In other conditions with mild cognitive impairment, such as prodromal Alzheimer's disease, thinning rates were 0.01 mm/year greater in subjects who progressed to mild cognitive impairment compared to subjects who maintained cognitive health[205]. While the absence of detectable cortical thinning and subcortical volume loss in this study is not proof of the absence of ongoing brain atrophy in HIV+ individuals,

the power analysis demonstrates that clinically-meaningful changes could have been detected, if present. These findings are consistent with a recent, smaller longitudinal study, which likewise found no significant changes in average cortical thickness and deep gray matter volumes over two years in treated HIV+ participants with undetectable viral loads[77]. Collectively, these findings support the hypothesis that effective viral suppression with stable cART could halt the previously reported progression of brain atrophy in HIV[49,66,67].

Improvements in neuropsychological test scores were observed to a similar degree in both groups in Letter Fluency and Digit Symbol Substitution tasks. Improvement was also seen in Trail Making Test Part A scores, with the HIV+ group showing greater improvements than controls. On average, these improvements were less than 0.5 SD from baseline, a threshold generally considered to indicate clinically-meaningful change[206]. The observed test score improvements likely reflect imperfect test-retest reliability and practice effects; in any case, the findings argue against substantial cognitive decline. However, a caveat of mixed-effects modeling is the assumption that patterns of longitudinal change are the same for all individuals, which may not be true. It is possible that the mixed-effects models masked unique cognitive trajectories that have clinical meaning[75]. Future studies should consider alternative approaches such as group-based trajectory analysis, which identifies distinct cognitive trajectories. This approach was applied to a large sample of HIV+ participants drawn from the CNS HIV Anti-Retroviral Therapy Effects Research (CHARTER) cohort. Consistent with our findings, a decline in even one neuropsychological test was uncommon, with the large majority of HIV+ participants remaining cognitively stable over 3 years[75].

The absence of worsening cognitive function also agrees with a recent Multicenter AIDS Cohort study and another CHARTER study. These studies found that stability was the rule, with only small subsets of HIV+ participants having deterioration in neuropsychological performance or HAND status[47,76]. Those studies supported the possibility that cardiovascular disease contributed to cognitive decline, with lower high-density lipoprotein concentrations and hypercholesterolemia predicting decline[47,76]. Here, we focused on cART-treated, aviremic individuals, excluding those with evidence of white matter hyperintensities attributable to microvascular injury *a priori,* to test the hypothesis that HIV, rather than vascular comorbidities, causes brain injury. Future studies should evaluate brain volumes and neuropsychological performance in HIV+ individuals over a longer period to clarify whether very subtle progressive

effects continue. Studies specifically concentrating on older HIV+ individuals (>55 y) are also needed, as increasing age and HIV infection may have synergistic effects on brain structure and function.

Smaller cortical and subcortical volumes and worse cognitive performance in the HIV+ group may reflect brain injury that occurred soon after seroconversion, possibly during the time of untreated infection. Viral markers and markers of immune activation are elevated in the CSF during this phase of the infection[6]. These viral and immunopathogenic changes are believed to be associated with neuronal damage[53]. If the infection is left untreated, high levels of HIV replication continue, leading to increased production of toxic viral proteins and neuro-inflammatory responses resulting in potentially permanent damage[6]. Supporting this hypothesis, cross-sectional studies investigating brain volumes and cognitive function in primary HIV infection (defined as <1 year after exposure) have reported reduced putamen and cortical gray matter volumes[53,61,103], and poorer cognitive performance in tasks involving executive function, attention/working memory, language, and speed of information processing[61,103,207]. This demonstrates that neuronal injury is present early in the infection. Our results are also consistent with a large body of cross-sectional work with chronic HIV+ subjects reporting volume reductions throughout the subcortical regions[5,48,50,51,62,186,208], cortical thickness reductions in the primary sensory and motor cortices, temporal lobe, and middle cingulate cortex[100,101,208], and weaker performance on neuropsychological tests compared to controls[5,100,186,208].

Supporting the idea that these differences relate to events prior to cART initiation, previous studies demonstrated that a history of more severe immunosuppression, indexed by nadir CD4 cell counts, is related to smaller brain volumes and worse neuropsychological performance[7,62-64,208]. Here, we observed a significant correlation between lower nadir CD4 and smaller subcortical volumes, but not with cortical thickness or neuropsychological performance. While this corresponds with previous work[101,208], the literature is not consistent because smaller cortical volumes and worse neuropsychological performance have been previously linked with lower nadir CD4[7,62,63]. Discrepancies between the results most likely reflect differences in sample size[7], disease severity[62,63], and neuropsychological test selection[173]. Taken together, our results could support the hypothesis that neurobiological changes occurring early in infection may be responsible for the cognitive impairment found in chronic HIV+ individuals. This

suggests that early initiation of cART may have neurocognitive benefits. However, future longitudinal work assessing brain structure and function in primary HIV infection is required to verify this hypothesis.

The effect of treatment CNS penetration effectiveness, indexed by CPE score, on brain volumes and neuropsychological test performance was also explored. No correlations with any brain volume measures or neuropsychological test scores were observed. This suggests that higher penetrating regimens do not influence brain structure or function. However, given the limited number of treatment regimens prescribed (CPE score range: 5-13), this sample of HIV+ participants were not appropriate to demonstrate the potential neuroprotective or neurotoxic effects of cART.

This study has limitations. First, recent evidence suggested that cardiovascular risk factors are more common in HIV+ individuals and relate to cognitive deficits[83]. Although we excluded participants with overt imaging evidence of cerebrovascular disease, data on vascular risk factors were not acquired. We cannot definitively exclude that vascular injury contributes to the smaller brain volumes and cognitive deficits. Second, this study focused on the direct effects of HIV, by including cART-treated, aviremic HIV+ participants with minimal comorbidities, and no white matter hyperintensities. This limits the generalizability to individuals with similar characteristics. Indeed, HIV+ individuals with lesions or other comorbid conditions may be more likely to experience ongoing brain injury despite full viral suppression. Finally, although the HIV+ group performed worse on neuropsychological tests than the HIV- controls, we did not collect information on the functional limitations of daily living needed to categorize participants with respect to the HAND categories; our focus was on the change within the individual over time [75]. The ability to detect change in neuropsychological performance depends on the tests used. It is possible that different tests would yield different results. For example, our neuropsychological assessment did not include measures of non-verbal learning and memory or tests of abstractions. However, no evidence of deterioration on the Trail Making Test Part B were observed, which was demonstrated to be the cognitive test most likely to show decline over 36 months across a battery of 15 neuropsychological tests administered to 701 HIV+ individuals in a longitudinal CHARTER cohort [75]. In that study, and here, improvements in some tests were observed, presumably due to practice effects. These effects could yield stable performance despite underlying progressive

brain injury, but the absence of detectably worse brain volume loss in the same HIV+ sample here argues against this interpretation.

In conclusion, we used multiple neuroimaging methods to assess brain structure and cognitive function in a cohort of treated, virologically well-controlled HIV+ participants, and demographically similar HIV- controls. Although we observed smaller cortical thickness and subcortical volumes, and poorer cognitive function in the HIV+ group, there was no significant brain volume loss or neuropsychological decline over two years. These findings support the hypothesis that brain injury due to HIV could occur principally during untreated infection. This suggests that early initiation of cART and full viral suppression may preserve long-term brain health.

## 4.6. Chapter 4 Reference List


5. Ances BM, Orteg M, Vaida F, Heaps J, Paul R. Independent Effects of HIV, Aging and HAART on Brain Volumetric Measures. J Acquir Immune Defic Syndr **2012**; 59(5): 469-77.
6. Gonzalez-Scarano F, Martin-Garcia J. The neuropathogenesis of AIDS. Nat Rev Immunol **2005**; 5(1): 69-81.
7. Heaton RK, Clifford DB, Franklin DR, et al. HIV-associated neurocognitive disorders persist in the era of potent antiretroviral therapy: CHARTER Study. Neurology **2010**; 75(23): 2087-96.
45. Antinori A, Arendt G, Becker JT, et al. Updated research nosology for HIV-associated neurocognitive disorders. Neurology **2007**; 69(18): 1789-99.
47. Heaton RK, Franklin DR, Deutsch R, et al. Neurocognitive change in the era of HIV combination antiretroviral therapy: the longitudinal CHARTER study. Clin Infect Dis **2015**; 60(3): 473-80.
48. Becker JT, Sanders J, Madsen SK, et al. Subcortical brain atrophy persists even in HAART-regulated HIV disease. Brain Imaging Behav **2011**; 5(2): 77-85.
49. Cardenas VA, Meyerhoff DJ, Studholme C, et al. Evidence for ongoing brain injury in human immunodeficiency virus-positive patients treated with antiretroviral therapy. J Neurovirol **2009**; 15(4): 324-33.
50. Kallianpur KJ, Shikuma C, Kirk GR, et al. Peripheral blood HIV DNA is associated with atrophy of cerebellar and subcortical gray matter. Neurology **2013**; 80(19): 1792-9.

51. Chiang M, Dutton RA, Hayashi KM, et al. 3D pattern of brain atrophy in HIV/AIDS visualized using tensor-based morphometry. Neuroimage **2007**; 34(1): 44-60.
53. Wright PW, Pyakurel A, Vaida FF, et al. Putamen volume and its clinical and neurological correlates in primary HIV infection. AIDS **2016**; 30(11): 1789-94.
61. Ragin AB, Du H, Ochs R, et al. Structural brain alterations can be detected early in HIV infection. Neurology **2012**; 79(24): 2328-34.
62. Cohen RA, Harezlak J, Schifitto G, et al. Effects of Nadir CD4 Count and Duration of HIV Infection on Brain Volumes in the HAART Era. J Neurovirol **2010**; 16(1): 25-32.
63. Ellis RJ, Badiee J, Vaida F, et al. CD4 nadir is a predictor of HIV neurocognitive impairment in the era of combination antiretroviral therapy. AIDS **2011**; 25(14): 1747-51.
64. Hua X, Boyle CP, Harezlak J, et al. Disrupted cerebral metabolite levels and lower nadir CD4+ counts are linked to brain volume deficits in 210 HIV-infected patients on stable treatment. Neuroimage Clin **2013**; 3: 132-42.
66. Stout JC, Ellis RJ, Jernigan TL, et al. Progressive cerebral volume loss in human immunodeficiency virus infection: a longitudinal volumetric magnetic resonance imaging study. HIV Neurobehavioral Research Center Group. Arch Neurol **1998**; 55(2): 161-8.
67. Pfefferbaum A, Rogosa DA, Rosenbloom MJ, et al. Accerelated aging of selective brain structures in human immunodeficiency virus infection: a controlled, longitudinal magnetic resonance imaging study. Neurobiol Aging **2014**; 35(7): 1755-68.
70. Letendre S, Marquie-Beck J, Capparelli E, et al. Validation of CNS Penetration-Effectiveness Rank for Quantifying Antiretroviral Penetration into the Central Nervous System. Arch Neurol **2008**; 65(1): 65-70.
75. Brouillette M, Yuen T, Fellows LK, Cysique LA, Heaton RK, Mayo NE. Identifying Neurocognitive Decline at 36 Months among HIV-Positive Participants in the CHARTER Cohort Using Group-Based Trajectory Analysis. PLoS ONE **2016**; 11(5): 1-17.
76. Sacktor N, Skolasky RL, Seaberg E, et al. Prevalence of HIV-associated neurocognitive disoders in the Multicenter AIDS Cohort Study. Neurology **2016**; 86(4): 334-40.

77. Corrêa DG, Zimmermann N, Tukamoto G, et al. Longitudinal Assessment of Subcortical Gray Matter Volume, Cortical Thickness, and White Matter Integrity in HIV-Positive Patients. J Magn Reson Imaging **2016**; 44(5): 1262-9.

83. Su T, Wit FW, Caan MW, et al. White matter hyperintensities in relation to cognition in HIV-infected men with sustained suppressed viral load on cART. AIDS **2016**; 30(15): 2329-39.

100. Thompson PM, Dutton RA, Hayashi KM, et al. Thinning of the cerebral cortex visualized in HIV/AIDS reflects CD4+ T lymphocyte decline. Proc Natl Acad Sci USA **2005**; 102(43): 15647-52.

101. Kallianpur KJ, Kirk GR, Sailasuta N, et al. Regional Cortical Thinning Associated with Detectable Levels of HIV DNA. Cereb Cortex **2011**; 22(9): 2065-75.

103. Ragin AB, Wu Y, Gao Y, et al. Brain alterations within the first 100 days of HIV infection. Ann Clin Transl Neurol **2015**; 2(1): 12-21.

106. Sled JG, Zijdenbos AP, Evans AC. A nonparametric method for automatic correction of intensity nonuniformity in MRI data. IEEE Trans Med Imaging **1998**; 17(1): 87-97.

111. Collins DL, Neelin P, Peters TM, Evans AC. Automatic 3D intersubject registration of MR volumetric data in standardized Talairach space. J Comput Assist Tomogr **1994**; 18(2): 192-205.

113. Ashburner J, Friston KJ. Voxel-Based Morphometry - The Methods. Neuroimage **2000**; 11(6): 805-21.

122. Eskildsen SF, Coupe P, Fonov V, et al. BEaST: Brain Extraction based on nonlocal Segmentation Technique. Neuroimage **2012**; 59(3): 2362–73.

136. Fonov V, Evans AC, Botteron K, McKinstry R, Collins DL. Unbiased average age-appropriate atlases for pediatric studies. Neuroimage **2011**; 54(1): 313-27.

138. Collins DL, Holmes CJ, Peters TM, Evans AC. Automatic 3-D model-based neuroanatomical segmentation. Hum Brain Mapp **1995**; 3(3): 190-208.

158. Eskildsen SF, Østergaard LR. Active Surface Approach for Extraction of the Human Cerebral Cortex from MRI. Med Image Comput Comput Assist Interv **2006**; 9: 823-30.

173. Brouillette M, Mayo N, Fellows LK, et al. A better screening tool for HIV-associative neurocognitive disorders: is it what clinicians need? AIDS **2015**; 29: 895-902.

183. Genovese CR, Lazar NA, Nichols T. Thresholding of Statistical Maps in Functional Neuroimaging Using the False Discovery Rate. Neuroimage **2002**; 15(4): 870-8.

186. Janssen MAM, Meulenbroek O, Steens SCA, et al. Cognitive function, wellbeing and brain correlates in HIV-1 infected patients on long-term combination antiretroviral therapy. AIDS **2015**; 29(16): 2139-48.

190. Coupe P, Yger P, Prima S, Hellier P, Kervrann C, Barillot C. An optimized blockwise nonlocal means denoising filter for 3D magnetic resonance images. IEEE Trans Med Imaging **2008**; 27(4): 425-41.

200. Janssen MAM, Koopmans PP, Kessels RPC. Cognitive Decline in Relation to Psychological Wellbeing and HIV Disease- and Treatment Characteristics in HIV-Infected Patients on cART: A One-Year Follow-Up Study. AIDS Behav **2016**: 1-7.

201. Casaletto KB, Cattie J, Franklin DR, et al. The Wide Range Achievement Test-4 Reading subtest "holds" in HIV-infected invdividuals. J Clin Exp Neuropsychol **2014**; 36(9): 992-1001.

202. Guizard N, Fonov VS, Garcia-Lorenzo D, Nakamura K, Aubert-Broche B, Collins DL. Spatio-Temporal Regularization for Longitudinal Registration to Subject-Specific 3d Template. PLoS ONE **2015**; 10(8).

203. Aubert-Broche B, Fonov VS, Garcia-Lorenzo D, et al. A new method for structural volume analysis of longitudinal brain MRI data and its application in studying the growth trajectories of anatomical brain structures in childhood. Neuroimage **2013**; 82(15): 393-402.

204. Eskildsen SF, Østergaard LR. Evaluation of five algorithms for mapping brain cortical surfaces. 2008 XXI Brazilian Symposium on Computer Graphics and Image Processing **2008**: 137-44.

205. Pacheco J, Goh JO, Kraut MA, Ferrucci L, Resnick SM. Greater cortical thinning in normal older adults predicts later cognitive impairment. Neurobiol Aging **2015**; 36(2): 903-8.

206. Norman GR, Sloan JA, Wyrwich KW. Interpretation of Changes in Health-related Quality of Life: The Remarkable Unvisaility of Half a Standard Deviation. Med Care **2003**; 41(5): 582-92.

207. Prakash A, Hou J, Liu L, Gao Y, Kettering C, Ragin AB. Cognitive function in early HIV infection. J Neurovirol **2016**: 1-10.
208. Sanford R, Cruz ALF, Scott SC, et al. Regionally Specific Brain Volumetric and Cortical Thickness Changes in HIV-infected Patients in the HAART era. J Acquir Immune Defic Syndr **2017**; 74(5): 563-70.

## Chapter 5: Longitudinal Trajectories of Brain Volume and Cortical Thickness in Treated and Untreated Primary HIV Infection

We previously reported that people living with HIV on suppressive cART had significant brain volume reductions and poorer cognitive function compared to controls, but changes in brain volume and cognitive function over time were similar between the groups[209]. While this finding argues against an ongoing, destructive process to be the cause of the brain alterations and cognitive function, the timing of the brain alterations and the impact cART has on these changes remain uncertain.

In the following longitudinal study, we combined multiple advanced neuroimaging methods with complementary strengths, TBM and cortical modeling, to map the longitudinal trajectory of structural brain changes in early infection and assessed whether cART stabilizes or reverses the structural alterations. This study included 65 well-characterized, treated and untreated participants starting in primary HIV infection (defined as <1 year after exposure), 30 of whom commenced cART at some point during follow-up.

We observed that prior to cART initiation longer duration of untreated infection (i.e. deferring treatment) was correlated with brain atrophy and cortical thinning. After cART initiation, structural deterioration was no longer observed. These findings demonstrated that brain atrophy begins early in untreated HIV infection and worsens with the continued absence of treatment, but initiating cART prevents further brain atrophy. This means that the cognitive difficulties and brain volume reductions that has become common in the cART era most likely reflects changes that occurred principally during untreated infection, emphasizing the importance of starting treatment early to mitigate significant brain injury and cognitive decline.

# Longitudinal Trajectories of Brain Volume and Cortical Thickness in Treated and Untreated Primary HIV Infection

Ryan Sanford[1], Dieter J. Meyerhoff[2], Richard W. Price[3], Dietmar Fuchs[4], Henrik Zetterberg[5,6,7,8], Beau M. Ances[9], Serena Spudich[10] and D. Louis Collins[1]

[1] Department of Biological and Biomedical Engineering, Montreal Neurological Institute, Montréal, Canada

[2] Department of Radiology and Biomedical Imaging, University of California-San Francisco School of Medicine, San Francisco, USA

[3] Department of Neurology, University of California-San Francisco School of Medicine, San Francisco, USA

[4] Division of Biological Chemistry, Innsbruck Medical University, Innsbruck, Austria

[5]Department of Psychiatry and Neurochemistry, The Sahlgrenska Academy at the University of Gothenburg, Mölndal, Sweden

[6]Clinical Neurochemistry Laboratory, Sahlgrenska University Hospital, Mölndal, Sweden

[7]Department of Molecular Neuroscience, UCL Institute of Neurology, Queen Square, London, UK

[8]UK Dementia Research Institute at UCL, London, UK

[9] Department of Neurology, University of Washington, St. Louis, USA

[10] Department of Neurology, Yale School of Medicine, New Haven, USA

*Clinical Infectious Diseases. 2018; Volume: 67; Issue: 11.*

## 5.1. Abstract

**Background:** HIV penetrates the brain in early infection. We used neuroimaging to longitudinally examine the impact the virus and combination antiretroviral therapy (cART) has on brain structure in treated and untreated participants starting in primary HIV infection (PHI).

**Methods:** Sixty-five participants enrolled during PHI and underwent longitudinal MRI, 30 of whom commenced cART during follow-up. Cross-sectional MRI was acquired from 16 chronic HIV infection (CHI) and 19 HIV-negative participants. Brain volume and cortical thickness were estimated using tensor-based morphometry (TBM) and cortical modeling, respectively. Mixed-

effects models mapped brain morphometric changes before and after cART initiation. The relationships between brain morphometry estimates and blood and CSF biomarkers were also tested. Region-of-interest analyses were performed to compare brain volume and cortical thickness between the groups cross-sectionally.

**Results:** Prior to cART initiation, longer duration of untreated infection correlated with volume loss in the thalamus, caudate, and cerebellum, and with cortical thinning in the frontal and temporal lobes, and cingulate cortex. After cART, no further volume loss was found by TBM. However, small increases of cortical thickness in the right frontal and temporal lobe correlated with longer cART duration. No correlations were observed with blood or CSF measures. The PHI group had cortical thickness reductions only in the right frontal lobe compared with the HIV-negative group, but had larger volumes in the thalamus, caudate, putamen, brainstem, and cortical gray matter compared with CHI group.

**Conclusion:** Subcortical atrophy and cortical thinning occur during untreated infection, but may be arrested by cART. These findings emphasize the importance of early cART.

## 5.2. Introduction

HIV penetrates the central nervous system (CNS) soon after seroconversion. Despite the use of combination antiretroviral therapy (cART), people living with HIV continue to experience neurological impairment[6,208,209]. The etiology of this mild, but quality-of-life limiting brain dysfunction in most of these individuals is unclear.

Recently, a longitudinal study demonstrated that well-treated, aviremic chronic HIV infection (CHI) participants had significant brain volume reductions compared to controls at all visits, but changes in brain volume over time were similar in both groups[209]. Although this result argues against an active, destructive process to be the cause of the brain alterations, the timing and cause of these changes remain uncertain.

It has been hypothesized that structural brain alterations may occur in primary HIV infection (PHI; defined as <1 year after exposure), possibly before cART initiation. Several studies have demonstrated that prominent inflammation[38,54,55], immune activation[56-58] and blood-brain barrier (BBB) disruption[59] were evident during the first year of infection, and progressively worsened in the absence of cART[54,57,59]. All of these factors have been linked to neuronal injury during this period[60], and could contribute, in part, to brain volume reductions

previously reported in PHI individuals[53,61,103]. However, the natural course of structural brain changes that occurs in early infection, and the impact cART has on these changes have not been well-characterized[53,61,103,210].

In this longitudinal study, we: 1) sought to map the trajectory of structural brain changes in early infection; 2) assessed whether cART stabilizes or reverses structural alterations; and 3) explored the relationship between brain morphometric measures and blood and cerebrospinal fluid (CSF) biomarkers. A large sample of treated and untreated PHI participants, and smaller samples of CHI participants and HIV-negative controls, underwent structural MRI. Regional brain volume and cortical thickness was characterized with advanced neuroimaging processing tools tensor-based morphometry (TBM) and cortical modeling, respectively. These approaches are useful for examining regional brain morphometry because they do not require *a priori* anatomical hypotheses, and they have previously been shown to be effective in detecting brain changes in people living with HIV[49,100,208,209]. It is advantageous to use these methods in tandem because they provide complimentary information; while TBM is best suited to detect spatially localized volume changes in subcortical regions[49], cortical modeling is well-suited extracting cortical morphometric measures (i.e. thickness)[208].

## 5.3. Methods

### 5.3.1. Participants

Sixty-five PHI, 19 HIV-negative, and 16 CHI participants were studied at UCSF from December 14$^{th}$, 2005 to December 22$^{nd}$, 2011. PHI was defined as infection within 12 months prior to enrolment, confirmed by the Serological Testing Algorithm for Recent HIV Seroconversion[211]. HIV transmission date was estimated as 14 days before onset of seroconversion symptoms, or as the date halfway between the last negative and first HIV positive test[60]. Sixty-one PHI participants (94%) were cART-naïve at enrolment. CHI participants had a history of HIV diagnosis for at least 3 years, and were either cART-naïve (n=9) or had elected to interrupt therapy for at least 3 months before entering the study (n=7; mean time off therapy: 11.7 months). HIV-negative controls were recruited from the San Francisco community, and matched to PHI participants for age, sex and education. Exclusion criteria included confounding active neurologic illness, active substance use (except tobacco, marijuana and alcohol), and hepatitis B or C co-infection. The Institutional Review Board at University of California San Francisco (UCSF) approved the study. Written informed consent was obtained from all participants.

### 5.3.2. Specimen Sampling, Processing, and Laboratory Analysis

Participants underwent detailed medical and neurological examinations, and collection of blood and CSF specimens at each visit. Details of the laboratory analysis have been previously described[212]. In brief, blood samples were analyzed for CD4+ and CD8+ T-lymphocyte counts using flow cytometry. CSF samples were analyzed for neurofilament light chain (NFL), at enrolment in PHI only, with the NF-light enzyme-linked immunosorbent assay kit (UmanDiagnostics, Umeå, Sweden)[60]. Paired blood and CSF samples were analyzed for white blood cell (WBC) count and albumin, while paired blood and cell-free CSF samples were analyzed for HIV RNA and neopterin concentrations[212]. These measures are considered biomarkers of viral burden (blood and CSF HIV RNA), immune status (CD4+ and CD8+ T-lymphocyte counts), inflammation (blood and CSF neopterin, and WBC counts), BBB permeability (CSF:blood albumin ratio), and neuronal injury (CSF NFL).

### 5.3.3. MRI acquisition

All participants underwent MRI using the same Bruker (Billerica, MA) MedSpec 4T with Siemens (Erlangen, Germany) TRIO console in San Francisco. The scanning protocol included a $T_1$-weighted three-dimensional magnetization-prepared rapid acquisition gradient echo sequence [repetition time (TR)/echo time (TE)/inversion time (TI)=2300/3.0/950ms; voxel=1.0mm$^3$]. PHI participants completed longitudinal MRI scans, whereas HIV-negative and CHI participants only completed a baseline scan. MRI and laboratory data were acquired at enrolment, 6 weeks, and every 6 months thereafter. While some MRI and laboratory data were not acquired on the same date, they were associated with the same study interval. MRIs were obtained a median of 12 days (IQR: 6, 23.5) from each associated laboratory visit.

### 5.3.4. MRI processing

All PHI $T_1$-weighted data was processed using a longitudinal processing pipeline, as previously described[203,209]. Pre-processing included denoising[190], intensity inhomogeneity removal[106] and brain masking[122]. Images were linearly registered to the Montreal Neurological Institute ICBM152 template using a nine-parameter affine transform[111]. To ensure the registrations to the ICBM152 space were consistent across all time points, a subject-specific template was created using an unbiased template creation approach[136]. This process yielded nonlinear transformations that mapped each visit to the ICBM152 space in a consistent manner reducing the intra-subject variability in brain volume measures across visits, increasing the

statistical power to detect within-subject changes[138,203]. Cross-sectional $T_1$-weighted data for HIV-negative and CHI participants followed similar processing procedures, except the scans were nonlinearly registered directly to the ICBM152 template[138]. All data were carefully inspected for unacceptable processing outcomes. All data passed visual quality control and were available for TBM and cortical modeling.

### 5.3.5. Tensor-based morphometry

TBM provides a voxel-wise estimate of brain structure volume relative to the ICBM152 template, corrected for overall brain size. Structural volumes were calculated by taking the Jacobian determinant of the deformation field from the nonlinear transform[113].

### 5.3.6. Cortical modeling

Cortical modeling provides a quantitative measure of cortical thickness. Cortical thickness estimates were extracted with Fast Accurate Cortical Extraction by deforming polygonal meshes to fit the gray-white matter and pial surface boundaries[158]. Thickness estimates were mapped to the ICBM152 average cortical template using an iterative feature-based registration algorithm[162], and blurred with a 20-mm surface-based kernel.

### 5.3.7. Statistical analysis

To assess the longitudinal trajectory of brain volume and cortical thickness before and after cART initiation in PHI, a piecewise mixed-effects model was applied to the whole brain on a voxel-by-voxel basis. This involved fitting a linear model to the visits before cART initiation, and a different linear model to the visits after cART initiation. Both models were constrained to meet at cART initiation[54]. Age was included as a fixed-effect, as well as a participant-specific random intercept.

At the visits before cART initiation in PHI, a multivariable mixed-effects model assessed the relationship between the brain morphometric measures and markers of inflammation, immune status, viral burden and BBB integrity. This model included age, CD4+ and CD8+ T-lymphocyte counts, blood and CSF HIV RNA and neopterin, CSF WBC, and albumin ratio as fixed effects, and a participant-specific random intercept. Given that CSF NFL was only acquired at enrolment, a fixed-effects model was constructed to assess the correlation of the HIV-related factors at baseline, including CSF NFL, with baseline brain morphometric measures. All whole brain statistical maps were corrected for multiple comparisons using the standard false discovery rate (FDR) with a false-positive rate of 5%[183].

The small HIV-negative and CHI groups limited the ability to perform meaningful whole brain voxel-wise comparisons. Instead, we performed region-of-interest analyses based on prior hypotheses to compare brain volumes and cortical thickness between the groups. Volumes from the thalamus and caudate, and cortical thickness from the right frontal and temporal lobes were extracted from the baseline scan in untreated PHI, HIV-negative and CHI participants. These regions were chosen because we found that they were significantly correlated with the duration of untreated infection in the piecewise mixed-effects model in the PHI group (see Results). Volumes were also extracted from the putamen, 3rd ventricle, brainstem and cortical gray matter because these regions were shown in previous work to be affected in PHI[53,61,103]. General linear models were used to cross-sectionally compare these brain volumes between the groups at baseline, while controlling for age.

## 5.4. Results

### 5.4.1. Participants

Table 5.1 summarizes baseline demographic and clinical characteristics of the participants. The PHI group completed a total of 184 MRI scans over 6 years. Treatment was commenced in 30 PHI participants during follow-up, independent of the study, at a median of 10.9 months (IQR: 6.2, 22.0) after HIV transmission. Those that started treatment were significantly older ($p$=0.04) and more educated ($p$<0.001) at the initial visit compared to those that deferred treatment. At enrolment, the median duration of infection after HIV transmission was 3.7 months in the PHI group, while the CHI participants had a median duration of 90 months since HIV diagnosis, though initial infection date was unknown. The HIV-negative participants were comparable to the PHI participants with respect to age, sex and education, while CHI participants were only comparable to the PHI participants with respect to sex and education.

Table 5.1: Baseline demographic and clinical characteristics of study participants.

| | | | | *P* value[a] | |
|---|---|---|---|---|---|
| | HIV-negative (n=19) | Primary HIV infection (n=65) | Chronic HIV infection (n=16) | PHI vs HIV- | PHI vs CHI |
| Age [years, mean (SD)] | 34.5 (9.9) | 36.9 (9.0) | 45.1 (10.3) | 0.36 | 0.01 |
| Sex [n, (% male)] | 19 (100) | 65 (100) | 15 (94) | 1.00 | 0.17 |

| | | | | | |
|---|---|---|---|---|---|
| Education [years, mean (SD)] | 16.1 (2.6) | 15.4 (2.3) | 14.3 (2.3) | 0.34 | 0.09 |
| Duration of HIV infection [months, median (IQR)][b] | NA | 3.7 (2.0, 5.2) | 90 (48, 220) | NA | <0.01 |
| CD4+ T-lymphocyte count [cells/µl, median (IQR)] | 790 (745, 1003) | 579 (412, 748) | 223 (145, 310) | <0.01 | <0.01 |
| CD8+ T-lymphocyte count [cells/µl, median (IQR)] | 476 (335, 732) | 901 (641, 1151) | 1029 (695, 1366) | <0.01 | 0.50 |
| CD4/CD8 ratio [median (IQR)] | 1.9 (1.3, 2.4) | 0.6 (0.4, 0.9) | 0.2 (0.2, 0.3) | <0.01 | <0.01 |
| Blood HIV RNA [$log_{10}$, mean (SD)] | NA | 4.3 (0.9) | 4.6 (0.8) | NA | 0.32 |
| CSF HIV RNA [$log_{10}$, mean (SD)] | NA | 2.5 (0.8) | 3.9 (1.1) | NA | <0.01 |
| Blood neopterin [nmol/L, median (IQR)] | NC | 13.0 (7.8, 20.4) | 18.4 (11.1, 22.3) | NA | 0.13 |
| CSF neopterin [nmol/L, median (IQR)] | NC | 9.0 (6.6, 12.8) | 23.9 (19.4, 43.6) | NA | <0.001 |
| CSF white blood cell count [cells/µl, mean (SD)] | 1.8 (1.5) | 7.7 (8.3) | 8.3 (6.8) | <0.01 | 0.80 |
| CSF:blood albumin ratio [mean (SD)] | 5.3 (1.9) | 5.6 (2.3) | 7.6 (3.5) | 0.60 | 0.05 |
| CSF neurofilament light chain [pg/mL, median (IQR)][c] | NC | 519 (408, 793) | NC | NA | NA |

Abbreviations: NA = not applicable; SD = standard deviation; IQR = Interquartile range; NC = not collected

[a] Comparisons were made using Wilcoxon signed-rank test for continuous variables and chi-square test for categorical variables.

[b] Duration of HIV infection for PHI was estimated by date of recent seroconversion as confirmed by laboratory measures. CHI duration of infection reflects the period since known HIV diagnosis.

[c] CSF NFL only measured in PHI participants at baseline.

By the study conclusion, the PHI participants who initiated cART had been receiving treatment for a median of 7.9 months (IQR: 3.7, 29.9). Significant improvements in almost all

blood and CSF biomarkers, except albumin ratio, were observed when comparing the first and last MRI visit (Table 5.2).

Table 5.2: Comparison of first and last MRI visit in the PHI participants who initiated cART.

| | | | Difference between visits | |
|---|---|---|---|---|
| | First visit (n=29)[a] | Last visit (n=29)[a] | 95% CI | *P* value[b] |
| CD4+ T-lymphocyte count [cells/µl, median (IQR)] | 441 (372, 628) | 531 (469, 758) | 89 (26,176) | 0.004 |
| CD8+ T-lymphocyte count [cells/µl, median (IQR)] | 881 (619, 1142) | 693 (574, 914) | -225 (-379, -60) | 0.004 |
| CD4/CD8 [median (IQR)] | 0.5 (0.4, 0.9) | 0.9 (0.6, 1.1) | 0.3 (0.2, 0.4) | <0.001 |
| Blood HIV RNA [$log_{10}$, mean (SD)] | 4.4 (1.0) | 1.8 (0.6) | -2.6 (-3.1, -2.1) | <0.001 |
| CSF HIV RNA [$log_{10}$, mean (SD)] | 2.7 (0.7) | 1.7 (0.2) | -1.0 (-1.3, -0.6) | <0.001 |
| Blood neopterin [nmol/L, median (IQR)] | 11.5 (8.0, 21.0) | 6.2 (4.6, 9.0) | -7.5 (-11.2, -3.5) | <0.001 |
| CSF neopterin [nmol/L, median (IQR)] | 9.0 (6.8, 11.6) | 7.1 (5.2, 9.5) | -2.0 (-7.5, 0.3) | 0.07 |
| CSF white blood cell count [cells/µl, mean(SD)] | 7.7 (6.4) | 3.3 (4.4) | -3.8 (-7.8, -0.1) | 0.03 |
| CSF:blood albumin ratio [mean (SD)] | 5.8 (1.9) | 5.5 (1.9) | -0.22 (-1.1, 0.6) | 0.54 |

Abbreviations: SD = standard deviation; IQR = Interquartile range

[a] One subject who initiated treatment only had one visit.

[b] *p* value calculated using Wilcoxon signed-rank test for paired samples (CD4+ and CD8+ cell counts, CD4/CD8 ratio, albumin ratio and CSF white blood cell count) and paired *t*-test (blood and CSF HIV RNA).

### 5.4.2. Cross-sectional comparison of brain volumes and cortical thickness

Volumes in the thalamus, caudate, putamen, 3rd ventricle, cortical gray matter and brainstem, and cortical thickness in the right temporal and frontal lobes were extracted from the baseline MRI scan in untreated PHI, HIV-negative and CHI participants (Table 5.3). The cortical thickness in the right frontal lobe was significantly reduced in the PHI compared to HIV-negative

controls, whereas the other regions did not significantly differ. Significant differences in most brain regions were observed when PHI and CHI groups were compared, where CHI participants had smaller brain volumes, thinner cortices, and enlarged 3rd ventricle.

Table 5.3: Cross-sectional comparison of brain volumes at baseline.

| | | | | *p* value[a] | |
|---|---|---|---|---|---|
| | HIV- [mean (SD)] | PHI [mean (SD)] | CHI [mean (SD)] | PHI vs HIV- | PHI vs CHI |
| Thalamus ($mm^3$)[b] | 7663.0 (877.2) | 7816.0 (661.0) | 7108.3 (954.2) | 0.25 | 0.02 |
| Caudate ($mm^3$)[b] | 5871.8 (666.9) | 5744.7 (598.6) | 5215.0 (435.0) | 0.61 | 0.03 |
| Putamen ($mm^3$)[b] | 5395.9 (531.7) | 5188.4 (494.0) | 4661.2 (688.1) | 0.22 | 0.07 |
| 3rd Ventricle ($mm^3$) | 1513.5 (491.2) | 1691.5 (521.9) | 2310.1 (1054.8) | 0.28 | 0.03 |
| Brainstem ($mm^3$) | 33899.7 (3792.3) | 34895.8 (3408.7) | 32755.4 (3335.7) | 0.31 | 0.06 |
| Cortical gray matter ($mm^3$) | 609,920 (73996.8) | 616,862 (60774.6) | 558,856 (71997.4) | 0.71 | 0.008 |
| Right superior temporal lobe (mm)[c] | 3.1 (0.6) | 3.1 (0.6) | 2.8 (0.5) | 0.78 | 0.13 |
| Right frontal lobe (mm)[c] | 3.2 (0.5) | 2.9 (0.5) | 2.4 (0.5)[d] | 0.03 | 0.008 |

Abbreviations: SD = standard deviation

[a] *p* values calculated from a general linear model while controlling for age.

[b] Volumes from the left and right hemisphere were averaged.

[c] Average cortical thickness within anatomical brain region.

[d] One CHI participant was considered an outlier and removed because cortical thickness was >5.9σ.

### 5.4.3. Brain volume and cortical thickness changes prior to cART initiation in PHI

When brain volume and cortical thickness estimates were evaluated by TBM and cortical modeling, respectively, we observed that before cART initiation longer duration of untreated infection was significantly correlated with volume loss in the right cerebellum, bilateral thalami, left caudate and left temporal lobe (Figure 5.1A), and with cortical thinning in bilateral frontal and temporal lobes, and the cingulate cortex (Figure 5.1B). Within these regions, atrophy rates ranged from 0.27% to 1.22%/year (median: 0.63%/year [IQR: 0.55-0.73%/year]) (see Figure S5 in section A.5.1. in Appendix) when volumes were estimated by TBM, and cortical thinning rates ranged from 0.02mm to 0.48mm/year (median: 0.25 mm/year [IQR: 0.22-0.30mm/year]) (see Figure S5 in section A.5.2. in Appendix).

### 5.4.4. Brain volume and cortical thickness changes after cART initiation in PHI

After cART, no further significant brain volume loss was found by TBM (Figure 5.1A). However, small but significant increases of cortical thickness in the right frontal and temporal lobes were correlated with longer cART duration (Figure 5.1B).

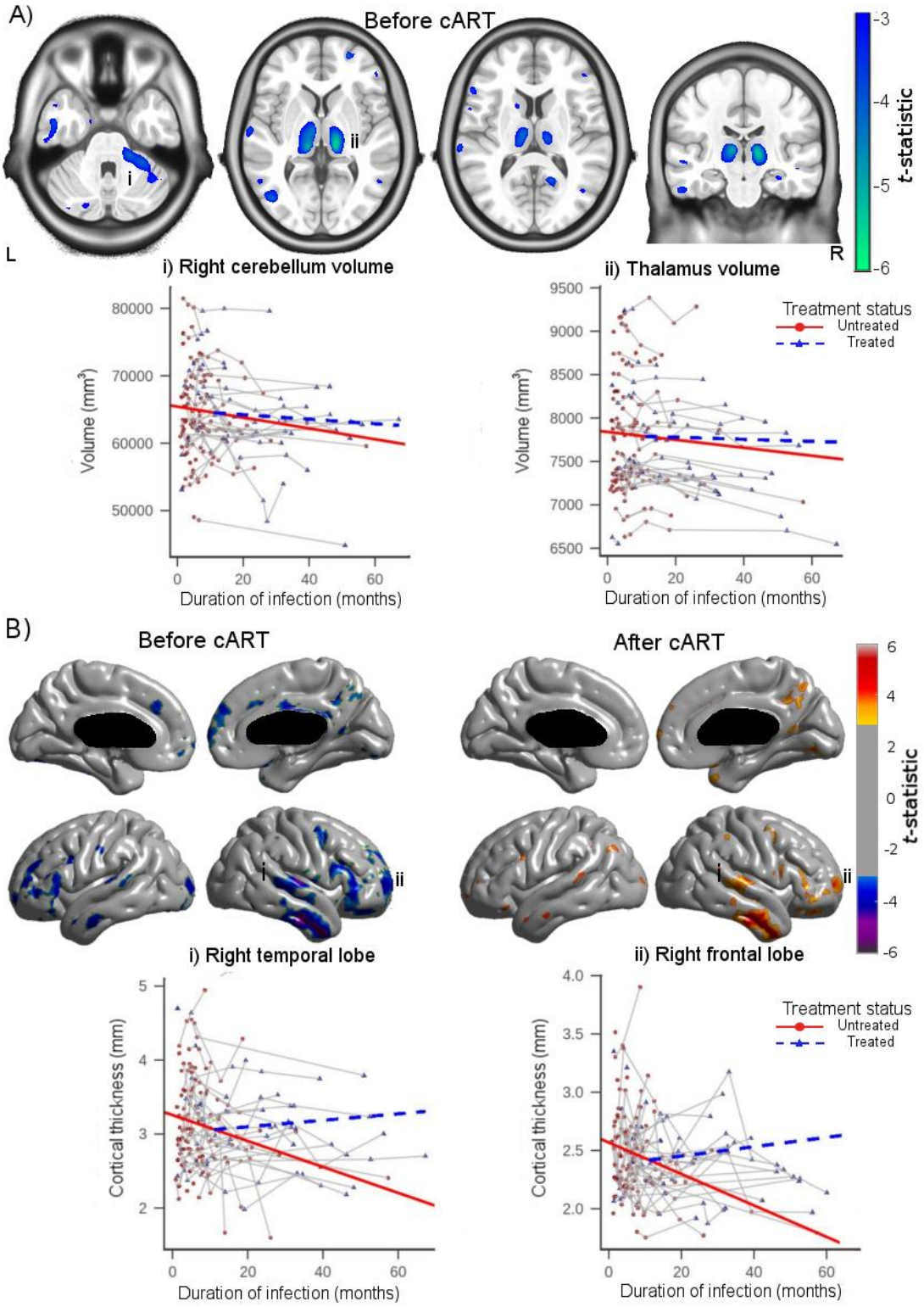


Figure 5.1: A) Upper row: Brain volume loss associated with longer duration of untreated infection as revealed with TBM. Lower row: Volume of the right cerebellum (left plot) and bilateral thalami (right plot) in relation with the duration of infection. B) Upper row: Cortical thinning associated with longer duration of untreated infection (left) and longer cART duration (right). Lower row: Cortical thickness of the right superior temporal gyrus (left) and right frontal lobe (right) in relation to the duration of infection for all PHI participants.

### 5.4.5. Brain volume and cortical thickness correlations with blood and CSF measures in untreated PHI

At the visits before cART in PHI, the relationship between brain volumes and blood and CSF measures were tested. Increasing CSF HIV RNA tended to be correlated with volume loss in the thalamus, while CD4+ cell count was positively correlated with cortical thickness in small areas of the left frontal lobe. However, these correlations did not reach statistical significance after correction for multiple comparisons. The remaining blood and CSF measures, including CSF NFL, were not significantly associated with any brain morphometric measures.

## 5.5. Discussion

While several studies have investigated the effects of HIV on the brain in early infection, the natural course of structural brain changes that occur during this period, and the impact cART has on these changes are not completely characterized. We observed that before cART initiation, PHI participants experienced progressive subcortical atrophy and cortical thinning that worsened in the absence of treatment. However, after cART was commenced structural deterioration was no longer observed.

We demonstrated that during untreated infection, PHI participants had a median atrophy and thinning rate of 0.63%/year and 0.25mm/year, respectively. These rates were of greater magnitude than that of normal ageing with previous studies reporting atrophy rates of 0.2%/year[213] and thinning rates of 0.01mm/year[205] in similarly aged healthy individuals, suggesting that untreated PHI individuals may experience greater-than-age related brain changes. However, given that longitudinal control data was not acquired, we cannot definitively conclude that the observed atrophy is a result of the infection. Future studies with longitudinal data on treated and untreated PHI participants and matched HIV-negative controls are warranted to clarify whether structural atrophy is caused by the virus or confounded by general processes such as ageing.

These findings, along with reports from previous studies[54-57,59,60,210], support the presumed initiation of HIV neuropathogenesis in early infection. The virus penetrates the CNS after initial systemic viral infection, infecting and activating local immune cells within the CNS compartment. These cells begin to release viral proteins and produce inflammatory factors resulting in prominent inflammation[38,54,55], immune activation[56-58], and BBB disruption[59], all of which facilitate neuronal injury and brain volume loss[6,60]. If the infection

remains untreated, we demonstrate here that brain atrophy and cortical thinning continues, while others report that markers of immune status, inflammation and BBB permeability progressively worsen[54,57,59]. Although the observed atrophy was not associated with any blood or CSF biomarkers, this could be an indication that a single biomarker is insufficient to infer underlying structural brain alterations; instead, a combination of these biomarkers may be more suitable for neurological prognosis[88].

The brain regions affected during untreated infection correspond with previous studies that examined people living with HIV. These studies reported volume reductions throughout the subcortical regions[5,48,50,51,208,209] and cerebellum[68,214], and cortical thickness reductions in the frontal and temporal lobes, and cingulate cortex[100,101,208,209]. The data in aggregate add to the growing body of evidence that demonstrate the brain is not spared in early infection. This suggests that the brain volume reductions reported in people living with HIV may reflect changes that occurred, in part, during the period of untreated infection.

In the subset of PHI participants who commenced cART, we observed improvements in markers of inflammation, immune status and viral burden, which demonstrates the effectiveness of cART. While this is not surprising, given that cART has been successful in treating systemic HIV infection, the impact it has on the brain is less known. Here, we did not find brain atrophy nor cortical thinning after cART initiation. Notably, we did not observe further subcortical atrophy with TBM. This is worth noting because while this suggests that treatment prevents additional subcortical atrophy, it points to possible permanent and irreversible changes. Interestingly, small increases in cortical thickness were found in the right frontal and temporal lobes suggesting that cortical volume partially recovers with treatment. This finding is consistent with a previous magnetic resonance spectroscopy study performed in acute HIV, where increased N-acetylaspartate (NAA) in the frontal gray and white matter was associated with cART[55]. However, extra caution must be exercised when interpreting these results, considering that 30 PHI participants started cART during follow-up, yielding only 61 post-cART scans, the likelihood of false-positive errors increases. Nevertheless, our findings suggest that cART can arrest structural atrophy, emphasizing the importance of early treatment. It also lends further support to the idea that events prior to cART may be responsible, in part, for the structural differences found in CHI[209].

To further assess the existence and extent of brain changes in PHI, we extracted volumes from the thalamus, caudate, putamen, 3rd ventricle, cortical gray matter and brainstem, and cortical thickness from the right temporal and frontal lobes in the PHI, HIV-negative and CHI groups. In contrast to previous PHI work[53,61,103], only the cortical thickness in the right frontal lobe was significantly reduced in the PHI group compared to HIV-negative controls. Discrepancies with prior work most likely reflect differences in sample size[53,103], duration of untreated infection[61,103], number of participants receiving cART[61,103], and the brain regions investigated[53,61,103]. As expected, the untreated CHI group had smaller brain volumes, thinner cortices and enlarged 3rd ventricle compared to PHI participants. This result is not surprising given that the CHI group had been infected for a median of 90 months and most participants were cART-naïve. This is in agreement with a large body of cross-sectional work that reported smaller subcortical volumes[5,48,51,208,209] and thinner cortices[100,101,208,209] in CHI individuals. Taken together, these findings provide further insight into the natural course of brain volume changes in untreated PHI, where it appears that the right frontal lobe may be preferentially susceptible to the virus, whereas macroscopic changes as seen on MRI in the remaining brain regions may not be detectable after a median time of 3.7 months of infection. Meanwhile, the CHI group consistently had worse brain volume and cortical thickness measures. Presumably, brain volumes in the PHI group would approach the volumes observed in the CHI group in the continued absence of treatment. Although causal inferences cannot be made with cross-sectional data, these conclusions are supported by our longitudinal data; altogether, the data provides additional suggestive evidence for brain atrophy progressing in the absence of treatment, arguing for early treatment.

This study has limitations. First, the HIV-negative and CHI groups were small, limiting the ability to perform exploratory whole brain voxel-wise statistics, reducing the generalizability, and exposing the results to false-positive errors. Second, since longitudinal control data was not acquired, we cannot determine when the structural brain changes begin to occur or estimate any component related to ageing. Third, given that data on lifestyle was not acquired, we cannot definitively exclude that lifestyle modifications after cART initiation contributes to the post-cART results. Finally, the study participants were young adult men with a history of drug use, limiting the generalizability of the results to individuals with similar characteristics.

In conclusion, our findings provide a unique narrative regarding the natural course of brain volume changes in early HIV infection. We reported that subcortical atrophy and cortical thinning begins early in HIV infection, principally during untreated infection, and worsens in the continued absence of cART. However, initiating cART may halt further structural deterioration. These results highlight the importance of early cART, and demonstrate that effective cART in PHI may be instrumental in preserving long-term brain health.

## 5.6. Chapter 5 Reference List


5. Ances BM, Orteg M, Vaida F, Heaps J, Paul R. Independent Effects of HIV, Aging and HAART on Brain Volumetric Measures. J Acquir Immune Defic Syndr **2012**; 59(5): 469-77.
6. Gonzalez-Scarano F, Martin-Garcia J. The neuropathogenesis of AIDS. Nat Rev Immunol **2005**; 5(1): 69-81.
38. Valcour V, Chalermchai T, Sailasuta N, et al. Central nervous system viral invasion and inflammation during acute HIV infection. The Journal of Infectious Diseases **2012**; 206: 275-82.
48. Becker JT, Sanders J, Madsen SK, et al. Subcortical brain atrophy persists even in HAART-regulated HIV disease. Brain Imaging Behav **2011**; 5(2): 77-85.
49. Cardenas VA, Meyerhoff DJ, Studholme C, et al. Evidence for ongoing brain injury in human immunodeficiency virus-positive patients treated with antiretroviral therapy. J Neurovirol **2009**; 15(4): 324-33.
50. Kallianpur KJ, Shikuma C, Kirk GR, et al. Peripheral blood HIV DNA is associated with atrophy of cerebellar and subcortical gray matter. Neurology **2013**; 80(19): 1792-9.
51. Chiang M, Dutton RA, Hayashi KM, et al. 3D pattern of brain atrophy in HIV/AIDS visualized using tensor-based morphometry. Neuroimage **2007**; 34(1): 44-60.
53. Wright PW, Pyakurel A, Vaida FF, et al. Putamen volume and its clinical and neurological correlates in primary HIV infection. AIDS **2016**; 30(11): 1789-94.
54. Young AC, Yiannoutsos CT, Hegde M, et al. Cerebral metabolite changes prior to and after antiretroviral therapy in primary HIV infection. Neurology **2014**; 83(18): 1592-600.
55. Sailasuta N, Ross W, Ananworanich J, et al. Change in Brain Magnetic Resonance Spectroscopy after Treatment during Acute HIV Infection. PLOS ONE **2012**; 7(11): e49272.

56. Spudich S, Gisslen M, Hagberg L, et al. Central Nervous System Immune Activation Characterizes Primary Human Immunodeficiency Virus 1 Infection Even in Participants with Minimal Cerebrospinal Fluid Viral Burden. J Infect Dis **2011**; 204: 753-60.

57. Suh J, Sinclair E, Peterson J, et al. Progressive increase in central nervous system immune activation in untreated primary HIV-1 infection. J Neuroinflammation **2014**; 11(199): 1-8.

58. Kessing CF, Spudich S, Valcour V, et al. High Number of Activated CD8+ T Cells Targeting HIV Antigens Are Present in Cerebrospinal Fluid in Acute HIV Infection. J Acquir Immune Defic Syndr **2017**; 75(1): 108-17.

59. Rahimy E, Li F-Y, Hagberg L, et al. Blood-Brain Barrier Disruption Is Initiatied During Primary HIV Infection and Not Rapidly Altered by Antiretroviral Therapy. The Journal of Infectious Diseases **2017**; 215: 1132-40.

60. Peluso MJ, Meyerhoff DJ, Price RW, et al. Cerebrospinal Fluid and Neuroimaging biomarker Abnormalities Suggest Early Neurological Injury in a Subset of Inidivduals During Primary HIV Infection. J Infect Dis **2013**; 207: 1703-12.

61. Ragin AB, Du H, Ochs R, et al. Structural brain alterations can be detected early in HIV infection. Neurology **2012**; 79(24): 2328-34.

68. Clifford KM, Samboju V, Cobigo Y, et al. Progressive Brain Atrophy Despite Persistent Viral Suppression in HIV Patients Older Than 60 Years. J Acquir Immune Defic Syndr **2017**; 76(3): 289-97.

88. Price RW, Epstein LG, Becker JT, Cinque P, Pulliam L, McArthur JC. Biomarkers of HIV-1 CNS Infection and Injury. Neurology **2007**; 69: 1781-8.

100. Thompson PM, Dutton RA, Hayashi KM, et al. Thinning of the cerebral cortex visualized in HIV/AIDS reflects CD4+ T lymphocyte decline. Proc Natl Acad Sci USA **2005**; 102(43): 15647-52.

101. Kallianpur KJ, Kirk GR, Sailasuta N, et al. Regional Cortical Thinning Associated with Detectable Levels of HIV DNA. Cereb Cortex **2011**; 22(9): 2065-75.

103. Ragin AB, Wu Y, Gao Y, et al. Brain alterations within the first 100 days of HIV infection. Ann Clin Transl Neurol **2015**; 2(1): 12-21.

106. Sled JG, Zijdenbos AP, Evans AC. A nonparametric method for automatic correction of intensity nonuniformity in MRI data. IEEE Trans Med Imaging **1998**; 17(1): 87-97.

111. Collins DL, Neelin P, Peters TM, Evans AC. Automatic 3D intersubject registration of MR volumetric data in standardized Talairach space. J Comput Assist Tomogr **1994**; 18(2): 192-205.

113. Ashburner J, Friston KJ. Voxel-Based Morphometry - The Methods. Neuroimage **2000**; 11(6): 805-21.

122. Eskildsen SF, Coupe P, Fonov V, et al. BEaST: Brain Extraction based on nonlocal Segmentation Technique. Neuroimage **2012**; 59(3): 2362–73.

136. Fonov V, Evans AC, Botteron K, McKinstry R, Collins DL. Unbiased average age-appropriate atlases for pediatric studies. Neuroimage **2011**; 54(1): 313-27.

138. Collins DL, Holmes CJ, Peters TM, Evans AC. Automatic 3-D model-based neuroanatomical segmentation. Hum Brain Mapp **1995**; 3(3): 190-208.

158. Eskildsen SF, Østergaard LR. Active Surface Approach for Extraction of the Human Cerebral Cortex from MRI. Med Image Comput Comput Assist Interv **2006**; 9: 823-30.

162. Järnum H, Eskildsen SF, Steggensen EG, et al. Longitudinal MRI study of cortical thickness, perfusion, and metabolite levels in major depressive disorder. Acta Psychiatr Scand **2011**; 124(6): 435-46.

183. Genovese CR, Lazar NA, Nichols T. Thresholding of Statistical Maps in Functional Neuroimaging Using the False Discovery Rate. Neuroimage **2002**; 15(4): 870-8.

190. Coupe P, Yger P, Prima S, Hellier P, Kervrann C, Barillot C. An optimized blockwise nonlocal means denoising filter for 3D magnetic resonance images. IEEE Trans Med Imaging **2008**; 27(4): 425-41.

203. Aubert-Broche B, Fonov VS, Garcia-Lorenzo D, et al. A new method for structural volume analysis of longitudinal brain MRI data and its application in studying the growth trajectories of anatomical brain structures in childhood. Neuroimage **2013**; 82(15): 393-402.

205. Pacheco J, Goh JO, Kraut MA, Ferrucci L, Resnick SM. Greater cortical thinning in normal older adults predicts later cognitive impairment. Neurobiol Aging **2015**; 36(2): 903-8.

208. Sanford R, Cruz ALF, Scott SC, et al. Regionally Specific Brain Volumetric and Cortical Thickness Changes in HIV-infected Patients in the HAART era. J Acquir Immune Defic Syndr **2017**; 74(5): 563-70.

209. Sanford R, Fellows LK, Ances BM, Collins DL. Association of Brain Structure Changes and Cognitive Function With Combination Antiretroviral Therapy in HIV-Positive Individuals. JAMA Neurol **2018**; 75(1): 72-9.
210. Kelly SG, Taiwo BO, Wu Y, et al. Early suppressive antiretroviral therapy in HIV infection is associated with measurable changes in the corpus callosum. J Neurovirol **2014**; 20(5): 514-20.
211. Zetola NM, Pilcher CD. Diagnosis and management of acute HIV infection. Infect Dis Clin North Am **2007**; 21: 19-48.
212. Spudich S, Nilsson AC, Lollo ND, et al. Cerebrospinal fluid HIV infection and pleocytosis: Relation to systemic infection and antiretroviral treatment. BMC Infect Dis **2005**; 5(98).
213. Fox NC, Schott JM. Imaging cerebral atrophy: normal ageing to Alzheimer's disease. Lancet **2004**; 363: 392-4.
214. Klunder AD, Chiang M, Dutton RA, et al. Mapping Cerebellar Degeneration in HIV/AIDS. Neuroreport **2008**; 19(17): 1655-9.

## Chapter 6: Association of Cerebral Small Vessel Disease with Brain Structure and Cognitive Function in HIV+ Individuals

Up to this point, we have presented a series of investigations that argues against an active, destructive process as the cause of HAND and, instead, argues that it most likely reflects brain changes that occurred during the time of untreated infection. However, this explanation fails to consider other factors that also may contribute to the cognitive impairment. Recent evidence has emerged suggesting that one of key underpinnings of HAND may be cerebral small vessel disease (CSVD), which is the most common cause of vascular cognitive impairment in general ageing populations[215]. This contribution could be worsened as HIV+ individuals could have increased risk of developing CSVD[10,83,216].

In the following study, we investigated 120 treated HIV+ participants with well-controlled infections and 55 demographically similar controls. A subset of participants was also longitudinally followed over a two-year period. We sought to: 1) examine whether HIV+ participants had more severe CSVD, as index by the total volume of WMH, compared to controls; 2) test the relationship between CSVD and standard clinical markers of HIV disease (including CD4 current and nadir and cART regimen) in the HIV+ group; 3) assess the magnitude to which HIV and CSVD contribute to changes in brain structure and cognitive function; and 4) longitudinally track CSVD severity to determine whether HIV is associated with greater change in CSVD severity over time.

We reported that HIV infection was not associated with CSVD. This finding was further supported by the longitudinal data as the HIV+ and control participants experienced similar increases in WMH lesion loads over two years. These results signify that HIV most likely does not significantly impact the mechanisms that lead CSVD, rather the presence of CSVD in people living with HIV is most likely incidental brought on by traditional vascular processes. As expected, we found that CSVD was significantly associated with reduced brain volumes and worse cognitive function in all participants. Combining the findings from all the studies presented in this dissertation, they suggest that while early HIV-induced brain changes leads to downstream cognitive deficits, subsequent CSVD may inflict additional brain injury. The combination of these processes most likely has a cumulative detrimental effect on brain structure and cognitive function. This means that HAND in the cART era is most likely a mixture of injury from early HIV and current CSVD.

# Association of Cerebral Small Vessel Disease with Brain Structure and Cognitive Function in HIV+ Individuals

Ryan Sanford[1], MEng; Jeremy Strian[2], PhD; Mahsa Dadar[1], PhD; Josefina Maranzano[1], MD; Alexandre Bonnet[3], MD; Nancy E. Mayo[4], PhD; Susan C. Scott[4], PhD; Lesley K. Fellows[1], MD CM, DPhil; Beau M. Ances[2], MD, PhD; and D. Louis Collins[1], PhD.

[1]Montreal Neurological Institute, McGill University, 3801 University Street, Montréal, Québec, Canada H3A 2B4

[2] Department of Neurology, Washington University, Box 8111, 660 South Euclid, St. Louis, Missouri, USA 63110

[3] Service de Neurologie, Centre Hospitalier Universitaire Pontchaillou 2, rue Henri le Guilloux, 35033 Rennes cedex 9, France

[4] Division of Clinical Epidemiology, McGill University, 3801 University Street, Montréal, Québec, Canada H3A 2B4

*AIDS. Accepted (in press).*

## 6.1. Abstract

**Objective:** Investigate whether cerebral small vessel disease (CSVD) is more common in virologically-suppressed HIV-positive participants compared to controls and examine the potential synergistic effects of HIV and CSVD on brain and cognition.

**Design:** Cross-sectional analysis of 119 treated, virologically-supressed HIV-positive and 55 HIV-negative participants. 46 HIV-positive and 30 HIV-negative participants had follow-up two-years later. All participants underwent MRI and neuropsychological testing.

**Methods:** Volume of white matter hyperintensities (WMH) was used as a surrogate measure of CSVD severity. Tensor-based morphometry and cortical modeling estimated brain volumes and cortical thickness, respectively. Rasch measurement theory was applied to neuropsychological test scores to estimate overall cognition. Linear models compared WMH loads, brain volumes and cognition between the groups, assessed the association of WMH loads with brain volumes and cognition, and tested the interaction between HIV and WMH loads on brain volumes and cognition. Mixed-effects models compared the change in WMH loads between groups.

**Results:** WMH loads and change in WMH loads were similar between the groups. HIV-positive participants had poorer cognitive function, thinner cortex and reduced subcortical volumes compared to HIV-negative controls. Higher WMH loads were associated with reduced cortical thickness and subcortical volumes and worse cognition, regardless of HIV serostatus. No significant interactions between HIV and WMH loads on the brain or cognition were observed.

**Conclusions:** These findings suggest that the contributions of HIV and CSVD to brain atrophy and cognitive impairment are independent but additive processes. This argues that optimizing vascular health may mitigate brain injury and cognitive decline, especially in treated, virologically-suppressed individuals.

## 6.2. Introduction

Despite the introduction of suppressive combination anti-retroviral therapy (cART), people living with HIV continue to experience HIV-associated neurocognitive disorders (HAND) at rates similar to that of the pre-cART era[7]. Such impairments remain clinically relevant as they can impact performance in every day activities and reduce overall quality of life[7].

Analysis of longitudinal data has provided a clearer understanding into the cause of this impairment[209,217,218]. These studies suggested that the cognitive deficits reflect, at least in part, injury that occurred soon after initial infection before cART was started[209,217,218]. However, there are likely other contributing factors. In particular, cerebral small vessel disease (CSVD) could be a key contributor to the continued presence of HAND[83,84,219,220]. CSVD is the most common cause of vascular impairment in the general population[215], and there has been indirect evidence that people living with HIV may have increased risk of CSVD[83,216].

However, whether CSVD is more common in HIV-positive compared to HIV-negative individuals remains unclear. A recent study reported that people living with HIV had greater burden of magnetic resonance imaging (MRI)-visible white matter hyperintensities (WMH), a standard quantitative marker of CSVD[215], compared to controls[83]. However, other studies have found no association between HIV serostatus and different measures of CSVD[84,219-222]. In addition, while the negative impact of CSVD on brain structure and function is well-known in the ageing population[83,84,219,220], the potential synergistic effects between CSVD and HIV on the brain and cognition are not well-characterized. One study reported that the presence of WMH in HIV-positive participants was associated with decreased cortical volumes in the frontal

lobe[223]. However, this study did not have a HIV-negative comparison group making it difficult to disentangle effects related to HIV and CSVD.

In this observational study, we investigated a large sample of virologically suppressed HIV-positive participants and demographically similar controls. A subset of these participants was longitudinally followed over a two-year period. We sought to: 1) examine whether the HIV-positive participants had worse CSVD compared to HIV-negative controls; 2) evaluate the relationship between CSVD and standard clinical markers of HIV infection severity in the HIV-positive group; 3) assess the extent to which HIV and CSVD contribute to changes in brain volumetrics and cognitive function; and 4) provide evidence of the longitudinal evolution of CSVD, to assess whether HIV is associated with greater rate of change in CSVD. The burden of WMH due to vascular etiologies, as seen on $T_2$-weighted MRI, was used as a surrogate marker of CSVD severity[215]. We characterized brain volumetrics by applying multiple advanced neuroimaging processing methods such as tensor-based morphometry (TBM) and cortical modeling and assessed cognitive function with a battery of neuropsychological tests.

## 6.3. Methods

### 6.3.1. Participants

Washington University in St. Louis (WUSTL) Institutional Review Board approved the study. Written informed consent was obtained from all participants. HIV-positive participants were selected from ongoing studies conducted by the infectious disease clinic and the AIDS clinical trial unit at WUSTL from February 2, 2012 to April 18, 2017. Demographically similar HIV-negative controls were recruited from the St. Louis community using leaflets and from a research participant registry at WUSTL. Participants were not enrolled if they had a history of confounding neurological disorders, current or past opportunistic central nervous system (CNS) infection, traumatic brain injury (loss of consciousness >30 minutes), major psychiatric disorders, or were actively abusing substances or had a dependence diagnosis according to Diagnostic and Statistics Manual of Mental Disorders fourth edition criteria. The present study included HIV-positive and HIV-negative participants that were greater than 40 years old and who had MRI ($T_1$ and $T_2$-weighted scans) and neuropsychological testing. All HIV-positive participants were on stable cART for at least 6 months and had an undetectable viral load (<50 copies/ml). A total of 120 HIV-positive and 55 HIV-negative participants were included. From this cohort, 46 HIV-positive

and 30 HIV-negative participants had follow-up examination approximately two years later (HIV-positive:2.1±0.2 years; HIV-negative:1.8±0.3 years).

Factors commonly associated with cardiovascular disease, including blood pressure, body mass index (BMI), waist circumference and smoking, were collected from all participants. Participants were considered to have hypertension if they had had a resting systolic blood pressure ≥140 mmHg or diastolic blood pressure ≥90 mmHg. Smoking status was defined as a current smoker or not.

### 6.3.2. Neuropsychological assessment

All participants underwent a comprehensive neuropsychological assessment that consisted of ten standard tests recommended to assess HAND, including[45]: Grooved Pegboard (dominant and non-dominant), Hopkins Verbal Learning Test–Revised immediate and delayed recall, Trail Making Test Part A and B, Digit Symbol Substitution Task, Letter-Number Sequencing, Letter Fluency (FAS), and Action (verb naming) Fluency.

Rasch Measurement Theory was applied to the neuropsychological test scores, yielding an estimate of overall cognitive ability. This approach uses item response theory to determine the extent to which a set of items (e.g. neuropsychological tests) and responses to those items reflect a single latent construct (i.e. cognitive ability)[173,208]. Rasch analysis arranges items and participant responses on the same scale (logits) such that items that most participants correctly answer are considered easy items and participants who incorrectly respond are considered to have less cognitive ability. Likewise, items that few participants pass are harder items, and participants who pass them have more cognitive ability[173,208]. This approach yields an estimate of each person's cognitive ability that can be treated as a continuous measure (i.e. higher score corresponds with more cognitive ability). This approach does not require normative data and accommodates for missing data, allowing all available neuropsychological test scores to be used[208].

### 6.3.3. MRI acquisition

All participants underwent neuroimaging using the same 3T Siemens Tim TRIO whole-body magnetic resonance scanner with a 12-channel transmit/receive head coil at WUSTL. The scanning protocol included $T_1$-weighted three-dimensional magnetization-prepared rapid acquisition gradient echo sequence [repetition time (TR)/echo time (TE)/inversion time (TI)=2400/3.16/1000ms; voxel=1.0mm$^3$] and $T_2$-weighted Fast Spin Echo sequence [TR/TE=3200/460ms; voxel=1.0mm$^3$].

### 6.3.4. MRI processing

Cross-sectional MRI data were processed using a previously described standard pipeline[203]. Pre-processing included intensity inhomogeneity removal[106] and brain masking[122]. Images were initially linearly registered to the Montreal Neurological Institute ICBM152 template using a nine-parameter affine transform, followed by non-linear registration[138]. For the longitudinal data, a subject-specific template was created using an unbiased template creation approach to ensure good registration to the ICBM152 space and to maintain intra-subject consistency across visits[209]. All data were carefully inspected for unacceptable processing outcomes. All data passed visual quality control.

### 6.3.5. WMH segmentation

Since WMH commonly appear as a consequence of CSVD, total volume of WMH was used as a surrogate marker for CSVD severity[215]. WMH were segmented using $T_1$ and $T_2$-weighted scans with a previously validated technique[224]. This approach has been shown to produce valid WMH segmentations that strongly correlate with manual segmentations in this data set and others[224]. In brief, this technique uses a set of features that best inform a random forest classifier of the likelihood that a voxel is a WMH lesion. The feature set includes $T_1$ and $T_2$ voxel intensities as well as an intensity and spatial WMH probability map were created by averaging manually segmented WMH maps[224]. The quality of all segmentations was visually assessed. One participant was removed due to a poor segmentation outcome. The burden of WMH was defined as the volume ($cm^3$) of all segmented WMH voxels in ICBM152 space, and is thus normalized for head size.

### 6.3.6. Tensor-based morphometry

TBM provides a voxel-wise estimate of brain structure volume relative to the ICBM152 template. Structural volumes were calculated by taking the log Jacobian determinant of the deformation field from the nonlinear transform[113].

### 6.3.7. Cortical modeling

Cortical modeling provides a quantitative measure of cortical thickness. Cortical thickness estimates were extracted with Fast Accurate Cortical Extraction by deforming polygonal meshes to fit the gray-white matter and pial surface boundaries[158]. Thickness estimates were mapped to the ICBM152 average cortical template using an iterative feature-based registration algorithm[158].

### 6.3.8. Statistical analysis

Linear models were used to determine the factors that were significantly associated with lesion loads in all participants. Significant factors were identified using a stepwise model selection approach, where factors that had $p<0.1$ were included in the final model. All models consistently included HIV serostatus, age, sex, and race. In the HIV-positive group, separate linear models tested whether standard clinical markers of HIV disease, including nadir and current CD4, duration of HIV infection, duration on cART and type of anti-retroviral medication (e.g. protease inhibitor), were associated with the burden of WMH, controlling for age, sex, and race.

Linear mixed-effects models were used to examine longitudinal changes in WMH lesion loads. This model included HIV serostatus, time (years from initial visit), age at initial visit, sex, and HIV serostatus by time interaction as fixed effects, along with participant-specific random intercepts.

Finally, linear models were used to determine the variables that were most associated with cognitive function, as indexed by the Rasch score, voxel-wise linear models were used to assess the factors related to regional brain volumes and vertex-wise linear models were used for cortical thickness in all participants. Optimal models were identified using a stepwise procedure as described above. All models included HIV serostatus, age, and sex as covariates. Whole-brain statistical maps were corrected for multiple comparisons using a standard false discovery rate with a false-positive rate of 5%. WMH lesion loads were log-transformed to normalize the distribution for all analyses. Statistical significance was set at $p < 0.05$ (two-sided) for all models.

## 6.4. Role of funding source

The study funders had no role in study design, data collection, analysis or interpretation, or writing of the manuscript. The corresponding author had full access to all study data and had final responsibility for the decision to submit for publication.

## 6.5. Results

### 6.5.1. Participants

Table 6.1 summarizes demographic and clinical characteristics of all participants. While the HIV-positive and HIV-negative groups were comparable with respect to age, education, and race, the HIV-positive group had significantly more males than the HIV-negative controls

($p$=0.001). Factors commonly associated with CVSD were similar between the two groups, except for smoking where the HIV-positive group had more current smokers.

Table 6.5: Demographic and clinical characteristics of study participants.

| | HIV-positive (n=119) [a] | HIV-negative (n=55) | $p$ value[b] |
|---|---|---|---|
| Age [years, mean (SD)] | 55.8 (7.9) | 56.2 (11.7) | 0.83 |
| Sex [n, % (male)] | 96 (81) | 28 (51) | **0.001** |
| Race [n, % (African American)] | 67 (56) | 32 (58) | 0.78 |
| Education [years, mean (SD)] | 13.2 (2.8) | 13.8 (2.2) | 0.14 |
| Duration of HIV infection [years, mean (SD)] | 16.4 (8.2) | NA | |
| Current CD4 [cells/µl, median (IQR)] | 580 (397, 767) | NA | |
| Nadir CD4 [cells/µl, median (IQR)] [c] | 121 (21, 272) | NA | |
| CPE score [median (IQR)] | 7.0 (7, 9) | NA | |
| cART duration [years, median (IQR)] [d] | 14.3 (7.3, 18.0) | NA | |
| Nucleoside reverse transcriptase inhibitor [n, (%)] | 86 (72) | NA | |
| Non-nucleoside reverse transcriptase inhibitor [n, (%)] | 7 (6) | NA | |
| Protease inhibitor [n, (%)] | 62 (52) | NA | |
| Integrase inhibitor [n, (%)] | 22 (18) | NA | |
| Fusion inhibitor [n, (%)] | 2 (2) | NA | |
| Blood pressure – Systolic [mmHg, mean (SD)] | 123.1 (10.5) | 125.4 (10.8) | 0.20 |
| Blood pressure – Diastolic [mmHg, mean (SD)] | 79.4 (8.0) | 82.0 (9.2) | 0.11 |
| Hypertension [n, % (hypertensive)] | 23 (19) | 7 (13) | 0.39 |
| BMI [mean (SD)] | 27.2 (6.1) | 28.5 (5.9) | 0.18 |
| Waist Circumference [inches, mean (SD)] | 39.7 (6.6) | 40.0 (5.8) | 0.78 |
| Currently smoking [n, % (smokes)] | 62 (52) | 18 (35) | **0.05** |
| Rasch score [mean (SD); higher is better] | -0.34 (1.16) | 0.26 (1.31) | **0.008** |

| | | | |
|---|---|---|---|
| WMH lesion loads [$cm^3$, median (IQR)] | 1.4 (0.8, 3.0) | 1.4 (0.9, 2.2) | 0.94 |

Abbreviations: NA, not applicable; NC, not collected; SD, standard deviation; IQR, interquartile range; CPE, CNS penetration effectiveness;

[a] One participant removed due to poor WMH segmentations.

[b] Comparisons were made using Wilcoxon signed-rank test for continuous variables and chi-square test for categorical variables.

[c] 25 HIV-positive participants were missing nadir CD4.

[d] 34 HIV-positive participants were missing cART duration.

### 6.5.2. Factors associated with WMH burden

The WMH burden was similar between the two groups (Figure 6.1). The most optimal linear model revealed that older age ($p$=0.001) and hypertension ($p$=0.002) were significantly associated with WMH burden, while smoking had a trend level effect ($p$=0.07) (Figure 6.3A). No significant interactions existed amongst these factors, HIV serostatus, and WMH lesion load. Within the HIV-positive group, clinical markers of HIV severity were not associated with WMH lesion load.

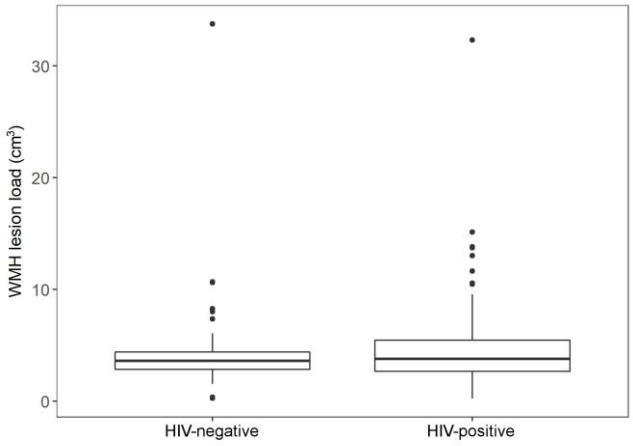


Figure 6.1: WMH lesion load in HIV-positive and HIV-negative participants. Note: Lesion loads were not log-transformed in the plot to facilitate interpretability.

### 6.5.3. Longitudinal changes in WMH burden

Statistically significant increases in WMH burden over an approximately two-year interval were seen for both groups through mixed-effects modeling, after correcting for HIV serostatus, age at initial visit, and sex (Figure 6.2). Observed changes in WMH lesion loads were similar for the HIV-positive and HIV-negative groups. No significant interactions between HIV serostatus and the time between scans or age were observed with WMH burden.

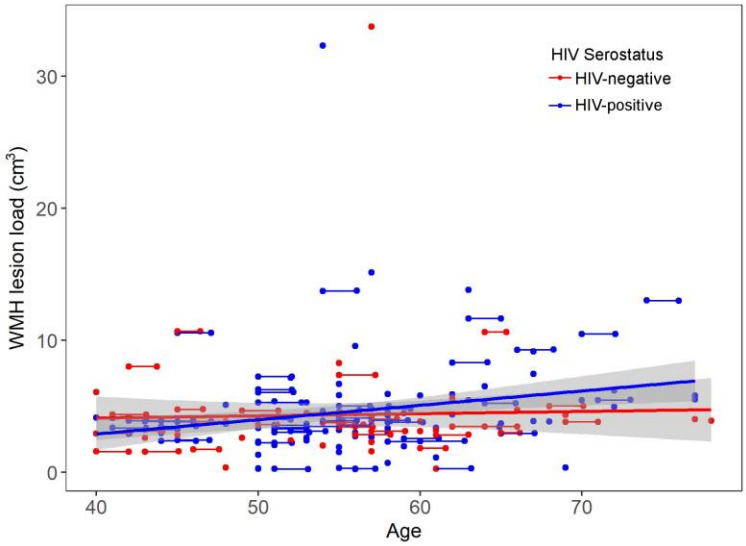


Figure 6.2: WMH burden over approximately two-years for HIV-positive (blue) and HIV-negative participants (red). The solid line represents the best linear fit for each group. The grey band indicates the 95% confidence interval on the linear fitted model.

### 6.5.4. Neuropsychological test performance

The HIV-positive group had significantly worse overall neuropsychological test performance, as measured by the Rasch score, compared to the controls (Table 6.1). The most optimal linear model revealed that age ($p$=0.0008), education ($p$=0.0005), HIV serostatus ($p$=0.004), and WMH burden ($p$=0.02) were significantly associated with overall neuropsychological test performance. Specifically, we observed that fewer years of education and older age were the strongest predictors of worse cognition, followed by HIV serostatus and greater burden of WMH (Figure 6.3B). Other variables, including hypertension, smoking, BMI, and waist circumference, were not associated with cognition.

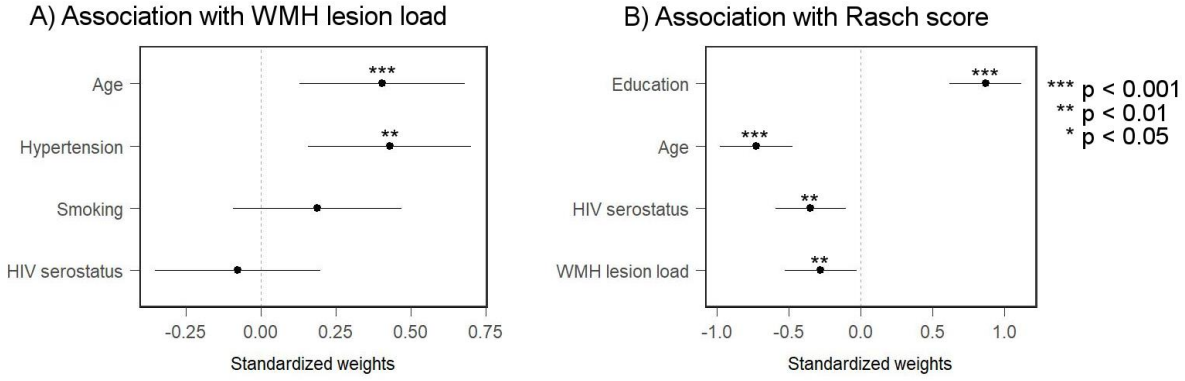


Figure 6.3: A) Standardized weights of factors that were associated with A) WMH lesion loads and B) overall neuropsychological test performance, as summarized by the Rasch score.

### 6.5.5. Brain volume and cortical thickness

Comparing regional brain measures between the groups revealed reduced cortical thickness and smaller subcortical volumes in the HIV-positive group compared to the HIV-negative group (Figure 6.4). Cortical thickness reductions were observed in bilateral primary sensory and motor cortex, superior temporal gyrus, anterior and middle cingulate cortex, and frontal lobe (Figure 6.4A). TBM revealed significantly smaller subcortical volumes in the thalamus, putamen, globus pallidus, brainstem, and midbrain in the HIV-positive group compared to the HIV- negative group (Figure 6.4B). These results remained significant even after including WMH lesion load, age, and sex in the model.

Increased burden of WMH lesion loads were significantly associated with reduced cortical thickness and smaller subcortical volumes in all participants; an effect that remained significant even after controlling for HIV serostatus, age, and sex. Cortical thickness reductions that were associated with WMH burden were predominately found in the bilateral frontal lobe, anterior cingulate cortex, and temporal lobe (Figure 6.4C), while smaller subcortical volumes were observed in the thalamus, putamen, globus pallidus, and brainstem (Figure 6.4D). When the interaction between HIV serostatus and lesion load was modeled, significant subcortical brain volume reductions were only observed in small areas of the thalamus and putamen for HIV-positive participants who had higher lesion loads (Figure 6.4E). No interaction was found in the cortex.

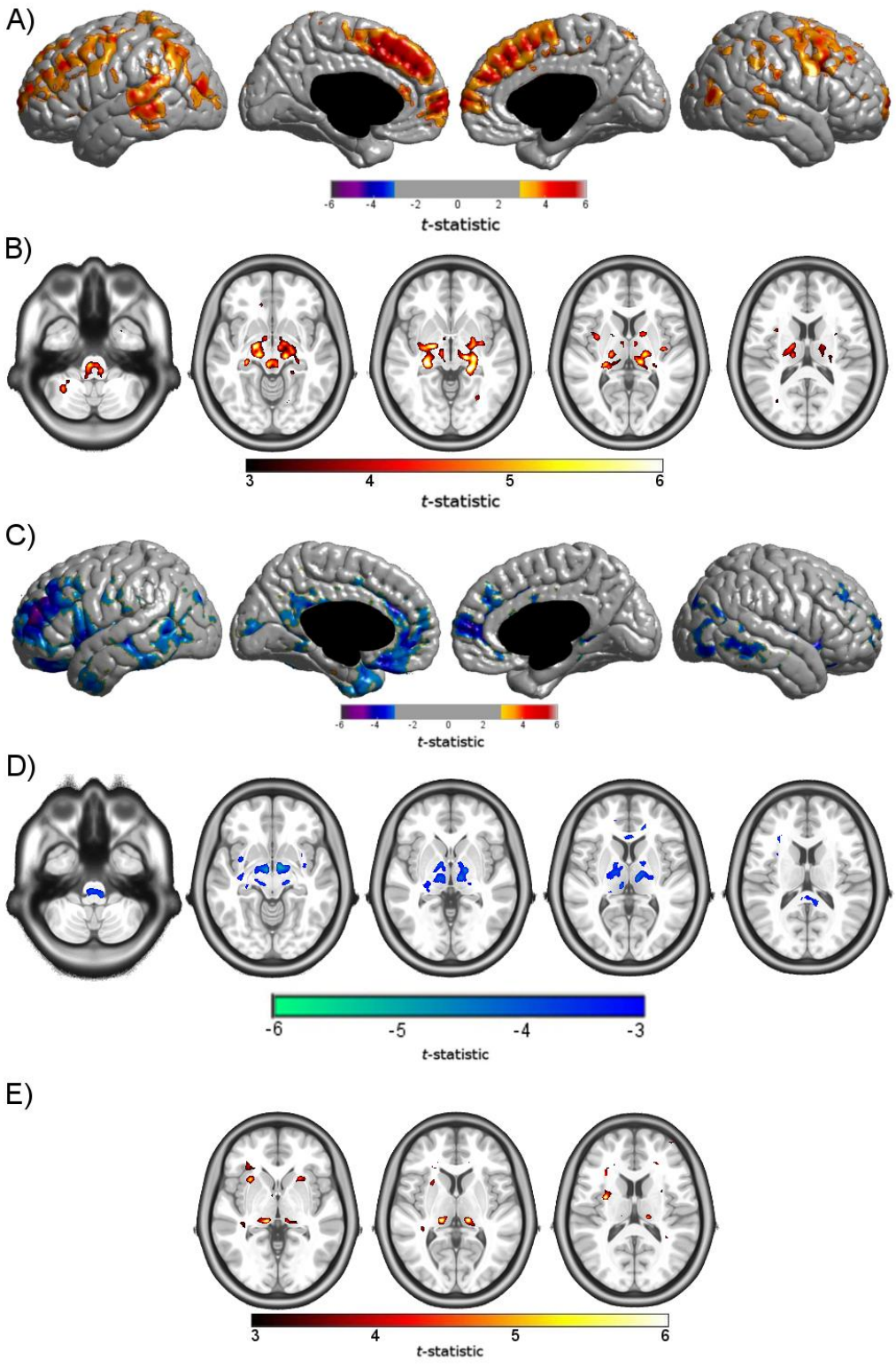


Figure 6.4: A) Cortical thickness reductions in HIV-positive participants compared to HIV-negative controls. B) Brain volume reductions in HIV-positive participants compared to HIV-negative controls as revealed with TBM. C) Cortical thickness reductions associated with greater WMH burden for all participants. D) Brain volume reductions associated with greater burden of WMH for all participants as revealed with TBM. E) Brain volume reductions in those with HIV and higher WMH lesion loads.

## 6.6. Discussion

There is some recent evidence that shows HIV infection alters the risk of developing CSVD[83,216], which may be a key contributor to HAND[83,84,219,220]. Despite the growing body of literature, it is not yet clear whether CSVD is more common in people living with HIV and, more importantly, the impact that CSVD has on the brain in people living with HIV is not well-characterized. In the present study, we observed that neither HIV infection nor indicators of the severity of the infection were associated with CSVD, as measured by WMH burden, in people with good viral suppression. However, worse CSVD was associated with reductions in cortical thickness and brain volumes and poorer cognitive test scores, an association that remained significant even after accounting for HIV serostatus.

Using the total volume of WMH of presumed vascular origin as a surrogate marker of CSVD, we observed that the higher WMH lesion loads, independent of HIV serostatus, were associated with reduced brain volumes and cortical thickness and poorer cognitive function in all participants[83,84,215,220,223]. The observed brains regions associated with CSVD were comparable to those seen in previous work which reported volume reductions throughout the basal ganglia[215] and cortical thickness reductions in the frontal lobes[141,223] in similarly aged HIV-negative individuals with CSVD. The interaction between HIV serostatus and CSVD only revealed small subcortical volume reductions, but no interaction was found in the cortex. Integrating these results with those from previous work[209,217,218], a potential unifying explanation regarding the development of cognitive impairment in people living with HIV could be formulated: Early HIV-related neurobiological changes results in downstream cognitive deficits[209,217,218], while subsequent CSVD may independently contribute to brain changes leading to additional cognitive problems. The combination of these independent processes most likely has a cumulative detrimental effect on brain structure and cognitive function resulting in the mild cognitive impairment that seems to be common in older people with long-standing, well-controlled HIV infection[208].

While the HIV-related brain injury may not be completely reversible with cART[218], further injury due to CSVD could be mitigated by addressing modifiable cardiovascular risk factors through lifestyle changes or medication. We observed that smoking and hypertension were associated with worse CSVD, and worse CSVD was associated with poorer cognitive function. This could mean that interventions focused on reducing smoking and controlling blood pressure

could lead to a reduction in CSVD severity, which, in turn, could lead to better brain health and cognition. Reduction of cardiovascular risk through positive lifestyle interventions has been shown to prevent further decline in cognition in the general population[225]. Future longitudinal interventional studies are warranted to assess the effectiveness of vascular health optimization on cognition in people living with HIV.

The WMH lesion loads were similar between the HIV-positive and HIV-negative groups suggesting that HIV-positive individuals do not have more severe CSVD. While this result lends support to previous findings[84,220,226] in a much larger sample of treated HIV-positive participants with good viral control, it differs from a recent study that reported an association between HIV and WMH lesion loads[83]. Discrepancies between these results may reflect cohort differences, where the prior study only included HIV-positive males, limiting its generalizability[83]. The longitudinal data reinforced our cross sectional finding that HIV was not associated with CSVD, showing that the HIV-positive group did not have more rapid worsening of CSVD: the change in WMH lesion loads over time was similar for both groups. Furthermore, no significant associations were observed between standard clinical measures of HIV disease and WMH burden, arguing against a direct causal link between HIV and CSVD. Finally, no associations were found with cART duration or specific anti-retroviral regimen. This is in contrast to prior work reporting that prolonged exposure to cART, specifically protease inhibitors, increases the risk of developing CSVD[87,216]. However, given the limited number of treatment regimens prescribed, this sample of HIV-positive participants was not appropriate for demonstrating a potential association between cART and CSVD.

Despite the uncertain evidence as to whether people living with HIV have increased risk of CSVD, multiple hypotheses have been introduced to explain such a possibility, including: 1) HIV infection and particular anti-retroviral medications may alter the pathogenic process underlying CSVD[83,216]; and 2) HIV serostatus may be an indicator of a sub-population that has altered prevalence of cardiovascular risk factors unrelated to the virus itself (e.g. smoking rates)[216,227]. Our findings would appear to indicate that HIV and cART do not affect the pathogenic process underlying CSVD in a clinically meaningful manner. Instead, we provide strong evidence that the presence of CSVD in people living with HIV is most likely due to traditional vascular factors, such as ageing and hypertension[84,219-222,226]. Interestingly, our results seem to offer some support for the latter hypothesis as the HIV-positive group had more

current smokers than HIV-negative group. However, this difference did not translate into greater WMH lesion loads, which could be explained, in part, by the relatively small and insignificant contribution that smoking has on the WMH, compared to ageing and hypertension. This may mean that the perceived relationship between HIV and CSVD in the current literature may really be driven by increased cardiovascular risk factors that are unrelated to the virus itself but, for complex reasons[227]. are more common in HIV-positive populations[216].

This study has limitations. First, since limited data on cardiovascular risk factors were acquired, we cannot make any conclusions regarding the prevalence of metabolic syndrome in people living with HIV. Indeed, metabolic syndrome is associated with CSVD and could be increased in people living with HIV due to HIV infection and cART[228]. Second, while the WMH segmentations using the $T_1$ and $T_2$-weighted data has been shown to provide valid estimates of lesion loads, without FLAIR data the full extent of the lesions could not be adequately captured[224]. However, it remains unknown whether the WMH portions not captured in this study are clinically significant[224]. Third, given that the participants were selected from ongoing studies, only a small number of participants have returned for follow-up visits, which reduced the statistical power of the longitudinal analysis. As more participants return for follow-up visits, additional analyses should be conducted to validate these results. Fourth, the study included participants greater than 40 years old, limiting the generalizability to similarly aged individuals. Additional studies focusing across a greater age spectrum (particularly older ≥55 years) are required as possible synergistic effects between HIV and ageing on CSVD may occur[226]. Finally, the HIV-positive group had more males than the HIV-negative group. While sex was included as a controlling factor in all models, there are substantial sex differences in the prevalence of cardiovascular disease[229]. This could be a confounding factor and warrants further investigation.

In conclusion, we provided additional insight into the clinical relevance of CSVD in people living with HIV. We show that while CSVD is not more common in the HIV-positive group compared to HIV-negative controls, the underpinnings of HAND in the cART era may reflect a combination of injury caused by early HIV infection and subsequent CSVD, likely amongst other factors. These results suggest that optimizing vascular health in people living with HIV, who are on stable cART and virologically suppressed, may be a useful route to improve brain health and protect against decline.

## 6.7. Chapter 6 Reference List


7. Heaton RK, Clifford DB, Franklin DR, et al. HIV-associated neurocognitive disorders persist in the era of potent antiretroviral therapy: CHARTER Study. Neurology **2010**; 75(23): 2087-96.

10. Brew BJ. Has HIV-associated neurocognitive disorders now transformed into vascular cognitive impairment. AIDS **2016**; 30(15): 2379-80.

45. Antinori A, Arendt G, Becker JT, et al. Updated research nosology for HIV-associated neurocognitive disorders. Neurology **2007**; 69(18): 1789-99.

83. Su T, Wit FW, Caan MW, et al. White matter hyperintensities in relation to cognition in HIV-infected men with sustained suppressed viral load on cART. AIDS **2016**; 30(15): 2329-39.

84. Watson C, Busovaca E, Foley JM, et al. White matter hyperintensities correlate to cognition and fiber tract integrity in older adults with HIV. J Neurovirol **2017**.

87. Ryom L, Lundgren JD, El-Sadr W, et al. Cardiovascular disease and use of contemporary protease inhibitors: the D:A:D international prospective multicohort study. Lancet HIV **2018**; 5(6): e291-e300.

106. Sled JG, Zijdenbos AP, Evans AC. A nonparametric method for automatic correction of intensity nonuniformity in MRI data. IEEE Trans Med Imaging **1998**; 17(1): 87-97.

113. Ashburner J, Friston KJ. Voxel-Based Morphometry - The Methods. Neuroimage **2000**; 11(6): 805-21.

122. Eskildsen SF, Coupe P, Fonov V, et al. BEaST: Brain Extraction based on nonlocal Segmentation Technique. Neuroimage **2012**; 59(3): 2362–73.

138. Collins DL, Holmes CJ, Peters TM, Evans AC. Automatic 3-D model-based neuroanatomical segmentation. Hum Brain Mapp **1995**; 3(3): 190-208.

141. Dadar M, Zeighami Y, Yau Y, et al. White matter hyperintensities are linked to future cognitive decline in de novo Parkinson's disease patients. Neuroimage Clin **2017**; 20: 892-900.

158. Eskildsen SF, Østergaard LR. Active Surface Approach for Extraction of the Human Cerebral Cortex from MRI. Med Image Comput Comput Assist Interv **2006**; 9: 823-30.

173. Brouillette M, Mayo N, Fellows LK, et al. A better screening tool for HIV-associative neurocognitive disorders: is it what clinicians need? AIDS **2015**; 29: 895-902.

203. Aubert-Broche B, Fonov VS, Garcia-Lorenzo D, et al. A new method for structural volume analysis of longitudinal brain MRI data and its application in studying the growth trajectories of anatomical brain structures in childhood. Neuroimage **2013**; 82(15): 393-402.

208. Sanford R, Cruz ALF, Scott SC, et al. Regionally Specific Brain Volumetric and Cortical Thickness Changes in HIV-infected Patients in the HAART era. J Acquir Immune Defic Syndr **2017**; 74(5): 563-70.

209. Sanford R, Fellows LK, Ances BM, Collins DL. Association of Brain Structure Changes and Cognitive Function With Combination Antiretroviral Therapy in HIV-Positive Individuals. JAMA Neurol **2018**; 75(1): 72-9.

215. Wardlaw JM, Smith EE, Biessels GJ, et al. Neuroimaging standards for research into small vessel disease and its contribution to ageing and neurodegeneration. Lancet Neurol **2013**; 12(8): 822-38.

216. Currier JS, Lundgren JD, Carr A, et al. Epidemiological Evidence for Cardiovascular Disease in HIV-Infected Patients and Relationship to Highly Active Antiretroviral Therapy. Circulation **2008**; 118: e29-e35.

217. Cole JH, Caan MWA, Underwood J, et al. No evidence for accelerated ageing-related brain pathology in treated HIV: longitudinal neuroimaging results from the Comorbidity in Relation to AIDS (COBRA) project. Clin Infect Dis **2018**; 66(12): 1899-909.

218. Sanford R, Ances BM, Meyerhoff DJ, et al. Longitudinal Trajectories of Brain Volume and Cortical Thickness in Treated and Untreated Primary HIV Infection. Clin Infect Dis **2018**; 67(11): 1697-704.

219. Haddow L, Laverick R, Leung I, et al. Measurement of Retinal Vessels as a Biomarker of Cerebrovascular Aging in Older HIV-Positive Men Compared With Controls. J Acquir Immune Defic Syndr **2018**; 77(2): 199-205.

220. Wu M, Fatukasi O, Yang S, et al. HIV disease and diabetes interact to affect brain white matter hyperintensities and cognition. AIDS **2018**; Publish Ahead of Print.

221. McArthur JC, Kumar JA, Johnson DW, et al. Incidental White Matter Hyperintensities on Magnetic Resonance Imaging in HIV-1 Infection. J Acquir Immune Defic Syndr **1990**; 3(3).

222. Haddow LJ, Dudau C, Chandrashekar H, Cartledge JD, Hyare H, Miller RF. Cross-sectional study of unexplained white matter lesions in HIV positive individuals undergoing brain magnetic resonance imaging. AIDS Patient Care STDS **2014**; 28: 341-9.
223. McMurtray A, Nakamoto B, Shikuma C, Valcour V. Cortical atrophy and white matter hyperintensities in HIV: The Hawaii Aging with HIV Cohort Study. J Stroke Cerebrovasc Dis **2008**; 17(4): 212-7.
224. Dadar M, Maranzano J, Ducharme S, Carmichael OT, Decarli C, Collins DL. Validation of T1w-based segmentations of white matter hyperintensity volumes in large-scale datasets of aging. Hum Brain Mapp **2018**; 39(3): 1093-107.
225. Kennedy G, Hardman RJ, Macpherson H, Scholey AB, Pipingas A. How Does Exercise Reduce the Rate of Age-Associated Cognitive Decline? A Review of Potential Mechanisms. J Alzheimers Dis **2016**; 55(1): 1-18.
226. Seider TR, Gongvatana A, Woods AJ, et al. Age exacerbates HIV-associated white matter abnormalities. J Neurovirol **2015**; 22(2): 201-12.
227. Reynolds NR. Cigarette smoking and HIV: more evidence for action. AIDS Educ Prev **2009**; 21(3 Suppl): 106-21.
228. Paula AA, Falcão MC, Pacheco AG. Metabolic syndrome in HIV-infected individuals: underlying mechanisms and epidemiological aspects. AIDS Research and Therapy **2013**; 10(1): 32.
229. Mosca L, Barrett-Connor E, Kass Wenger N. Sex/Gender Differences in Cardiovascular Disease Prevention. Circulation **2011**; 124(19): 2145-54.

## Chapter 7: Discussion

The introduction of cART has drastically reduced mortality and significantly improved the life expectancy of people living with HIV. Despite this, the prevalence of HAND remains frequent, even in those who are on suppressive cART continue to experience cognitive difficulties[37,46,65]. Such cognitive impairments are clinically relevant as they could impact performance in every day activities and reduce quality of life[8]. Despite the growing body of literature, the cause of the persistence of HAND and its underlying neuropathogenesis remains unclear.

It is well-known that cART has been widely successful in treating systemic HIV infection (i.e. reducing viral loads and improving immune function), but in the CNS, there appears to be a therapeutic paradox; very effective treatment regimens have failed to eliminate quality-of-life-limiting cognitive impairment. This led to the hypothesis that there must be an ongoing, subclinical process that continually alters the brain structure and cognitive function even when peripheral measures of viral load and immunocompetence are within acceptable limits[8,48]. Previous neuroimaging studies have supported this hypothesis by demonstrating that HIV+ individuals had greater rates of brain atrophy compared to controls over time[49,66,67]. However, the results reported in Chapters 3 and 4 do not support this conclusion, as we observed that cART-treated HIV+ individuals had smaller regional brain measures compared to a demographically similar control group but the rate of brain volume changes over time were similar between the groups. Our post hoc power analysis verified that we had sufficient statistical power to detect subtle brain changes, if they were present. In particular, we had the power to detect differences in annual brain volume loss between the groups as small as 0.1%/year in subcortical regions and 0.01 mm/year in the cortex. Although the absence of detectable brain atrophy is not proof of the absence of ongoing brain atrophy in the HIV+ group, the power analysis verified that clinically meaningful changes could have been detected. These findings contrast previous work because the majority of HIV+ participants in these prior studies had advanced disease and poor viral control[49,66,67], which does not generalize well to the majority of people living with HIV who are on stable treatment with undetectable viral loads. Meanwhile, the HIV+ participants included in Chapters 3 and 4 were on stable cART and had good viral suppression over the entire study duration, which is a more representative sample of the people living with HIV in the cART era. Collectively, these findings argue against an active, destructive process as the cause of HAND, while also highlighting the

importance of adhering to cART and maintaining viral suppression to protect the brain from further injury and cognitive decline.

The observed brain volume reductions and poorer cognitive function reported in Chapters 3 and 4 may reflect brain injury that occurred soon after initial infection, before starting treatment. Supporting this hypothesis, numerous studies have demonstrated that prominent inflammation[38,54,55], immune activation[56-58] and BBB disruption[59] were evident in early HIV infection, and progressively worsened in the absence of cART[54,57,59]. All of these factors have been linked to neuronal injury during this period[60], and presumably would contribute, in part, to the observed brain volume reductions and cognitive deficits reported in Chapters 3 and 4. However, this hypothesis cannot be verified with the cohort of HIV+ participants examined in Chapters 3 and 4 as they had chronic HIV infection (i.e. have had HIV for a long time). Moreover, there have been few neuroimaging studies in the current literature that have assessed the existence and extent brain changes in early HIV infection (primary HIV). These studies reported brain volume reductions in the putamen, third ventricle, brainstem, and cortical gray matter in early infection suggesting that brain alterations begin soon after initial[53,61,103]. However, the cross-sectional nature of the prior work is a limitation as the natural course of brain changes that occurs in early infection, and the impact cART has on these changes could not be examined.

To assess the longitudinal brain changes that occur in early infection, the study reported in Chapter 5 followed a group of treated and untreated HIV+ participants starting in primary HIV infection. The strength of this study lied in the longitudinal design, where several cART-naïve participants (i.e. never been on cART before) enrolled soon after initial infection (less than 1 year) and then started treatment at some point during follow-up. This design gave us the unique opportunity to examine the trajectory of early brain alterations before starting cART and assess whether commencing cART stabilizes or reverses these structural alterations. We observed that longer duration of untreated infection (i.e. prior to cART initiation) was associated with significant brain atrophy and cortical thinning. As hypothesized, these brain alterations were in complete agreement with the brain alterations observed in Chapters 3 and 4 and with previous HIV studies that have reported brain volume reductions in chronic HIV+ participants throughout the subcortical regions[5,48,50,51,208,209] and cerebellum[68,214], and cortical thickness reductions in the frontal and temporal lobes, and cingulate cortex[100,101,208,209]. These findings add to the growing body of literature that demonstrates the brain is not spared in early infection and provides

additional support for the hypothesis that brain alterations in untreated infection may be responsible for the cognitive impairment commonly found in people living with HIV.

After cART initiation, brain atrophy and cortical thinning were no longer observed. This was a notable finding because it demonstrated that initiating cART may halt further structural deterioration and while also suggesting that the brain injury may not be completely resolved, even after starting cART. Overall, the findings in Chapter 5 supports the idea that neurobiological events that principally occur prior to cART initiation may be responsible, in part, for HAND, and, more importantly, stresses the importance of starting treatment early to minimize the extent of brain injury and subsequent cognitive deficits.

The findings from Chapters 3-5 in aggregate strongly argues against an active, destructive process occurring in people living with HIV on suppressive cART and, instead, fully supports the hypothesis that the observed brain atrophy and cognitive difficulties principally occurs during untreated infection. However, this explanation only focuses on the detrimental effects of HIV and fails to consider other factors that could negatively impact cognition. In particular, CSVD has emerged as a possible major contributor of HAND as it is the most common cause of vascular cognitive impairment in normal ageing populations[10,83]. This effect may be further exacerbated with the possibility that HIV could alter the pathogenic process underlying CSVD[10,83].

The study in Chapter 6 sought to examine the clinical significance of CSVD in people living with HIV by using the total volume of WMH as a surrogate marker of CSVD severity. We observed that the WMH lesion loads were similar between the HIV+ and control group, suggesting that CSVD is not more common in people living with HIV. This result was consistent with prior work that also did not observe any associations between HIV and different measures of CSVD[84,220,223,226]. The longitudinal data in Chapter 6 reinforced the idea that people living with HIV do not have more severe CSVD, since the change in WMH lesion loads over time were similar between the two groups. Furthermore, no significant associations were observed between standard clinical measures of HIV disease and WMH lesion load, arguing against a direct causal link between HIV and CSVD. Greater WMH lesion loads were only associated with older age, smoking and hypertension. These observations point towards the idea that HIV and cART do not affect the pathogenic process underlying CSVD, instead, it is most likely caused by co-existing factors, including traditional vascular processes, such as ageing and hypertension[84,219-222,226] and by risk factors unrelated to HIV, such as smoking[216].

Regardless of the prevalence of CSVD in people living with HIV, we were still interested in the potential harmful effects that CSVD may have on the brain structure and cognitive function. Despite the growing body of literature examining CSVD in HIV, the potential synergistic effects between CSVD and HIV on the brain and cognition are not well-characterized. We observed that worse CSVD was associated with reductions in cortical thickness and brain volumes and poorer cognitive function in all participants, regardless of HIV serostatus. The brain regions that were associated CSVD were similar to those seen in previous work which reported volume reductions throughout the basal ganglia[215,230] and cortical thickness reductions in the frontal lobes[141,223] in individuals with CSVD. Furthermore, these findings were in complete agreement with the current body of evidence showing that CSVD is most likely a major contributor of cognitive impairment[81,83,84,86,219-221,223]. Together, this demonstrates that while CSVD is not more common in people living with HIV compared to controls, the brain atrophy and cognitive impairment commonly found in the cART era may not be caused entirely by HIV, rather some components may have a vascular origin.

Integrating all the results from the investigations presented in this dissertation, along with reports from other studies[6,39,54-57,59,60,210], a unique narrative regarding the neuromechanisms that lead to HAND in the cART era could be formed (Figure 7.1). The virus penetrates the CNS soon after initial systemic infection, infecting and activating local immune cells within the CNS compartment. These cells begin to release viral proteins and produce inflammatory factors resulting in prominent inflammation[38,54,55], immune activation[56-58], and BBB disruption[59], all of which facilitate neuronal injury and brain atrophy[6,60]. If the infection remains untreated, we demonstrated that the brain atrophy continues, and markers of immune status, inflammation and BBB permeability progressively worsen[54,57,59]. Once cART has been commenced, viral loads begin to decrease[231], markers of immune status and inflammation begin to improve[6,39,54], and brain atrophy is arrested. With good adherence to cART and excellent viral control, people living with HIV should not experience greater-than-age related brain atrophy or cognitive decline[217]. However, as people living with HIV start to reach older ages (thanks to cART), in which they become vulnerable to various age-related processes, they may begin to develop CSVD, which we showed is related to brain volume reductions and is a major contributor of cognitive impairment. Taken together, these results suggest that the combination of independent processes related to HIV and CSVD most likely has a cumulative

detrimental effect on brain structure and cognitive function leading to cognitive impairment. This means that underpinnings of HAND in the cART era is a mixture of injury caused by untreated HIV infection and subsequent CSVD.

While the results presented in Chapters 3-5 demonstrated that brain injury caused by HIV may not be completely resolved even after starting cART, the impact of CSVD on cognition could be minimized with positive lifestyle changes and certain therapies. For instance, we observed that smoking and hypertension were associated with worse CSVD, and worse CSVD was associated with poorer cognitive function. This could mean that interventions focused on reducing smoking and controlling blood pressure could lead to a reduction in CSVD severity, which, in turn, could lead to better brain health and cognition. Reduction of cardiovascular risk through positive lifestyle interventions has been shown to prevent further decline in cognition in the general population[225,232,233]. Future longitudinal interventional studies are warranted to assess the effectiveness of vascular health optimization on cognition in people living with HIV.

In conclusion, this dissertation presented a series of investigations that provides compelling evidence demonstrating that the persistence of HAND in the cART era may be a result of a combination of events that occurred prior to the initiation of cART and subsequent CSVD. More importantly, these findings stress the importance of starting cART early, maintaining excellent viral control and optimizing vascular health to help prevent further brain injury and cognitive decline.

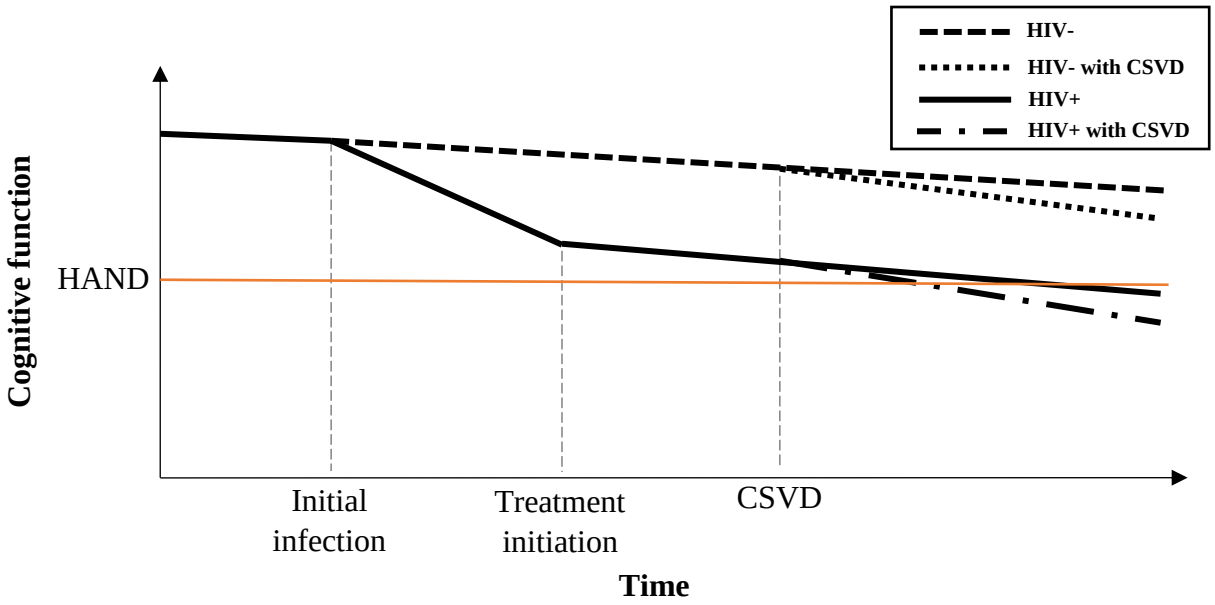


Figure 7.1: Illustration of the potential course of cognitive function in people living with HIV based on the results gathered in this dissertation. In brief, we demonstrated that brain injury and cognitive decline begin soon after initial infection before commencing treatment. After cART initiation and achieving good viral suppression, the changes in brain volume and cognition should stabilize. However, as treated HIV+ individuals begin age they may develop CSVD, which will cause additional damage to the brain structure and cognitive function. Taken together, this means that some cases of HAND may be a mixture of injury caused by HIV and CSVD. Illustration not drawn to scale.

# Chapter 8: Summary and Future Work

## 8.1. Summary and Clinical Implications

Even with the wealth of neuroimaging studies in the literature, the cause of the persistence of HAND in the era of stable treatment was unclear. Previous studies failed to disentangle the cause of impairment as they used sub-optimal MRI processing methods[5,61,62,102,185,187], included HIV+ participants that were not representative of the majority of people living with HIV today[49,66,67] and followed a cross-sectional design[5,48,51,53,83,100-103,185,187,195,196]. Given that HAND impacts everyday activities and reduces quality of life, a clearer understanding into the neuropathogenesis of HIV and disentangling the underpinnings of HAND was critical. In this dissertation, we used advanced MRI processing tools to extract measures of brain volume, atrophy and lesion burden. These measures were used as markers of disease severity and progression to assess the nature and extent of brain injury in the study participants. We were able to demonstrate that brain and cognitive changes found in people living with HIV in the cART era is a mixture of injury caused by early HIV infection and subsequent CSVD. These independent, but additive, processes have cumulative detrimental effects on brain structure and cognition function resulting in HAND that is commonly found in people living with HIV in the cART era.

The clinical implications of these findings are multiple as they stress the importance of commencing cART as soon as possible to mitigate irrecoverable brain injury and highlight the value of adhering to treatment and controlling viral loads to prevent progressive brain atrophy and cognitive decline. These results should open the door to novel HIV treatment strategies focused on potentially reversing the observed structural alterations. In addition, these findings demonstrate that optimizing vascular health in people living with HIV, who are on stable cART and virologically suppressed, may be a useful route to improve brain health and protect against decline.

## 8.2. Future Work

Although the findings described in this dissertation provide a clearer understanding into the underlying mechanisms of HAND in the cART era, further investigations are warranted. For instance, additional imaging modalities (e.g. diffusion tensor imaging and functional MRI) should be used in future work to gather a deeper understanding into the impact that HIV may have on other aspects of the brain (e.g. impact on the microstructures). Perhaps, the most important extension to this dissertation would be to investigate MRI-based biomarkers that could identify

HIV+ individuals who are at greatest risk of experiencing cognitive decline. While we show that stable cART and optimization of vascular health mitigates the risk of cognitive decline, several studies have demonstrated that small subsets of people living with HIV continue experience clinically meaningful cognitive decline[47,75,76]. These MRI-based biomarkers could be used to distinguish HAND from other neurodegenerative diseases, such as Alzheimer's disease. This is particularly important because the advent of cART has allowed people living with HIV to reach ages in which they could be vulnerable to Alzheimer's disease. The deep learning could be a viable option for MRI-based biomarker extraction as it has the ability to automatically extract relevant features and model complex, non-linear relationships.

A recent longitudinal study based on a European cohort of HIV+ individuals did not find any evidence of ongoing brain injury across multiple brain measurements[217], a finding that supports our conclusions. However, the time interval between visits was only two years, which may not be long enough to capture subtle brain changes. Future studies should evaluate brain volumes and cognitive function in HIV+ individuals over a longer period to clarify whether very subtle progressive effects exists. In addition, future work should concentrate on older HIV+ individuals (>55 years old), as increasing age and HIV infection may have synergistic effects on brain structure and function.

Chapter 5 provided a unique narrative regarding the natural course of structural brain changes in early HIV infection and the effect that cART has on these changes. However, extra caution should be exercised when interpreting the results as only a small subset of participants that started treatment had multiple post-cART visits, which increased the likelihood of false-positive errors. Ideally, additional studies should be conducted to validate these findings, but conducting longitudinal studies in early untreated HIV infection may no longer be feasible with the current treatment guidelines that recommends cART initiation at the time of diagnosis. This makes it difficult to acquire adequately sized longitudinal data on untreated HIV+ individuals soon after initial infection.

In Chapter 6, we reported that HIV was not associated with more severe CSVD, but worse CSVD significantly contributed to reductions in cortical thickness and brain volumes and cognitive deficits. These findings were revealed by quantifying CSVD severity through measuring the burden of WMH. Typically, WMH are segmented using FLAIR data, but since FLAIR data was not acquired, the segmentations were made using the $T_1$ and $T_2$-weighted scans. While the WMH

segmentations from the $T_1$ and $T_2$-weighted scans were shown to provide valid estimations of the lesion loads, the full extent of the lesions cannot be captured. Additional work is required to determine whether the WMH not captured are clinically relevant and associated with HIV.

The goal of this dissertation was to provide a clearer understanding into the neuropathogenesis of HIV and elucidate the cause of the persistence of HAND in the cART era. The four studies that compose the core of the dissertation provided evidence that neurobiological changes occur soon after initial infection, before starting treatment, that most likely results in downstream cognitive deficits, while subsequent cerebral small vessel disease may independently contribute to brain changes leading to additional cognitive problems. The combination of these independent processes most likely has cumulative detrimental effects on brain structure and cognitive function resulting in mild-to-moderate HAND, despite long-standing, well-controlled HIV infection. More importantly, these results stress the importance of starting cART early, adhering to cART, maintaining good viral control and optimizing vascular health to improve brain health and protect against cognitive decline.

## Master Reference List


1. Altman LK. Rare cancer seen in 41 homosexuals. New York Times. **1981**.
2. A Timeline of HIV and AIDS. Available at: https://www.hiv.gov/hiv-basics/overview/history/hiv-and-aids-timeline.
3. Levy JA. Pathogensis of human immunodeficiency virus infection. Microbiological Reviews **1993**; 57(1): 183-289.
4. Lima VD, Hogg RS, Harrigan PR, et al. Continued improvement in survival among HIV-infected individuals with newer forms of highly active antiretroviral therapy. AIDS **2007**; 21(6): 685-92.
5. Ances BM, Orteg M, Vaida F, Heaps J, Paul R. Independent Effects of HIV, Aging and HAART on Brain Volumetric Measures. J Acquir Immune Defic Syndr **2012**; 59(5): 469-77.
6. Gonzalez-Scarano F, Martin-Garcia J. The neuropathogenesis of AIDS. Nat Rev Immunol **2005**; 5(1): 69-81.
7. Heaton RK, Clifford DB, Franklin DR, et al. HIV-associated neurocognitive disorders persist in the era of potent antiretroviral therapy: CHARTER Study. Neurology **2010**; 75(23): 2087-96.
8. Mothobi NZ, Brew BJ. Neurocognitive dysfunction in highly active antiretroviral therapy era. Curr Opin Infect Dis **2012**; 25(1): 4-9.
9. O'Brien JT, Erkinjuntti T, Reisber B, et al. Vascular cognitive impairment. The Lancet Neurology **2003**; 2(2): 89-98.
10. Brew BJ. Has HIV-associated neurocognitive disorders now transformed into vascular cognitive impairment. AIDS **2016**; 30(15): 2379-80.
11. Gallo RC, Montagnier L. The Discovery of HIV as the Cause of AIDS. The New England Journal of Medicine **2003**; 349: 2283-5.
12. Barre-Sinoussi F, Chermann J-C, Rey F, et al. Isolation of a T-lymphotropic retrovirus from a patient at risk for acquired immune deficiency syndrome (AIDS). Science **1983**; 220: 868-71.
13. Gonçalves DU, Proietti FA, Ribas JGR, et al. Epidemiology, Treatment, and Prevention of Human T-Cell Leukemia Virus Type 1-Associated Diseases. Clinical Microbiology Reviews **2010**; 23(3): 577-89.

14. Gallo RC, Sarin PS, Gelmann EP, et al. Isolation of human T-cell leukemia virus in acquired immune deficiency syndrome (AIDS). Science **1983**; 220: 865-7.
15. Montagnier L, Chermann JC, Barre-Sinoussi F, et al. A new human T-lymphotropic retrovirus: characterization and possible role in lymphadenopathy and acquired immune deficiency syndromes: Cold Spring Harbor Laboratory, **1984**.
16. Gallo RC, Salahuddin SZ, Popovic M, et al. Frequent detection and isolation of cytopathic retroviruses (HTLV-III) from patients with AIDS and at risk for AIDS. Science **1984**; 224: 500-3.
17. Levy JA, Hoffman AD, Kramer SM, Landis JA, Simabukuro JM, Oshiro LS. Isolation of lymphocytopathic retroviruses from San Francisco patients with AIDS. Science **1984**; 225: 840-2.
18. Coffin J, Haase A, Levy JA, et al. Human immunodeficiency viruses. Science **1986**; 232: 697.
19. Maartens G, Celum C, Lewin SR. HIV Infection: epidemiology, pathogenesis, treatment, and prevention. Lancet **2014**; 384: 258-71.
20. Zheng Y, Lovsin N, Peterlin BM. Newly identified host factors modulate HIV replication. Immunology Letters **2005**; 97(2): 225-34.
21. Kirchhoff F. HIV Life Cycle: Overview. In: Science S. Encyclopedia of AIDS. New York, **2013**.
22. Garg H, Mohl J, Joshi A. HIV-1 Induced Bystander Apoptosis. Viruses **2012**; 3: 3020-43.
23. Alimonti JD, Ball TB, Fowke KR. Mechanisms of CD4 T lymphocyte cell death in human immunodeficiency virus infection and AIDS. Journal of General Virology **2003**; 84: 1649-61.
24. Finkel TH, Tudor-Williams G, Banda NK, et al. Apoptosis occurs predominantly in bystander cells and not in productively infected cells of HIV- and SIV-infected lymph nodes. Nature Medicine **1995**; 1: 129-34.
25. Garg H, Blumenthal R. Role of HIV Gp41 mediated fusion/hemifusion in bystander apoptosis. Cell Mol Life Sci **2008**; 65: 3134-44.
26. Mitsuya H, Weinhold KJ, Furman PA, et al. 3'-Azido-3'-deoxythymidine (BW A509U): an antiviral agent that inhibits the infectivity and cytopathic effect of human T-lymphotropic virus type III/lymphadenopathy-associated virus in vitro. Proceedings of

the National Academy of Sciences of the United States of America **1985**; 82(20): 7096-100.

27. Fischl MA, Richman DD, Grieco MH, Gottlieb MS. The Efficacy of Azidothymidine (AZT) in the Treatment of Patients with AIDS and AIDS-Related Complex. New England Journal of Medicine **1987**; 217: 185-91.
28. Lange JMA, Ananworanich J. The discovery and development of antiretroviral agents. Antiviral Therapy **2014**; 19: 5-14.
29. Gulick RM, Mellors JW, Havlir D, et al. Treate with Indinavir, Zidovudine, and Lamivudine in Adults with Human Immunodeficiency Virus Infection and Prior Antiretroviral Therapy. The New England Journal of Medicine **1997**; 337: 734-9.
30. Hammer SM, Squires KE, Hughes MD, et al. A Controlled Trial of Two Nucleoside Analogues plus Indinavir in Persons with Human Immunodeficiency Virus Infection and CD4 Cell Counts of 200 per Cubic Millimeter or Less. The New England Journal of Medicine **1997**; 337: 725-33.
31. Moore R, Chaisson R. Natural history of HIV infection in the era of combination antiretroviral therapy. AIDS **1999**; 13(14): 1933-42.
32. Ances BM, Ellis RJ. Dementia and Neurocognitive Disorders Due to HIV-1 Infection. Semin Neurol **2007**; 27(1): 86-92.
33. Guidelines for the Use of Antiretroviral Agents in HIV-1-Infected Adults and Adolescents. In: Services DoHaH, **2015**.
34. Das K, Arnold E. HIV-1 reverse transcriptase and antiviral drug resistance. Part 1. Current Opinion in Virology **2013**; 3(2): 111-8.
35. Metifiot M, Marchand C, Pommier Y. HIV Integrase Inhibitors: 20-Year Landmark and Challenges. Advances in Pharmacology **2013**; 67: 75-101.
36. Bai Y, Xue H, Wang K, et al. Covalent fusion inhibitors targeting HIV-1 gp41 deep pocket. Amino Acids **2013**; 44(2): 701-13.
37. Heaton RK, Franklin DR, Ellis RJ, et al. HIV-associated neurocognitive disorders before and during the era of combination antiretroviral therapy: Differences in rates, nature and predictors. J Neurovirol **2011**; 17(1): 3-16.

38. Valcour V, Chalermchai T, Sailasuta N, et al. Central nervous system viral invasion and inflammation during acute HIV infection. The Journal of Infectious Diseases **2012**; 206: 275-82.
39. Kramer-Hammerle S, Rothenaigner I, Wolff H, Bell JE, Brack-Werner R. Cells of the central nervous system as targets and reservoirs of the human immunodeficiency virus. Virus Research **2005**; 111: 194-213.
40. Scutari R, Alteri C, Perno C, Svicher V, Aquaro S. The Role of HIV Infection in Neurologic Injury. Brain Sciences **2017**; 7(4): 38.
41. Shaked I, Porat Z, Gersner R, Kipnis J, Schwartz M. Early activation of microglia as antigen-presenting cells correlates with T cell-mediated protection and repair of the injured central nervous system. Journal of Neuroimmunology **2004**; 146: 84-93.
42. Kipnis J, Avidan H, Caspi RR, Schwartz M. Dual effect of CD4+CD25+ regulatory T cells in neurodegeneration: a dialogue with microglia. Proceedings of the National Academy of Sciences of the United States of America **2004**; 101: 14663-9.
43. Barger SW, Hörster D, Furukawa K, Goodman Y, Krieglstein J, Mattson MP. Tumor necrosis factors alpha and beta protect neurons against amyloid beta-peptide toxicity: evidence for involvement of a kappa B-binding factor and attenuation of peroxide and Ca2+ accumulation. Proceedings of the National Academy of Sciences **1995**; 92(20): 9328-32.
44. Cheng B, Christakos S, Mattson MP. Tumor necrosis factors protect neurons against metabolic-excitotoxic insults and promote maintenance of calcium homeostasis. Neuron **1994**; 12(1): 139-53.
45. Antinori A, Arendt G, Becker JT, et al. Updated research nosology for HIV-associated neurocognitive disorders. Neurology **2007**; 69(18): 1789-99.
46. Heaton RK, Clifford DB, Franklin DR, et al. HIV-associated neurocognitive disorders persist in the era of potent anti-retroviral therapy. Neurology **2010**; 75(23): 2087-96.
47. Heaton RK, Franklin DR, Deutsch R, et al. Neurocognitive change in the era of HIV combination antiretroviral therapy: the longitudinal CHARTER study. Clin Infect Dis **2015**; 60(3): 473-80.
48. Becker JT, Sanders J, Madsen SK, et al. Subcortical brain atrophy persists even in HAART-regulated HIV disease. Brain Imaging Behav **2011**; 5(2): 77-85.

49. Cardenas VA, Meyerhoff DJ, Studholme C, et al. Evidence for ongoing brain injury in human immunodeficiency virus-positive patients treated with antiretroviral therapy. J Neurovirol **2009**; 15(4): 324-33.
50. Kallianpur KJ, Shikuma C, Kirk GR, et al. Peripheral blood HIV DNA is associated with atrophy of cerebellar and subcortical gray matter. Neurology **2013**; 80(19): 1792-9.
51. Chiang M, Dutton RA, Hayashi KM, et al. 3D pattern of brain atrophy in HIV/AIDS visualized using tensor-based morphometry. Neuroimage **2007**; 34(1): 44-60.
52. Thompson PM, Dutton RA, Hayashi KM, et al. 3D mapping of ventricular and corpus callosum abnormalities in HIV/AIDS. NeuroImage **2006**; 31(1): 12-23.
53. Wright PW, Pyakurel A, Vaida FF, et al. Putamen volume and its clinical and neurological correlates in primary HIV infection. AIDS **2016**; 30(11): 1789-94.
54. Young AC, Yiannoutsos CT, Hegde M, et al. Cerebral metabolite changes prior to and after antiretroviral therapy in primary HIV infection. Neurology **2014**; 83(18): 1592-600.
55. Sailasuta N, Ross W, Ananworanich J, et al. Change in Brain Magnetic Resonance Spectroscopy after Treatment during Acute HIV Infection. PLOS ONE **2012**; 7(11): e49272.
56. Spudich S, Gisslen M, Hagberg L, et al. Central Nervous System Immune Activation Characterizes Primary Human Immunodeficiency Virus 1 Infection Even in Participants with Minimal Cerebrospinal Fluid Viral Burden. J Infect Dis **2011**; 204: 753-60.
57. Suh J, Sinclair E, Peterson J, et al. Progressive increase in central nervous system immune activation in untreated primary HIV-1 infection. J Neuroinflammation **2014**; 11(199): 1-8.
58. Kessing CF, Spudich S, Valcour V, et al. High Number of Activated CD8+ T Cells Targeting HIV Antigens Are Present in Cerebrospinal Fluid in Acute HIV Infection. J Acquir Immune Defic Syndr **2017**; 75(1): 108-17.
59. Rahimy E, Li F-Y, Hagberg L, et al. Blood-Brain Barrier Disruption Is Initiatied During Primary HIV Infection and Not Rapidly Altered by Antiretroviral Therapy. The Journal of Infectious Diseases **2017**; 215: 1132-40.
60. Peluso MJ, Meyerhoff DJ, Price RW, et al. Cerebrospinal Fluid and Neuroimaging biomarker Abnormalities Suggest Early Neurological Injury in a Subset of Inidivduals During Primary HIV Infection. J Infect Dis **2013**; 207: 1703-12.

61. Ragin AB, Du H, Ochs R, et al. Structural brain alterations can be detected early in HIV infection. Neurology **2012**; 79(24): 2328-34.
62. Cohen RA, Harezlak J, Schifitto G, et al. Effects of Nadir CD4 Count and Duration of HIV Infection on Brain Volumes in the HAART Era. J Neurovirol **2010**; 16(1): 25-32.
63. Ellis RJ, Badiee J, Vaida F, et al. CD4 nadir is a predictor of HIV neurocognitive impairment in the era of combination antiretroviral therapy. AIDS **2011**; 25(14): 1747-51.
64. Hua X, Boyle CP, Harezlak J, et al. Disrupted cerebral metabolite levels and lower nadir CD4+ counts are linked to brain volume deficits in 210 HIV-infected patients on stable treatment. Neuroimage Clin **2013**; 3: 132-42.
65. Simioni S, Cavassini M, Annoni JM, et al. Cognitive dysfunction in HIV patients despite long-standing suppression of viremia. AIDS **2010**; 24(9): 1243-50.
66. Stout JC, Ellis RJ, Jernigan TL, et al. Progressive cerebral volume loss in human immunodeficiency virus infection: a longitudinal volumetric magnetic resonance imaging study. HIV Neurobehavioral Research Center Group. Arch Neurol **1998**; 55(2): 161-8.
67. Pfefferbaum A, Rogosa DA, Rosenbloom MJ, et al. Accerelated aging of selective brain structures in human immunodeficiency virus infection: a controlled, longitudinal magnetic resonance imaging study. Neurobiol Aging **2014**; 35(7): 1755-68.
68. Clifford KM, Samboju V, Cobigo Y, et al. Progressive Brain Atrophy Despite Persistent Viral Suppression in HIV Patients Older Than 60 Years. J Acquir Immune Defic Syndr **2017**; 76(3): 289-97.
69. Grant I, Franklin DR, Deutsch R, et al. Asymptomatic HIV-associated neurocognitive impairment increases risk of symptomatic decline. Neurology **2014**; 82(23): 2055-62.
70. Letendre S, Marquie-Beck J, Capparelli E, et al. Validation of CNS Penetration-Effectiveness Rank for Quantifying Antiretroviral Penetration into the Central Nervous System. Arch Neurol **2008**; 65(1): 65-70.
71. Holt JL, Kraft-Terry SD, Chang L. Neuroimaging studies of the aging HIV-1-infected brain. J Neurovirol **2012**; 18(4): 291-302.
72. Underwood J, Robertson KR, Wintson A. Could antiretroviral neurotoxicity play a role in the pathogenesis of cognitive impairment in treated HIV disease? AIDS **2015**; 29(3): 253-61.

73. Jernigan TL, Archibald SL, Fennema-Notestine C, et al. Clinical factors related to brain structure in HIV: the CHARTER study. J Neurovirol **2011**; 17(3): 248-57.
74. Robertson KR, Su Z, Margolis DM, et al. Neurocognitive effects of treatment interruption in stable HIV-positive patients in an observational cohort. Neurology **2010**; 74(16): 1260-6.
75. Brouillette M, Yuen T, Fellows LK, Cysique LA, Heaton RK, Mayo NE. Identifying Neurocognitive Decline at 36 Months among HIV-Positive Participants in the CHARTER Cohort Using Group-Based Trajectory Analysis. PLoS ONE **2016**; 11(5): 1-17.
76. Sacktor N, Skolasky RL, Seaberg E, et al. Prevalence of HIV-associated neurocognitive disoders in the Multicenter AIDS Cohort Study. Neurology **2016**; 86(4): 334-40.
77. Corrêa DG, Zimmermann N, Tukamoto G, et al. Longitudinal Assessment of Subcortical Gray Matter Volume, Cortical Thickness, and White Matter Integrity in HIV-Positive Patients. J Magn Reson Imaging **2016**; 44(5): 1262-9.
78. Chun TW, Fauci AS. HIV reservoirs: pathogenesis and obstacles to viral eradication and cure. AIDS **2012**; 26(10): 1261-8.
79. Brew BJ, Gray L, Lewin S, Churchill M. Is specific HIV eradication from the brain possible or needed? Expert Opinion on Biological Therapy **2013**; 13(3): 403-9.
80. Evering TH, Applebaum A, Mar ML, Garmon D, Dorfman D, Markowitz M. Rates of non-confounded HIV-associated neurocognitive disorders in men initiating combination antiretroviral therapy during primary infection. AIDS **2016**; 30(2): 203-10.
81. Wardlaw JM, Smith EE, Biessels GJ, et al. Neuroimaging standards for research into small vessel disease and its contribution to ageing and neurodegeneration. The Lancet Neurology **2013**; 12(8): 822-38.
82. Debette S, Markus HS. The clinical importance of white matter hyperintensities on brain magnetic resonance imaging: systematic review and meta-analysis. BMJ **2010**; 341(c3666).
83. Su T, Wit FW, Caan MW, et al. White matter hyperintensities in relation to cognition in HIV-infected men with sustained suppressed viral load on cART. AIDS **2016**; 30(15): 2329-39.

84. Watson C, Busovaca E, Foley JM, et al. White matter hyperintensities correlate to cognition and fiber tract integrity in older adults with HIV. J Neurovirol **2017**.
85. Benjamin L, Bryer A, Emsley HC, Khoo S, Solomon T, Connor MD. HIV infection and stroke: current perspectives and future directions. . Lancet Neurology **2012**; 11: 878-90.
86. Soontornniyomkij V, Umlauf A, Chung SA, et al. HIV protease inhibitor exposure predicts cerebral small vessel disease. AIDS (London, England) **2014**; 28(9): 1297-306.
87. Ryom L, Lundgren JD, El-Sadr W, et al. Cardiovascular disease and use of contemporary protease inhibitors: the D:A:D international prospective multicohort study. Lancet HIV **2018**; 5(6): e291-e300.
88. Price RW, Epstein LG, Becker JT, Cinque P, Pulliam L, McArthur JC. Biomarkers of HIV-1 CNS Infection and Injury. Neurology **2007**; 69: 1781-8.
89. Harrington PR, Haas DW, Ritola K, Swanstrom R. Compartmentalized human immunodeficiency virus type 1 present in cerebrospinal fluid is produced by short-lived cells. Journal of Virology **2005**; 79(13): 1772-88.
90. Kalehua AN, Nagel JE, Whelchel LM, et al. Monocyte chemoattractant protein-1 and macrophage inflammatory protein-2 are involved in both excitotoxin-induced neurodegeneration and regeneration. Exp Cell Res **2004**; 297(1): 197-211.
91. Fox NC, Schott JM. Imaging cerebral atrophy: normal ageing to Alzheimer's disease. The Lancet **2004**; 363(9406): 392-4.
92. Thompson PM, Jahanshad N. Novel Neuroimaging Methods to Understand How HIV Affects the Brain. Curr HIV/AIDS Rep **2015**; 12(2): 289-98.
93. Lau JC, Lerch JP, Sled JG, Henkelman RM, Evans AC, Bedell BJ. Longitudinal neuroanatomical changes determined by deformation-based morphometry in a mouse model of Alzheimer's disease. NeuroImage **2008**; 42(1): 19-27.
94. Hua X, Leow AD, Parikshak N, et al. Tensor-based morphometry as a neuroimaging biomarker for Alzheimer's disease: An MRI study of 676 AD, MCI, and normal subjects. NeuroImage **2008**; 43(3): 458-69.
95. Teipel SJ, Born C, Ewers M, et al. Multivariate deformation-based analysis of brain atrophy to predict Alzheimer's disease in mild cognitive impairment. NeuroImage **2007**; 38(1): 13-24.

96. Borghammer P, Østergaard K, Cumming P, et al. A deformation-based morphometry study of patients with early-stage Parkinson's disease. Eur J Neurol **2010**; 17(2): 314-20.
97. Tao G, Datta S, He R, Nelson F, Wolinsky JS, Narayana PA. Deep gray matter atrophy in multiple sclerosis: A tensor based morphometry. Journal of the Neurological Sciences **2009**; 282(1-2): 39-46.
98. Kipps CM, Duggins AJ, Mahant N, Gomes L, Ashburner J, McCusker EA. Progression of structural neuropathology in preclinical Huntinton's disease: a tensor based morphometry study. Journal of Neurology, Neurosurgery & Psychiatry **2004**; 76: 650-5.
99. Lyttelton O, Boucher M, Robbins S, Evans AC. An unbiased iterative group registration template for cortical surface analysis. Neuroimage **2007**; 34(4): 1535-44.
100. Thompson PM, Dutton RA, Hayashi KM, et al. Thinning of the cerebral cortex visualized in HIV/AIDS reflects CD4+ T lymphocyte decline. Proc Natl Acad Sci USA **2005**; 102(43): 15647-52.
101. Kallianpur KJ, Kirk GR, Sailasuta N, et al. Regional Cortical Thinning Associated with Detectable Levels of HIV DNA. Cereb Cortex **2011**; 22(9): 2065-75.
102. Becker JT, Maruca V, Kingsley LA, et al. Factors affecting brain structure in men with HIV disease in the post-HAART era. Neuroradiology **2012**; 54(2): 113-21.
103. Ragin AB, Wu Y, Gao Y, et al. Brain alterations within the first 100 days of HIV infection. Ann Clin Transl Neurol **2015**; 2(1): 12-21.
104. Prince JL, Links JM. Medical Imaging: Signals and Systems. In: Pearson, **2006**:381-403.
105. Frisoni GB, Fox NC, Jack CR, Scheltens P, Thompson PM. The clinical use of structural MRI in Alzheimer disease. Nature Reviews Neurology **2010**; 6: 67-77.
106. Sled JG, Zijdenbos AP, Evans AC. A nonparametric method for automatic correction of intensity nonuniformity in MRI data. IEEE Trans Med Imaging **1998**; 17(1): 87-97.
107. Narayana PA, Brey WW, Kulkarni MV, Sievenpiper CL. Compensation for surface coil sensitivity variation in magnetic resonance imaging. Magnetic Resonance Imaging **1988**; 6(3): 271-4.
108. Stollberger R, Wach P. Image of the active B1 field in vivo. Magnetic Resonance Imaging **1996**; 35: 246-51.
109. Wells WM, Grimson WEL, Kikinis R, Jolesz FA. Adaptive Segmentation of MRI Data. IEEE Transactions on Medical Imaging **1996**; 15(4).

110. Tustison NJ, Avants BB, Cook PA, et al. N4ITK: Improved N3 Bias Correction. IEEE Transactions on Medical Imaging **2010**; 29(6): 1310-20.
111. Collins DL, Neelin P, Peters TM, Evans AC. Automatic 3D intersubject registration of MR volumetric data in standardized Talairach space. J Comput Assist Tomogr **1994**; 18(2): 192-205.
112. Klein A, Andersson J, Ardekani BA, et al. Evaluation of 14 nonlinear deformation algorithms applied to human brain MRI registration. NeuroImage **2009**; 46(3): 786-802.
113. Ashburner J, Friston KJ. Voxel-Based Morphometry - The Methods. Neuroimage **2000**; 11(6): 805-21.
114. Chung MK, Worsley KJ, Paus T, et al. A Unified Statistical Approach to Deformation-Based Morphometry. NeuroImage **2001**; 14(3): 595-606.
115. Sotiras A, Davatzikos C, Paragios N. Deformable Medical Image Registration: A Survery. IEEE Transactions on Medical Imaging **2013**; 32(7): 1153-90.
116. Maes F, Collignon A, Vandermeulen D, Marchal G, Suetens P. Mulitmodality Image Registration by Maximization of Mutual Information. IEEE Transactions on Medical Imaging **1997**; 15(2): 187-98.
117. Dadar M, Fonov VS, Collins DL. A comparison of publicly available linear MRI stereotaxic registration techniques. NeuroImage **2018**; 174: 191-200.
118. Oliveira FPM, Tavares JMRS. Medical image registraton: a review. Computer Methods in Biomechanics and Biomedical Engineering **2014**; 17(2): 73-93.
119. Avants BB, Epstein CL, Grossman M, Gee JC. Symmetric diffeomorphic image registration with cross-correlation: Evaluating automated labeling of elderly and neurodegenerative brain. Medical Image Analysis **2008**; 12: 26-41.
120. Maes F, Vandermeulen D, Suetens P. Comparative evaluation of multiresolution optimization strategies for multimodality image registration by maximization of mutual information. Medical Image Analysis **1999**; 3(4): 373-86.
121. Pluim JPW, Maintz JBA, Viergever MA. Image Registration by Maximization of Combined Mutual Information and Gradient Information. Medical Image Computing and Computer-Assisted Intervention **2000**; 1935: 452-61.
122. Eskildsen SF, Coupe P, Fonov V, et al. BEaST: Brain Extraction based on nonlocal Segmentation Technique. Neuroimage **2012**; 59(3): 2362–73.

123. Smith SM. Fast robust automated brain extraction. Human Brain Mapping **2002**; 17(3): 143-55.
124. Krizhevsky A, Sutskever I, Hinton GE. ImageNet Classification with Deep Convolutional Neural Network. Advances in Neural Information Processing Systems 25 **2012**.
125. Wachinger C, Reuter M, Klein T. DeepNAT: Deep convolutional neural network for segmenting neuroanatomy. NeuroImage **2018**; 179: 434-45.
126. Kleesiek J, Urban G, Hubert A, et al. Deep MRI brain extraction: A 3D convolutional neural network for skull stripping. NeuroImage **2016**; 129: 460-9.
127. Despotovic I, Goosens B, Philips W. MRI Segmentation of the Human Brain: Challenges, Methods, and Applications. Computational and Mathematical Methods in Medicine **2015**.
128. Fischl B, Salat DH, Busa E, et al. Whole Brain Segmentation: Automated Labelling of Neuroanatomical Strucutures in the Human Brain. Neurotechnique **2002**; 33: 341-55.
129. Li SZ. Markov Random Field Modeling in Computer Vision. Berlin: Springer-Verlag, **1995**.
130. Leemput KV, Maes F, Vandermeulen D, Suetens P. Automated Model-Based Tissue Classification of MR Images of the Brain. IEEE Transactions on Medical Imaging **1999**; 18(10): 897-908.
131. Subbanna NK, Shah M, Francis SJ, et al. MS Lesion Segmentation using Markov Random Fields. In: MICCAI Workshop on Medical Image Analysis on Multiple Sclerosis. London, UK, 2009:37-48.
132. Chen H, Dou Q, Yu L, Qin J, Heng P. VoxResNet: Deep voxelwise residual networks for brain segmentation from 3D MR images. NeuroImage **2018**; 170: 446-55.
133. Mendrik AM, Vincken KL, Kuijf HJ, et al. MRBrainS Challenge: Online Evaluation Framework for Brain Image Segmentation in 3T MRI Scans. Computational Intelligence and Neuroscience **2015**; 2015: 16.
134. Evans AC, Janke AL, Collins DL, Baillet S. Brain templates and atlases. NeuroImage **2012**; 62(2): 911-22.
135. Fonov VS. ICBM 152 Nonlinear atlases version 2009. Available at: http://www.bic.mni.mcgill.ca/ServicesAtlases/ICBM152NLin2009.

136. Fonov V, Evans AC, Botteron K, McKinstry R, Collins DL. Unbiased average age-appropriate atlases for pediatric studies. Neuroimage **2011**; 54(1): 313-27.
137. Collins DL, Pruessner JC. Towards accurate, automatic segmentation of the hippocampus and amygdala from MRI by augmenting ANIMAL with a template library and label fusion. NeuroImage **2010**; 52(3): 1355-66.
138. Collins DL, Holmes CJ, Peters TM, Evans AC. Automatic 3-D model-based neuroanatomical segmentation. Hum Brain Mapp **1995**; 3(3): 190-208.
139. Aljabar P, Heckermann R, Hammers A, Hajnal JV, Rueckert D. Classifier Selection Strategies for Label Fusion Using Large Atlas Databases. Medical Image Computing and Computer-Assisted Intervention **2007**; 4791: 523-31.
140. Kamnitsas K, Ledig C, Newcombe VFJ, et al. Efficient multi-scale 3D CNN with fully connected CRF for accurate brain lesion segmentation. Medical Image Analysis **2017**; 36.
141. Dadar M, Zeighami Y, Yau Y, et al. White matter hyperintensities are linked to future cognitive decline in de novo Parkinson's disease patients. Neuroimage Clin **2017**; 20: 892-900.
142. Guizard N, Nakamura K, Coupe P, Fonov VS, Arnold DL, Collins DL. Non-Local Means Inpainting of MS Lesions in Longitudinal Image Processing. Frontiers in Neuroscience **2015**.
143. Prastawa M, Bullitt E, Ho S, Gerig G. A brain tumor segmentation framework based on outlier detection Medical Image Analysis **2004**; 8(3): 275-83.
144. Geremia E, Menze BH, Clatz O, Konukoglu E, Criminisi A, Ayache N. Spatial decision forests for MS lesion segmentation in multi-channel MR images. NeuroImage **2010**; 57(2): 378-90.
145. Zikic D, Glocker B, Konukoglu E, et al. Decision forests for tissue-specific segmentation and high-grade gliomas in multi-channel MR. Medical Image Computing and Computer-Assisted Intervention **2012**: 369-76.
146. Tustison N, Wintermark M, Durst C, Avants B. ANTS and Arboles. BRATS-MICCAI **2013**.

147. Dadar M, Pascoal TA, Manitsirikul S, et al. Validation of a Regression Technique for Segmentation of White Matter Hyperintensities in Alzheimer's Disease. IEEE Transactions on Medical Imaging **2017**; 36(8): 1758-68.
148. Dadar M, Maranzano J, Misquitta K, et al. Performance comparison of 10 different classification techniques in segmenting white matter hyperintensities in aging. NeuroImage **2017**; 157: 233-49.
149. Havaei M, Davy A, Warde-Farley D, et al. Brain tumor segmentation with Deep Neural Networks. Medical Image Analysis **2017**; 35: 18-31.
150. Kamnitsas K, Chen L, Ledig C, Rueckert D, Glocker B. Multi-scale 3D con- volutional neural networks for lesion segmentation in brain MRI. In: ISLES-MICCAI, 2015.
151. Brosch T, Tang LYW, Yoo Y, Li DKB, Traboulsee A, Tam R. Deep 3D Convolutional Encoder Networks With Shortcuts for Multiscale Feature Integration Applied to Multiple Sclerosis Lesion Segmentation. IEEE Transactions on Medical Imaging **2017**; 35(5): 1229-39.
152. Valverde S, Cabezas M, Roura E, et al. Improving automated multiple sclerosis lesion segmentation with a cascaded 3D convolutional neural network approach. NeuroImage **2017**; 155: 159-68.
153. Menze BH, Jakab A, Bauer S, et al. The Multimodal Brain Tumor Image Segmentation Benchmark (BRATS). IEEE Transactions on Medical Imaging **2015**; 34(10): 1993-2024.
154. Lepore N, Brun C, Chou Y, et al. Generalized Tensor-Based Morphometry of HIV/AIDS Using Multivariate Statistics on Deformation Tensors. IEEE Trans Med Imaging **2008**; 27(1): 129-41.
155. Good CD, Johnsrude IS, Ashburner J, Henson RN, Friston KJ, Frackowiak RS. A Voxel-Based Morphometric Study of Ageing in 465 Normal Adult Human Brains. NeuroImage **2001**; 14(1): 21-36.
156. Braak H, Braak E. Neuropathological stageing of Alzheimer-related changes. Acta Neuropathologica **1991**; 82(4): 239-59.
157. MacDonald D, Kabani N, Avis D, Evans AC. Automated 3-D Extraction of Inner and Outer Surface of Cerebral Cortex from MRI. NeuroImage **2000**; 12.
158. Eskildsen SF, Østergaard LR. Active Surface Approach for Extraction of the Human Cerebral Cortex from MRI. Med Image Comput Comput Assist Interv **2006**; 9: 823-30.

159. Kim JS, Singh V, Lee JK, et al. Automated 3-D extraction and evaluation of the inner and outer cortical surfaces using a Laplacian map and partial volume effect classification. NeuroImage **2005**; 27: 210-21.
160. Lorenson WE, Cline HE. Marching cubes: A high resolution 3-d surface construction algorithm. Computer Graphics **1987**; 21(4).
161. Dale AM, Fischl B, Sereno MI. Cortical surface-based analysis: segmentation and surface reconstruction. NeuroImage **1999**; 9: 179-94.
162. Järnum H, Eskildsen SF, Steggensen EG, et al. Longitudinal MRI study of cortical thickness, perfusion, and metabolite levels in major depressive disorder. Acta Psychiatr Scand **2011**; 124(6): 435-46.
163. Harvey PD. Clinical applications of neuropsychological assessment. Dialogues in Clinical Neuroscience **2012**; 14(1): 91-9.
164. Benedict RH, Schretlen B, Groninger L, Brandt J. Hopkins Verbal Learning Test - Revised: normative data and analysis of enter-form and test-retest reliability. The Clinical Neuropsychologist **1998**; 12: 43-55.
165. Spreen O, Strauss E. A Compendium of Neuropsychological Tests. New York: Oxford University Press, **1998**.
166. Piatt AL, Fields JA, Paolo AM, Koller WC, Troster AI. Lexical, semantic, and action verbal fluency in Parkinson's disease with and without dementia. Journal of Clinical and Experimental Neuropsychology **1999**; 21: 435-43.
167. Gladsjo JA, Schuman CC, Evans JD, Peavy GM, Miller SW, Heaton RK. Norms for letter and category fluency: demographic corrections for age, education, and ethnicity. Assessment **1999**; 6: 147-78.
168. Reitan RM, Wolfson D. The Halstead-Reitan Neuropsychological Test Battery. Tucson, Arizona: Neuropsychology Press, **1985**.
169. Wechsler D. Wechsler Adult Intelligence Scale, 3rd edition. San Antonio: The Psychological Corporation, **1997**.
170. Golden CJ. Stroop Color and Word Test. Chicago: Stoelting, **1978**.
171. Heaton RK, Chelune GJ, Talley JL, Kay GG, Curtis G. Revised Comprehensive Normans for an expanded Halstead-Reitan Battery: Demographically adjusted neuropsychological

norms for African American and Caucasian Adults. Lutz, Florida: Psychological Assessment Resources, Inc, **2004**.

172. Robertson KR, Parsons TD, Sidtis JJ, et al. Timed Gait test: normative data for the assessment of the AIDS dementia complex. Journal of Clinical and Experimental Neuropsychology **2006**; 28(7): 1053-64.
173. Brouillette M, Mayo N, Fellows LK, et al. A better screening tool for HIV-associative neurocognitive disorders: is it what clinicians need? AIDS **2015**; 29: 895-902.
174. Armitage P, Berry G, Matthews JNS. Statistical Methods in Medical Research: Wiley, **2002**.
175. Weir JM, Dunn JE. Smoking and mortality: A prospective study. Cancer **1970**; 25(1).
176. Locascio JJ, Atri A. An Overview of Longitudinal Data Analysis Methods for Neurological Research. Dement Geriatr Cogn Dis **2011**; 1: 330-57.
177. Pinheiro JC. Linear Mixed Effects Models for Longitudinal Data. Encyclopedia of Biostatistics **2005**.
178. Sullivan GM, Feinn R. Using Effect Size - or Why the P Value is Not Enough. Journal of Graduate Medical Education **2012**; 4(3): 279-82.
179. Sakpal TV. Sample Size Estimation in Clinical Trial. Perspectives in Clincal Research **2010**; 1(2): 67-9.
180. Poldrack RA, Baker CI, Durnez J, et al. Scanning the horizon: towards transparent and reproducible neuroimaging research. Nature Reviews Neuroscience **2017**; 18: 115-26.
181. Dunn O. Multiple Comparisons Among Means. Journal of American Statistical Association **1961**; 56(293): 52-64.
182. Worsley KJ, Andermann M, Koulis T, MacDonald D, Evans AC. Detecting changes in non-isotropic images. Human Brain Mapping **1999**; 9: 98-101.
183. Genovese CR, Lazar NA, Nichols T. Thresholding of Statistical Maps in Functional Neuroimaging Using the False Discovery Rate. Neuroimage **2002**; 15(4): 870-8.
184. Nichols TE, Holmes AP. Nonparametric permutation tests for functional neuroimaging: A primer with examples. Human Brain Mapping **2002**; 15(1): 1-25.
185. Küper M, Rabe K, Esser S, et al. Structural gray and white matter changes in patients with HIV. J Neurol **2011**; 258(6): 1066-75.

186. Janssen MAM, Meulenbroek O, Steens SCA, et al. Cognitive function, wellbeing and brain correlates in HIV-1 infected patients on long-term combination antiretroviral therapy. AIDS **2015**; 29(16): 2139-48.
187. Wade BSC, Valcour VG, Wendelken-Riegelhaupt L, et al. Mapping abnormal subcortical brain morphometry in an ederly HIV+ cohort. Neuroimage Clin **2015**; 9: 564-73.
188. Castelo JMB, Courtney MG, Melrose RJ, Stern CE. Putamen Hypertrophy in Nondemented Patients With Human Immunodeficiency Virus Infection and Cognitive Compromise. Arch Neurol **2007**; 64(9): 1275-80.
189. Ances BM, Hammoud DA. Neuroimaging of HIV Associated Neurocognitive Disorders (HAND). Curr Opin HIV AIDS **2014**; 9(6): 545-51.
190. Coupe P, Yger P, Prima S, Hellier P, Kervrann C, Barillot C. An optimized blockwise nonlocal means denoising filter for 3D magnetic resonance images. IEEE Trans Med Imaging **2008**; 27(4): 425-41.
191. Zijdenbos AP, Forghani R, Evans AC. Automatic 'pipeline' analysis of 3-D MRI data for clinical trials: application to multiple sclerosis. IEEE Trans Med Imaging **2002**; 21(10): 1280-91.
192. Ashburner J, Hutton C, Frackowiak R, Johnsrude I, Price C, Friston KJ. Identifying Global Anatomical Differences: Deformation-Based Morphometry Hum Brain Mapp **1998**; 6(5-6): 348-57.
193. Collins DL, Le Goualher G, Evans AC. Non-linear cerebral registration with sulcal constraints. In: Wells WM, Colchester A, Delp S. Medical Image Computing and Computer-Assisted Interventation — MICCAI'98: First International Conference Cambridge, MA, USA, October 11–13, 1998 Proceedings. Berlin: Springer, **1998**:974-84.
194. Nir TM, Jahanshad N, Busovaca E, et al. Mapping white matter integrity in elderly people with HIV. Hum Brain Mapp **2014**; 35(3): 975-92.
195. Wright PW, Vaida FF, Fernández RJ, et al. Cerebral white matter integrity during primary HIV infection. AIDS **2015**; 29(4): 433-42.
196. Plessis Sd, Vink M, Joska JA, et al. Prefrontal cortical thinning in HIV infection is associated with impaired striatal functioning. J Neural Transm **2016**; 123(6): 643-51.

197. Pfefferbaum A, Rosenbloom MJ, Sassoon SA, et al. Regional Brain Structural Dysmorphology in HIV Infection: Effects of AIDS, Alcoholism, and Age. Biol Psychiatry **2012**; 72(5): 361-70.
198. Moore DJ, Masliah E, Rippeth JD, et al. Cortical and subcortical neurodegeneration is associated with HIV neurocognitive impairment. AIDS **2006**; 20(6): 879-87.
199. Kuller LH, Lopez OL, Newman A, et al. Risk factors for dementia in the cardiovascular health cognition study. Neuroepidemiology **2003**; 22(1): 13-22.
200. Janssen MAM, Koopmans PP, Kessels RPC. Cognitive Decline in Relation to Psychological Wellbeing and HIV Disease- and Treatment Characteristics in HIV-Infected Patients on cART: A One-Year Follow-Up Study. AIDS Behav **2016**: 1-7.
201. Casaletto KB, Cattie J, Franklin DR, et al. The Wide Range Achievement Test-4 Reading subtest "holds" in HIV-infected invdividuals. J Clin Exp Neuropsychol **2014**; 36(9): 992-1001.
202. Guizard N, Fonov VS, Garcia-Lorenzo D, Nakamura K, Aubert-Broche B, Collins DL. Spatio-Temporal Regularization for Longitudinal Registration to Subject-Specific 3d Template. PLoS ONE **2015**; 10(8).
203. Aubert-Broche B, Fonov VS, Garcia-Lorenzo D, et al. A new method for structural volume analysis of longitudinal brain MRI data and its application in studying the growth trajectories of anatomical brain structures in childhood. Neuroimage **2013**; 82(15): 393-402.
204. Eskildsen SF, Østergaard LR. Evaluation of five algorithms for mapping brain cortical surfaces. 2008 XXI Brazilian Symposium on Computer Graphics and Image Processing **2008**: 137-44.
205. Pacheco J, Goh JO, Kraut MA, Ferrucci L, Resnick SM. Greater cortical thinning in normal older adults predicts later cognitive impairment. Neurobiol Aging **2015**; 36(2): 903-8.
206. Norman GR, Sloan JA, Wyrwich KW. Interpretation of Changes in Health-related Quality of Life: The Remarkable Unvisaility of Half a Standard Deviation. Med Care **2003**; 41(5): 582-92.
207. Prakash A, Hou J, Liu L, Gao Y, Kettering C, Ragin AB. Cognitive function in early HIV infection. J Neurovirol **2016**: 1-10.

208. Sanford R, Cruz ALF, Scott SC, et al. Regionally Specific Brain Volumetric and Cortical Thickness Changes in HIV-infected Patients in the HAART era. J Acquir Immune Defic Syndr **2017**; 74(5): 563-70.
209. Sanford R, Fellows LK, Ances BM, Collins DL. Association of Brain Structure Changes and Cognitive Function With Combination Antiretroviral Therapy in HIV-Positive Individuals. JAMA Neurol **2018**; 75(1): 72-9.
210. Kelly SG, Taiwo BO, Wu Y, et al. Early suppressive antiretroviral therapy in HIV infection is associated with measurable changes in the corpus callosum. J Neurovirol **2014**; 20(5): 514-20.
211. Zetola NM, Pilcher CD. Diagnosis and management of acute HIV infection. Infect Dis Clin North Am **2007**; 21: 19-48.
212. Spudich S, Nilsson AC, Lollo ND, et al. Cerebrospinal fluid HIV infection and pleocytosis: Relation to systemic infection and antiretroviral treatment. BMC Infect Dis **2005**; 5(98).
213. Fox NC, Schott JM. Imaging cerebral atrophy: normal ageing to Alzheimer's disease. Lancet **2004**; 363: 392-4.
214. Klunder AD, Chiang M, Dutton RA, et al. Mapping Cerebellar Degeneration in HIV/AIDS. Neuroreport **2008**; 19(17): 1655-9.
215. Wardlaw JM, Smith EE, Biessels GJ, et al. Neuroimaging standards for research into small vessel disease and its contribution to ageing and neurodegeneration. Lancet Neurol **2013**; 12(8): 822-38.
216. Currier JS, Lundgren JD, Carr A, et al. Epidemiological Evidence for Cardiovascular Disease in HIV-Infected Patients and Relationship to Highly Active Antiretroviral Therapy. Circulation **2008**; 118: e29-e35.
217. Cole JH, Caan MWA, Underwood J, et al. No evidence for accelerated ageing-related brain pathology in treated HIV: longitudinal neuroimaging results from the Comorbidity in Relation to AIDS (COBRA) project. Clin Infect Dis **2018**; 66(12): 1899-909.
218. Sanford R, Ances BM, Meyerhoff DJ, et al. Longitudinal Trajectories of Brain Volume and Cortical Thickness in Treated and Untreated Primary HIV Infection. Clin Infect Dis **2018**; 67(11): 1697-704.

219. Haddow L, Laverick R, Leung I, et al. Measurement of Retinal Vessels as a Biomarker of Cerebrovascular Aging in Older HIV-Positive Men Compared With Controls. J Acquir Immune Defic Syndr **2018**; 77(2): 199-205.
220. Wu M, Fatukasi O, Yang S, et al. HIV disease and diabetes interact to affect brain white matter hyperintensities and cognition. AIDS **2018**; Publish Ahead of Print.
221. McArthur JC, Kumar JA, Johnson DW, et al. Incidental White Matter Hyperintensities on Magnetic Resonance Imaging in HIV-1 Infection. J Acquir Immune Defic Syndr **1990**; 3(3).
222. Haddow LJ, Dudau C, Chandrashekar H, Cartledge JD, Hyare H, Miller RF. Cross-sectional study of unexplained white matter lesions in HIV positive individuals undergoing brain magnetic resonance imaging. AIDS Patient Care STDS **2014**; 28: 341-9.
223. McMurtray A, Nakamoto B, Shikuma C, Valcour V. Cortical atrophy and white matter hyperintensities in HIV: The Hawaii Aging with HIV Cohort Study. J Stroke Cerebrovasc Dis **2008**; 17(4): 212-7.
224. Dadar M, Maranzano J, Ducharme S, Carmichael OT, Decarli C, Collins DL. Validation of T1w-based segmentations of white matter hyperintensity volumes in large-scale datasets of aging. Hum Brain Mapp **2018**; 39(3): 1093-107.
225. Kennedy G, Hardman RJ, Macpherson H, Scholey AB, Pipingas A. How Does Exercise Reduce the Rate of Age-Associated Cognitive Decline? A Review of Potential Mechanisms. J Alzheimers Dis **2016**; 55(1): 1-18.
226. Seider TR, Gongvatana A, Woods AJ, et al. Age exacerbates HIV-associated white matter abnormalities. J Neurovirol **2015**; 22(2): 201-12.
227. Reynolds NR. Cigarette smoking and HIV: more evidence for action. AIDS Educ Prev **2009**; 21(3 Suppl): 106-21.
228. Paula AA, Falcão MC, Pacheco AG. Metabolic syndrome in HIV-infected individuals: underlying mechanisms and epidemiological aspects. AIDS Research and Therapy **2013**; 10(1): 32.
229. Mosca L, Barrett-Connor E, Kass Wenger N. Sex/Gender Differences in Cardiovascular Disease Prevention. Circulation **2011**; 124(19): 2145-54.

230. Appelman APA, Exalto LG, van der Graaf Y, Biessels GJ, Mali WPTM, Geerlings MI. White Matter Lesions and Brain Atrophy: More than Shared Risk Factors? A Systematic Review. Cerebrovascular Diseases **2009**; 28(3): 227-42.
231. Robertson KR, Robertson WT, Ford S, et al. Highly Active Antiretroviral Therapy Improves Neurocognitive Functioning. Journal of Acquired Immune Deficiency Syndrome **2004**; 36(1): 562-6.
232. Hillman CH, Erickson KI, Kramer AF. Be smart, exercise your heart: exercise effects on brain and cognition. Nature Reviews Neuroscience **2008**; 9: 58-65.
233. Ngandu T, Lehtisalo J, Solomon A, et al. A 2 year multidomain intervention of diet, exercise, cognitive training, and vascular risk monitoring versus control to prevent cognitive decline in at-risk elderly people (FINGER): a randomised controlled trial. The Lancet **2015**; 385(9984): 2255-63.

# Appendix

## A.3. Chapter 3 Appendix

### A.3.1. Rasch Analysis

Rasch analysis was applied to summarize neuropsychological performance; we have described the conceptual and mathematical advantages of this approach over more conventional averaging methods in detail elsewhere[1] .

The extent to which the scores on neuropsychological tests fit a unidimensional, hierarchical model representing the single latent construct of cognitive ability was tested using Rasch analysis. The partial credit model for ordered response categories was used within the Rasch Unidimensional Measurement Model program (RUMM 2030). To fit the data to the Rasch model, the continuous measurement scale for each neuropsychological test (termed items) was converted into unique ordered categories, the number of which depended on the distribution of the outcome.

The first step is to ensure hierarchically ordered thresholds such that a person with a higher level of cognitive ability is more likely to pass thresholds determined to be more difficult. With k ordered categories, the number of thresholds is k-1. Disordered thresholds were iteratively rescored by collapsing adjacent response options. After rescoring, higher values on these tests (items) now represent more cognitive ability.

Fit of the data to the model was evaluated using a $\chi 2$ goodness of fit test where a probability value >0.05 indicates fit. Two other measures of test fit were also used: item-fit residuals between -2.5 and 2.5 and item Chi-square tests >0.05. Reliability was also estimated, using the person separation index (PSI).

Pairs of items with residual correlation >0.4 were examined and one of the items was removed; the choice was based on both theoretical and statistical considerations. Once the best fitting set of tests was identified, unidimensionality was assessed by the principal component analysis (PCA) of the fit residuals. If the first PCA explains >10% of residual variance, this is an indicator of lack of unidimensionality. Items that remain highly correlated once the effect of the latent trait is removed also indicate lack of unidimensionality. Once a fitting model was obtained, items were examined for differential item functioning (DIF) across sex, age, education, race and HIV status. DIF was considered present for items with *p*-values on a two-way ANOVA that were significant at the level of 0.05 after applying the Bonferroni correction for multiple comparisons. Targeting of patient ability to item difficulty was examined via the person-item distribution plot.

### A.3.2. Statistical Analysis

Regional brain volume and cortical thickness estimates were modeled by fitting the following linear equation at each voxel:

$$\boldsymbol{Vol} = \boldsymbol{\beta_0} + \boldsymbol{\beta_1} \cdot \boldsymbol{Age} + \boldsymbol{\beta_2} \cdot \boldsymbol{Gender} + \boldsymbol{\beta_3} \cdot \boldsymbol{Edu} + \boldsymbol{\beta_4} \cdot \boldsymbol{Ethnicity} + \boldsymbol{\beta_5} \cdot \boldsymbol{Covariate\ of\ interest} + \boldsymbol{\varepsilon}$$

Here, *Vol* is the value of the Jacobian determinant, tissue density, or cortical thickness estimate, *Covariate of interest* is HIV status, nadir CD4, current CD4, current viral load, viral suppression status (detectable versus undetectable), CPE score, treatment status (treated versus untreated), or cognitive function as summarized by Rasch analysis, and $\varepsilon$ is the residual. Discrete variables (gender, ethnicity, HIV status, viral suppression status, and treatment status) were treated as binary variables. Each linear model was applied in a voxel-wise fashion creating a 3D statistical map allowing the patterns of significance to be visualized. Both positive and negative correlations were tested in all models.

The final linear model was chosen by minimizing the Akaike Selection Criterion (AIC)[2]. Increasing the number of parameters in the model improves the fit, but it comes at the cost of increasing complexity. The AIC balances the goodness of fit and the number of parameters by penalizing the number of covariates in the model. The model that has the lowest AIC is suggested to be the most optimal model. While there were no group differences in education and ethnicity, these variables were included in the final linear model because they minimized the AIC.

### A.3.3. Rasch Analysis Results

All available neuropsychological test scores were entered into a Rasch analysis, to determine if they could be summarized as reflecting a single latent construct. The sample available for the Rasch analysis (N=388; 284 HIV-infected, 104 HIV-uninfected) was larger than the sample available for the imaging analysis; in the latter, participants were excluded if they were missing neuroimaging, demographic or clinical information required for the primary analysis.

Neuropsychological tests scores were initially modelled with between seven and 13 categories; ten of the 16 tests had disordered thresholds. After rescoring, the number of levels per item was reduced to between two and eight. Due to response dependency, three items with correlations greater than 0.4 were removed: Hopkins Verbal Learning Delayed Recall, one measure from the Stroop test, and Grooved Pegboard, Dominant Hand. Grooved Pegboard, Non-

Dominant Hand was found to have DIF by age (i.e. suggesting that the item was not measuring the same ability in all participants), and was also dropped.

The final model consisted of 12 NP tests (Table S1). Reliability of the final model was 0.85, regardless of whether extreme values were included. Items and persons fit the model, with fit residuals having a mean 0.10 (SD: 1.06) and -0.29 (SD: 1.03), respectively. (Ideal fit residuals have a mean of 0 and standard deviation of 1.) All item fit residuals fell between -2.5 and 2.5 and none were statistically significant. Global fit was confirmed (nonsignificant global item trait $X^2$ of 85.24 on 72 df, p=0.14). Targeting of person ability to item difficulty was good, with a fluid distribution of both persons and items across seven logits, from -3 to 4, though items were available over nine logits, from -4 to 5 (Figure S1).

The final model was used to estimate the performance of each participant on the latent construct of 'cognitive ability', and these scores were then entered into the analyses relating brain structural indices to neuropsychological performance described in the main paper.

Table S1: Neuropsychological tests that contributed to the Rasch model (mean raw scores ± SD).

| | **HIV-infected** | **HIV-uninfected** |
|---|---|---|
| Hopkins Verbal Learning Total Learning Score | 21.2 ± 5.24 | 24.2 ± 4.37 |
| Symbol Search | 26.5 ± 8.36 | 33.6 ± 6.81 |
| Letter Number Sequencing | 7.79 ± 3.81 | 9.14 ± 2.71 |
| Digit-Symbol | 8.92 ± 3.23 | 10.79 ± 3.09 |
| Trail-Making Test A | 36.5 ± 19.7 | 26.1 ± 7.74 |
| Trail-Making Test B | 97.0 ± 50.0 | 72.7 ± 41.3 |
| Stroop 1 Time | 33.6 ± 8.17 | 29.0 ± 5.35 |
| Stroop 3 Time | 76.1 ± 30.5 | 56.6 ± 11.4 |
| Verbal Fluency | 12.4 ± 5.56 | 14.9 ± 6.42 |
| FAS Fluency | 38.1 ± 43.7 | 38.8 ± 12.2 |
| Animal Fluency | 19.0 ± 5.12 | 22.8 ± 4.94 |
| Test of Memory Malingering | 46.0 ± 5.20 | 48.7 ± 1.94 |

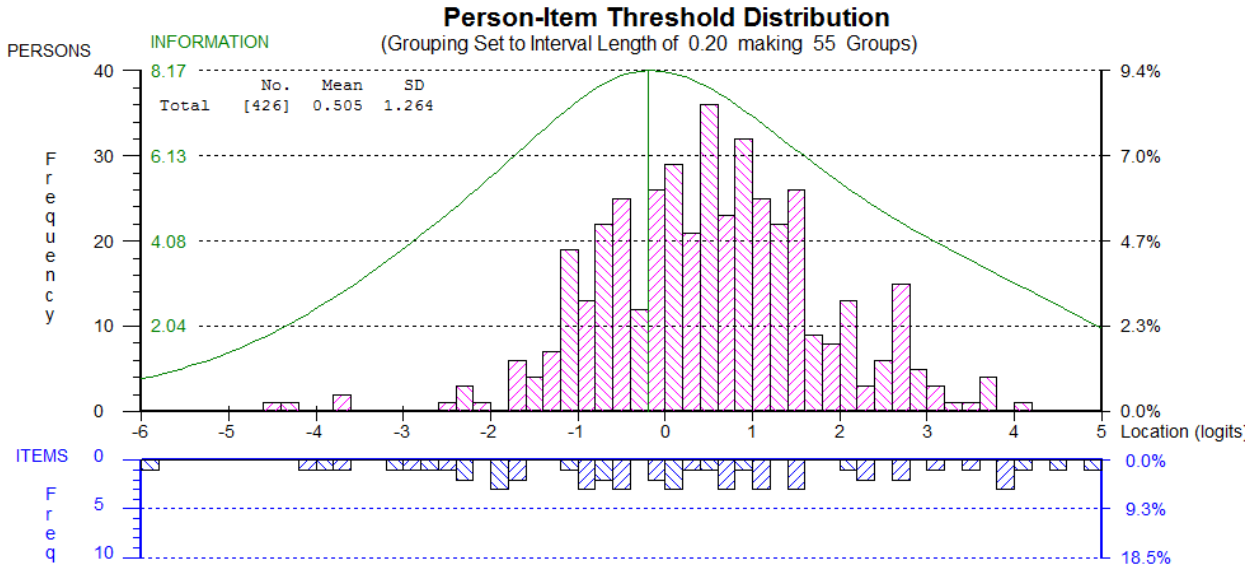


Figure S1: Distribution of persons (HIV-infected and HIV-uninfected groups collapsed) located according to position along a continuum of 'cognitive ability' (top panel), and the distribution of the items retained in the Rasch model that measure this latent construct (bottom panel). Items were available to assess the full range of ability demonstrated by the sample, with good coverage in the range of ability showed by most of the sample (i.e. items were well-targeted to the ability of the persons in this sample).

## A.4. Chapter 4 Appendix

### A.4.1. Statistical Analysis

We used multivariable mixed-effects modeling to compare raw neuropsychological test scores and brain volume estimates between the HIV+ and HIV- groups, and to determine if HIV serostatus significantly influences changes in these measures over the study period. Mixed-effects models have become a powerful statistical technique for longitudinal data analysis because they can account for intra-subject correlations, missing data, and biases due to attrition[3]. Any mixed effects model requires a combination of fixed and random effects. The fixed effects structure can provide estimates for overall group responses (i.e. group comparisons) and response changes over time. The interaction between these fixed effects can be used to compare the response changes over time by group. The random effects structure models subject-specific responses to account for within-subject correlations and minimizes biases in estimation due to attrition.

The mixed-effects models included all available data from both visits. To assess neuropsychological performance and regional brain volumes in the mixed-effects model, these measures were considered as the dependent variable in the models. The fixed effects structure included HIV serostatus, time (years from baseline visit), average age (mean age of at baseline and follow-up), sex, and the interaction between HIV serostatus and time. Within the HIV+ and HIV- groups, separate mixed-effects models assessed the change in neuropsychological performance or brain volumes between visits by including time, age and sex as a fixed effects to determine if greater-than-age related changes occurred in these measures over time. With only HIV+ participants, neuropsychological performance and brain volumes were regressed against current CD4, CD4 nadir and duration of infection. The random effects structure for all models included a subject-level random intercept.

In all the models raw neuropsychological test scores, voxel-wise brain volumes, vertex-wise cortical thickness estimates, age, education, time, measures of immune status (current and nadir CD4 cell counts), CPE score, and duration of HIV infection were treated as continuous variables, while gender and ethnicity were treated as binary variables (i.e. 0 and 1).

Optimal model structures were selected by minimizing the Akaike Information Criterion (AIC)[2], while the fit of different mixed-effects models were compared via the likelihood ratio test. If two mixed-effects models had similar AIC values, and the model with more fixed effects did not significantly improve model fit, the simplest model was chosen. All mixed-effects models were estimated with the maximum-likelihood method. To verify that this study had sufficient

statistical power to detect clinically-meaningful structural brain volume changes over two years in the HIV+ group compared to HIV- controls, the minimum detectable difference between the groups in the change in brain volumes over time was calculated.

Table S6: Neuropsychological test scores at baseline and follow-up.

| Neuropsychological test | HIV+ | | | HIV- | | | Group statistics | |
|---|---|---|---|---|---|---|---|---|
| | **Baseline [mean (SD)]** | **Follow-up [mean (SD)]** | ***p* for change over time [a]** | **Baseline [mean (SD)]** | **Follow-up [mean (SD)]** | ***p* for change over time [a]** | **HIV+ vs. HIV- [a]** | **Group x time [a]** |
| Trail Making Test A [b] (time to completion, sec) | 32.5 (11.0) | 30.9 (12.4) | 0.08 | 26.0 (7.6) | 27.9 (9.5) | 0.1 | 0.01* | 0.03* |
| Trail Making Test B [b] (time to completion, sec) | 93.7 (38.0) | 84.9 (34.1) | 0.2 | 62.4 (16.4) | 65.2 (21.1) | 0.2 | <0.001** | 0.1 |
| HVLT-R – immediate recall [c] (number of correct words) | 20.8 (4.7) | 21.6 (5.22) | 0.3 | 23.4 (4.7) | 23.4 (5.4) | 0.9 | 0.05* | 0.6 |
| HVLT-R – delayed recall [c] (number of correct words) | 7.5 (2.4) | 7.1 (4.1) | 0.6 | 8.5 (3.1) | 8.1 (2.8) | 0.4 | 0.2 | 0.9 |
| Digit Symbol Substitution Task [c] (number of correct marks) | 65.3 (15.3) | 67.5 (16.9) | 0.02* | 76.6 (15.9) | 77.3 (13.1) | 0.7 | <0.001** | 0.3 |
| Letter-Number Sequencing [c] (number of correct marks) | 8.3 (3.2) | 8.6 (2.3) | 0.7 | 10.9 (2.7) | 10.9 (3.0) | 0.8 | <0.001** | 0.5 |
| Action Fluency [c] (number of verbs) | 12.6 (4.9) | 13.0 (5.7) | 0.7 | 15.6 (7.4) | 15.0 (7.5) | 0.2 | 0.1 | 0.3 |
| Letter Fluency [c] (number of words) | 33.4 (11.2) | 36.6 (10.2) | 0.003* | 40.1 (12.7) | 43.6 (12.2) | 0.02* | 0.01* | 0.8 |

** $p<0.001$; * $p=0.001$-$0.05$

[a] Statistical models included all available data from both time points adjusting for age, sex, and education with mixed-effects modeling. Participant level intercept was included as a random effect. *P* value derived from likelihood ratio testing.
[b] Lower scores indicate better performance.
[c] Higher scores indicate better performance

## A.4.2. Supplementary Figures

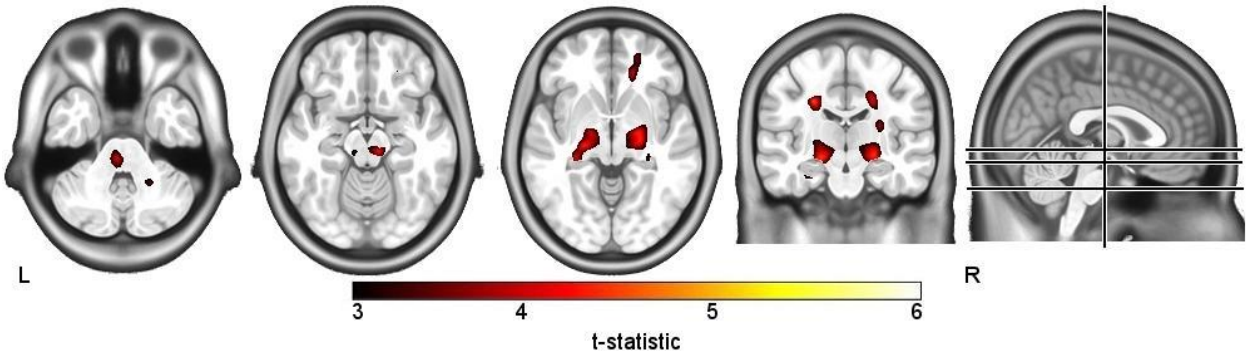


Figure S2: White matter tissue reductions in HIV+ patients revealed with voxel-based morphometry.

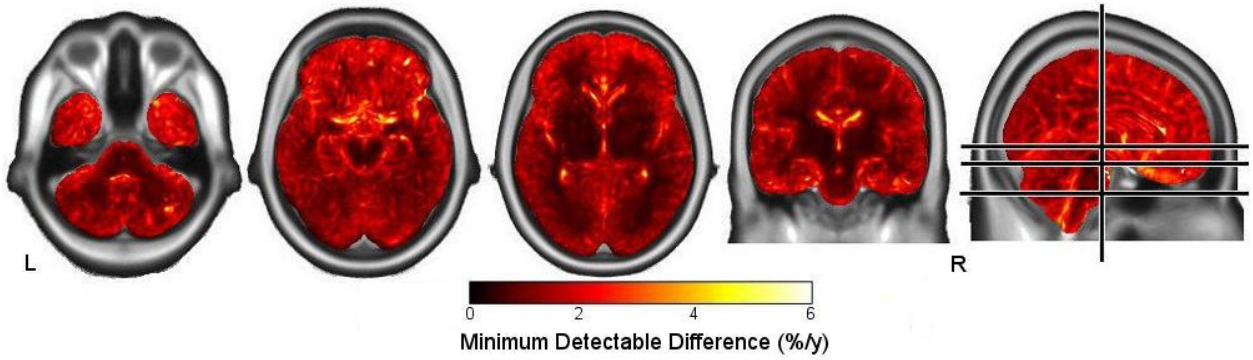


Figure S3: Visualization of the smallest difference between the groups in brain volume change over time that could be detected with tensor-based morphometry.

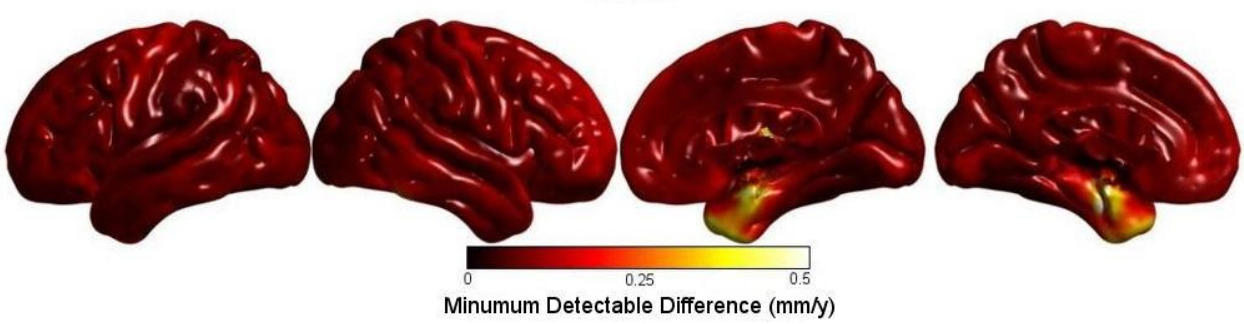


Figure S4: Visualization of the smallest difference between the groups in cortical thickness changes over time that could be detected from cortical thickness estimates.

## A.5. Chapter 5 Appendix

### A.5.1. Supplementary Figures

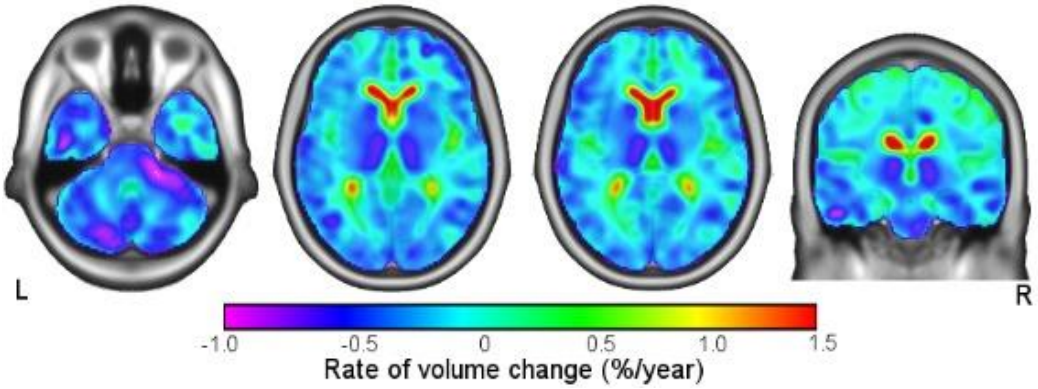


Figure S5: Rate of volume change prior to cART initiation from TBM.

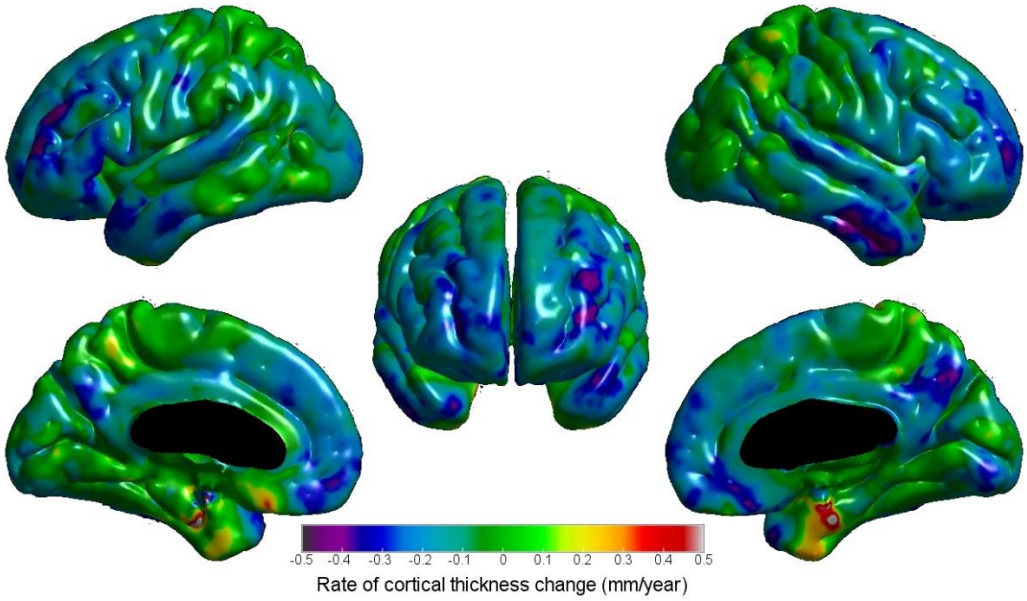


Figure S6: Rate of cortical thickness change prior to cART initiation from cortical modeling.

## Appendix Reference


1. Brouillette M, Mayo N, Fellows LK, et al. A better screening tool for HIV-associative neurocognitive disorders: is it what clinicians need? AIDS **2015**; 29: 895-902.
2. Akaike H. A New Look at the Statistical Model Identification. IEEE Trans Autom Control **1974**; AC-19(6): 716-23.
3. Locascio JJ, Atri A. An Overview of Longitudinal Data Analysis Methods for Neurological Research. Dement Geriatr Cogn Dis **2011**; 1: 330-57.